AD-A170 137 A STUDY OF CUMULUS PARAMETERIZATION IN A GLOBAL CIRCULATION MODEL(U) ILLINOIS UNIV AT URBANA DEPT OF ATMOSPHERIC SCIENCES S SOONG ET AL. JUN 85 1/2

UNCLASSIFIED AFGL-TR-85-0160 F19628-82-K-0030 F/G 4/2 NL

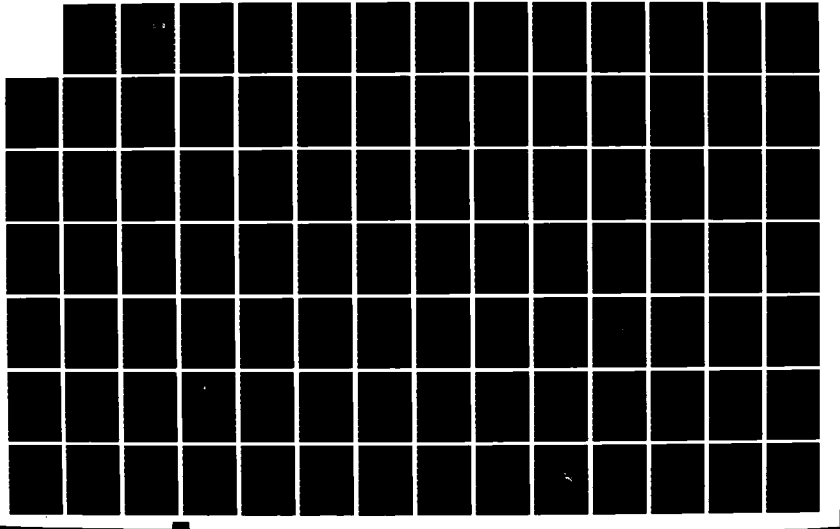

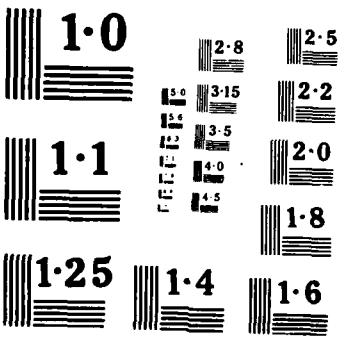
1·0
1·1
1·25
1·4
1·6
1·8
2·0
2·2
2·5
2·8
3·15
3·5
4·0
4·5

AFGL-TR-85-0160

A STUDY OF CUMULUS PARAMETERIZATION IN A GLOBAL CIRCULATION MODEL

Su-Tzai Soong
Yoshi Ogura
Wen-Shung Kau[1]

University of Illinois
Department of Atmospheric Sciences
Urbana, IL 61801

June 1985

Final Report
8 April 1982-8 June 1985

AIR FORCE GEOPHYSICS LABORATORY
AIR FORCE SYSTEMS COMMAND
UNITED STATES AIR FORCE
HANSCOM AIR FORCE BASE, MASSACHUSETTS 01731

[1]Present affiliation: National Taiwan University
Taipei, Taiwan

"This technical report has been reviewed and is approved for publication"

CHIEN-HSIUNG YANG
Contract Monitor

H. STUART MUENCH, Acting Chief
Atmospheric Prediction Branch

FOR THE COMMANDER

KENNETH R. HARDY, Acting Director
Atmospheric Sciences Division

This report has been reviewed by the ESD Public Affairs Office (PA) and is releasable to the National Technical Information Service (NTIS).

Qualified requestors may obtain additional copies from the Defense Technical Information Center. All others should apply to the National Technical Information Service.

If your address has changed, or if you wish to be removed from the mailing list, or if the addressee is no longer employed by your organization, please notify AFGL/DAA, Hanscom AFB, MA 01731. This will assist us in maintaining a current mailing list.

Unclassified

SECURITY CLASSIFICATION OF THIS PAGE

A170137

REPORT DOCUMENTATION PAGE

1a. REPORT SECURITY CLASSIFICATION: Unclassified	1b. RESTRICTIVE MARKINGS
2a. SECURITY CLASSIFICATION AUTHORITY	3. DISTRIBUTION/AVAILABILITY OF REPORT: Approved for public release; Distribution unlimited.
2b. DECLASSIFICATION/DOWNGRADING SCHEDULE	
4. PERFORMING ORGANIZATION REPORT NUMBER(S)	5. MONITORING ORGANIZATION REPORT NUMBER(S): AFGL-TR-85-0160
6a. NAME OF PERFORMING ORGANIZATION: University of Illinois; 6b. OFFICE SYMBOL (If applicable)	7a. NAME OF MONITORING ORGANIZATION: Air Force Geophysics Laboratory
6c. ADDRESS (City, State and ZIP Code): Department of Atmospheric Sciences, Urbana, IL 61801	7b. ADDRESS (City, State and ZIP Code): Hanscom AFB, Massachusetts 01731
8a. NAME OF FUNDING/SPONSORING ORGANIZATION; 8b. OFFICE SYMBOL (If applicable)	9. PROCUREMENT INSTRUMENT IDENTIFICATION NUMBER: F19628-82-K-0030
8c. ADDRESS (City, State and ZIP Code)	10. SOURCE OF FUNDING NOS.

PROGRAM ELEMENT NO.	PROJECT NO.	TASK NO.	WORK UNIT NO.
61102F	2310	G7	AC

11. TITLE (Include Security Classification): A Study of Cumulus Parameterization in a Global Circulation Model

12. PERSONAL AUTHOR(S): Su-Tzai Soong, Yoshi Ogura, Wen-Shung Kau

13a. TYPE OF REPORT	13b. TIME COVERED	14. DATE OF REPORT (Yr., Mo., Day)	15. PAGE COUNT
Final Report	FROM 8Apr82 TO 8Jun85	1985 June	122

16. SUPPLEMENTARY NOTATION

17 COSATI CODES		
FIELD	GROUP	SUB GR

18. SUBJECT TERMS (Continue on reverse if necessary and identify by block number): cumulus parameterization; the Arakawa-Schubert scheme; the Kuo scheme; global moist forecast model; rainfall prediction

19. ABSTRACT (Continue on reverse if necessary and identify by block number)

Parallel to the effort of the Air Force Geophysics Laboratory (AFGL) in developing a Moist Global Forecast Model, we carried out a research project in cumulus parameterization under the sponsorship of the Meteorology Division of the AFGL. The objectives of this research are: (1) to critically evaluate the Kuo and Arakawa-Schubert (A-S) cumulus parameterization schemes for numerical weather prediction; and (2) to improve these cumulus parameterization schemes for the purpose of improving precipitation forecasts on the global scale. The results of our research on the A-S

20. DISTRIBUTION AVAILABILITY OF ABSTRACT	21. ABSTRACT SECURITY CLASSIFICATION
UNCLASSIFIED UNLIMITED ☐ SAME AS RPT ☒ DTIC USERS ☐	Unclassified

22a. NAME OF RESPONSIBLE INDIVIDUAL	22b. TELEPHONE NUMBER (Include Area Code)	22c. OFFICE SYMBOL
Chien-Hsiung Yang	(617) 861-3913	AFGL/LYP

DD FORM 1473, 83 APR EDITION OF 1 JAN 73 IS OBSOLETE

~~Unclassified~~

SECURITY CLASSIFICATION OF THIS PAGE

scheme of cumulus parameterization, including an improved computational algorithm for computing the cloud spectrum under the quasi-equilibrium approximation, have been presented in Scientific Report No. 1 (Kao and Ogura, 1985).

The major improvements to the Kuo scheme include the prediction of cloud top height and the incorporation of the effect of entrainment on cloud temperature and mixing ratio profiles. This improvement enables the Kuo scheme to parameterize shallow to medium clouds as well as deep clouds. Tests of the Kuo scheme using a semi-prognostic approach and a Cloud Cluster Model indicate that the improved version verifies better with observation during weaker convective periods.

A set of experimental predictions were made and the results clearly demonstrated the ability of the AFGL model to predict large-scale stratiform precipitation. With the incorporation of the present modified Kuo scheme, the area of convective precipitation can also be well predicted. However, the predicted convective precipitation area is generally broader and the amount of rainfall smaller than observations. This problem may be attributed to the resolution of the AFGL model in that it cannot resolve the narrow band of the cold front, the major mesoscale rain-producing system. The implementation of the A-S scheme in the AFGL model also produced a reasonable distribution of convective precipitation. The precipitation area is more concentrated and sometimes it is produced in an observed clear area. This result may have been caused by the current implementation of the A-S scheme in the AFGL model, in which the cloud base is assumed to be 500 m above the ground surface. This assumption is valid in the tropics, but it may produce unrealistic convective rainfall in dry areas.

Preface

One of the central problems in numerical weather prediction is to relate the sub-grid scale condensation, evaporation, and vertical transports of heat and moisture by cumulus clouds to the variables predicted by the model. This problem is known as the cumulus parameterization. The most important element of any cumulus parameterization scheme is the prediction of the rainfall rate and the vertical distributions of the convective heating and moistening profiles. The rainfall rate is directly related to the total amount of heat added to and moisture removed from the large-scale system by condensation and evaporation. The vertical distributions of heat and moisture by clouds can change the large-scale stability and moisture structure of the atmosphere which, in turn, can affect the future development of large-scale weather systems.

Several cumulus parameterization schemes have been proposed in the past. The simplest and most commonly used scheme is the one proposed by Kuo (1965, 1974) based on the assumption that the convective precipitation is related to the vertically integrated moisture convergence. In this scheme, usually only one type of cloud is produced at a given time and the cloud heating and moistening profiles are proportional to the temperature and humidity differences between the cloud and the environment. Another scheme gaining increasing attention is the one proposed by Arakawa and Schubert (1974) which takes into account the coexistence of a spectrum of clouds. The quasi-equilibrium approximation, which requires that clouds stabilize the atmosphere as the large-scale motion generates moist convective instability, permits the determination of cloud properties.

Parallel to the effort of the Air Force Geophysics Laboratory (AFGL) in developing a Moist Global Forecast Model, we carried out a research project in cumulus parameterization under the sponsorship of the Meteorology Division of the AFGL. The objectives of this research are: (1) to critically evaluate the Kuo and Arakawa-Schubert (A-S) cumulus parameterization schemes for numerical weather prediction; and (2) to improve these cumulus parameterization schemes for the purpose of improving precipitation forecasts on the global scale. The results of our research on the A-S scheme of cumulus parameterization, including an improved computational algorithm for computing the cloud spectrum under the quasi-equilibrium approximation, have been presented in Scientific Report No. 1 (Kao and Ogura, 1985). Part I of this report contains the results of our research on the Kuo scheme. The major improvements to the Kuo scheme include the prediction of cloud top height and the incorporation of the effect of entrainment on cloud temperature and mixing ratio profiles. This improvement enables the Kuo scheme to parameterize shallow to medium clouds as well as deep clouds. Tests of the Kuo scheme using a semi-prognostic approach and a Cloud Cluster Model indicate that the improved version verifies better with observation during weaker convective periods. Part II contains the results of applying the improved Kuo scheme and the A-S scheme of cumulus parameterization in the AFGL Moist Global Forecast Model. In contrast to the forecast using the original code of cumulus parameterization in the AFGL model, both the improved Kuo scheme and the A-S scheme predicted the area of convective precipitation reasonably well.

Acknowledgments

We would like to thank Dr. Y.-L. Chen of the University of Hawaii for providing the verification data used in this study, C.-Y. Kao for helping the implementation of the A-S scheme in the AFGL model, Sandra Weaver for editorial work, and Karen Garrelts and Norene McGhiey for typing and arranging this report. This research was sponsored by the Air Force Geophysics Laboratory, Hanscom Air Force Base, Massachusetts, under Contract F19628-82-K-0030. The numerical modeling work was carried out on computers at the National Center for Atmospheric Research, which is supported by the National Science Foundation. Other computation was carried out on computers at the University of Illinois. The Research Board of the University of Illinois provided partial support of local computations.

TABLE OF CONTENTS

PART ONE

A Cumulus Parameterization Study with Special Attention to the Kuo Scheme

1. Introduction

It is recognized that the latent heat released in cumulus convection and the vertical transports of heat and moisture in clouds play key roles in determining the structure of the temperature and moisture fields in the atmosphere. However, since the horizontal scale of cumulus clouds is at least an order of magnitude smaller than the grid scale used in representing large and mesoscale flows, the net effect of convection and condensation upon the large-scale flows must be parameterized in terms of the known large-scale variables.

Several cumulus parameterization schemes are used in large-scale and mesoscale models. Each scheme is different in a way directed by convenience and by the type of problem and integration model involved. The most important elements of any cumulus parameterization scheme are the prediction of the rainfall rate and the convective heating and moistening profiles. The rainfall rate determines the total amount of heat added to the large-scale system by condensation, while the vertical distribution of heat and moisture by clouds can change the large-scale stability and moisture structure in ways that can either enhance or suppress the development of large-scale systems. The simplest and most popular scheme of cumulus parameterization is based on the assumption that convective precipitation is related to the vertically integrated moisture convergence. Kuo (1965, 1974) parameterized the release of latent heat by relating convective activity to the moisture converging into a conditionally unstable atmospheric column. This report will focus on this scheme. Section 2 reviews some of the Kuo-type cumulus

parameterization schemes, while Section 3 presents a semi-prognostic test of the Kuo scheme, Section 4 describes the present modified Kuo scheme, and Section 5 presents the results of the semi-prognostic studies with the present scheme. Section 6 presents the prognostic model results using a Cloud Cluster Model.

2. Review of Cumulus Parameterization Schemes Based on Moisture Convergence

A cumulus parameterization based on the total column moisture convergence was first proposed by Charney and Eliassen (1964). The application of this method to tropical cyclones has established the concept of CISK (Conditional Instability of the Second Kind). In this method, cumulus clouds are permitted to penetrate deeply into the unsaturated atmosphere in areas of low-level mass convergence. Extensive use of this method has led to several related but not identical techniques. Kuo (1965, 1974) refined this concept by distributing cumulus heat and moisture vertically with a simple cloud model. The amount of cumulus heating is assumed to be proportional to the vertically integrated moisture convergence. This technique has often been referred to as the Kuo scheme of cumulus parameterization. In this section, we will review several variations of Kuo's parameterization.

2.1. Kuo (1965):

Kuo's scheme stipulates that cumulus convection always occurs in regions of deep layers of conditionally unstable stratification and mean low-level convergence and that the vertical profiles of temperature and water vapor mixing ratio inside the cloud follow those of a non-entraining moist adiabatic process. The vertical distributions of convective heating and

moistening can be determined by the mixing of environmental and cloudy air after the decay of the cloud so that the convective heating and moistening is proportional to the temperature and mixing ratio differences between the cloud and the surrounding atmosphere.

The net convergence of moisture into a vertical column of air of a unit cross section produced by the large-scale flow and by the evaporation from the surface is expressed by

$$M_t = -\frac{1}{g}\int_o^{P_s} (\nabla\cdot\vec{V}q)dP + \rho_o C_D V_o (q_g - q_o) \qquad (1)$$

where g is the gravity, V is the horizontal velocity, q is the water vapor mixing ratio, ρ is the density, P_s is the surface pressure, C_D is the drag coefficient and subscripts g and 0 denote the surface and anemometer levels. The amount of moisture convergence needed to create a deep cumulus cloud of unit area and pressure depth ($P_b - P_t$) is

$$M_c = \frac{1}{g}\int_{P_t}^{P_b} \left[\frac{C_p}{L}(T_c - T) + q_c - q\right]dP \qquad (2)$$

where subscript C denotes cloud variables, P_b and P_t are the pressures at the base and top of the cloud, L is the latent heat of condensation, C_p is the specific heat at constant pressure and T is the temperature.

The variable M_c has two components: one is the moisture required to raise the cloud temperature to T_c and the other to raise the cloud mixing ratio to q_c. Therefore,

$$M_c = I_q + I_T \qquad (3)$$

where

$$I_\theta = \frac{1}{g}\int_{P_t}^{P_b} \frac{C_p}{L}(T_c - T)dP \tag{4}$$

and

$$I_q = \frac{1}{g}\int_{P_t}^{P_b} (q_c - q)dP \tag{5}$$

The fractional area of a grid square that will be covered by newly formed convective clouds in a time interval $\Delta\tau$ is

$$a = M_t \cdot \Delta\tau / M_c \tag{6}$$

The variable $\Delta\tau$ can be considered to be the cloud time-scale parameter (Krishnamurti et al., 1983). In practice, the time interval of a large-scale prediction model, Δt, is commonly used in place of $\Delta\tau$.

Since Kuo's scheme stipulates that the cloud will mix its temperature and mixing ratio with those of the environmental air, the large-scale temperature T and mixing ratio q after mixing are expressed by

$$T_{t+\Delta t} = T^* + a(T_c - T^*)$$

$$q_{t+\Delta t} = q' + a(q_c - q^*)$$

where T^* is the temperature at time $t + \Delta t$ before cumulus parameterization and q' is the mixing ratio at the previous time step. In this process, all of the moisture convergence is used to build clouds, leaving the environmental mixing ratio unaffected by the large-scale flow. In other words, $a(q_c-q^*)$ in Kuo's scheme includes the terms of large-scale advection, surface evaporation, cloud condensation and cloud transport of moisture. The combination of these processes will moisten the atmosphere and is commonly called the cloud moistening effect in Kuo's scheme. When cloud condensation and cloud transport alone are considered, they will, in general, dry the atmosphere and are called the cloud drying effect. To compute the cloud drying effect using Kuo's scheme, large-scale advection and surface evaporation should be subtracted from $a(q_c-q^*)$ profiles.

2.2 Kuo (1974)

Kuo's 1965 scheme of cumulus parameterization has been remarkably successful in hurricane simulation studies (Rosenthal, 1970). However, it underestimated the convective rainfall and heating rates in large-scale tropical applications. This defect is primarily related to the allocation of M_t into I_θ and I_q. Since I_q is typically twice as large as I_θ in the tropics, Kuo's 1965 scheme uses about 1/3 of the moisture supply to heat the atmosphere and 2/3 to moisten the atmosphere. Observations show that almost all of the moisture supply goes to heat the atmosphere. Kuo (1974) recognized this shortcoming and revised the scheme to provide a more reasonable subdivision of this moisture supply.

In deriving the new scheme, the equations for the potential temperature θ and the water vapor mixing ratio q of the large-scale system are written in p-coordinates as

$$\frac{d\theta}{dt} - Q_r - \frac{L}{c_p \pi}\overline{c} = \frac{L}{c_p \pi}\overline{c^*} - \overline{\frac{\partial \omega' \theta'}{\partial p}} \tag{7}$$

$$\frac{dq}{dt} - T_q + \overline{c} = -\overline{c}^* - \overline{\frac{\partial \omega' q'}{\partial P}} \tag{8}$$

and

$$\frac{d()}{dt} = \frac{\partial()}{\partial t} + \vec{V}\cdot\nabla() + \frac{\partial()}{\partial P}$$

where $\overline{c}$ and $\overline{c}^*$ are the condensation rates produced by large-scale and cloud convective motions, respectively, and Q_r is the heating rate by radiation and turbulent diffusion. T_q is the rate of mixing ratio change by turbulent diffusion and π is the non-dimensional pressure defined as:

$$\pi = (P/P_o)^{R/C_p}$$

The terms on the right hand sides of (7) and (8) are the cumulus effect on θ and q.

In order to correct the disproportion of M_t into I_θ and I_q, Kuo proposed that the fraction (1-b) of the moisture supply M_t is condensed during cumulus convection and is precipitated out as rain while the remaining fraction b of M_t is stored in the air to increase the humidity:

$$R = \frac{1}{g}\int_o^{P_s} \overline{c^*}\, dp = (1-b)M_t \tag{9}$$

$$\frac{1}{g}\int_o^{P_s} \frac{\partial q}{\partial t}\, dP = bM_t \tag{10}$$

where R is the rainfall, and b is the parameter for partitioning the moisture.

The rate of the release of latent heat by deep cumulus convection due to condensation can now be written as:

$$aQ_c = \frac{L}{c_p \pi} \bar{c}^* = g(1-b) \frac{L}{c_p \pi} M_t \frac{N_{k\theta}(P)}{(P_b - P_t)} \tag{11}$$

where Q_c is the latent heating effect by one unit area of cloud, $N_{k\theta}(p)$ is the vertical distribution function of Q_c. Kuo proposed that $N_{k\theta}(p)$ could be determined by the cloud - environment temperature differences. Therefore, it can be written as

$$N_{k\theta}(P) = \frac{(\theta_c - \bar{\theta})}{\langle \theta_c - \bar{\theta} \rangle} \tag{12}$$

which satisfies the condition:

$$\int_{P_t}^{P_b} N_{k\theta}(P) \, dp = (P_b - P_t) \quad .$$

The angle brackets represent the vertical averaging operator which is defined by:

$$\langle \; \rangle = \int_{P_t}^{P_b} () \, dP/(P_b - P_t) \tag{13}$$

In Kuo's 1965 scheme (previous section) entrainment was not considered because only deep clouds were included. The influence of entrainment on θ_c can be taken into consideration either by the employment of a simple empirical formula or by the use of a simple entrainment model. Kuo proposed the following equation expressed in T instead of θ:

$$T_c - T = T_s - \left[1 + \sum_{j=1}^{J} \alpha_j (1 - P/P_o)^{\gamma_j}\right] T \qquad (14)$$

where T_s is the temperature along the moist adiabatic process, the summation is over the different types of cumulus, α_j is a constant that is determined by the vertical extent of the particular type of cumulus, and γ_j is another constant which is most probably ≥ 2. Similar equations can be used to compute the entrainment effect on the cloud mixing ratio $(q_c - q)$. Kuo also proposed a simple formula to compute the cloud vertical velocity which, together with T_c and q_c computed from (14), can be used to compute the vertical transports of heat and moisture by cumulus clouds [see (7) and (8)]. Kuo argued that the vertical sensible heat transport is much smaller than aQ_c and that its effect is only to shift the level of maximum heating rate to a slightly higher altitude. The computation of $\overline{c}^*$ and the flux divergence of heat and moisture complete Kuo's 1974 cumulus parameterization.

In the above formulations Kuo did not give a formal expression for the b parameter to close the system. He only assumed that b is much smaller than 1 in regions of low-level convergence in the tropics, which implies that all of the moisture convergence brought about by the large-scale flow is precipitated out as rain.

2.3 Anthes (1977)

Following Kuo's 1974 scheme, Anthes (1977) argued that the vertical distribution of heating by condensation is not adequately represented by the cloud-environment temperature differences. Therefore, he proposed to use the actual cloud condensation profile from a cloud model for the vertical heating distribution function:

$$N_{A\theta}(P) = C^*/\langle C^* \rangle \tag{15}$$

The vertical distribution of condensational heating is therefore given by

$$aQ_c = \frac{L}{c_p \pi} \frac{g(1-b)}{(P_b - P_t)} M_t N_{A\theta}(P) \tag{16}$$

which is the same as (11) except for the vertical heating distribution function.

He also proposed that b is a function of the mean relative humidity in the column, increasing from near zero in a saturated column to 1 as the mean relative humidity approaches a critical value RH_c. Therefore b is given by

$$b = \begin{cases} \left\{ \frac{1-\langle RH \rangle}{1-RH} \right\}^n & \langle RH \rangle \geq RH_c \\ 1 & \langle RH \rangle < RH_c \end{cases} \tag{17}$$

where n is a positive exponent of order 1 which may be empirically adjusted.

The moisture equation at gridpoints with convection is written as

$$\frac{\partial q}{\partial t} = \frac{\partial q}{\partial t}^+ - \overline{\frac{\partial \omega' q'}{\partial P}} \tag{18}$$

where $\partial q^+/\partial t$ is the combined moistening effect due to water vapor convergence by the large-scale flow and the removal of water vapor by condensation. Given a value of b, the vertical integration of $\partial q/\partial t$ is

$$\frac{1}{g}\int_o^{P_s}\frac{\partial q}{\partial t}\,dP = \frac{1}{g}\int_o^{P_s}\frac{\partial q^+}{\partial t}\,dP = bM_t$$

He proposed the following form for the vertical distribution of $\partial q^+/\partial t$:

$$\frac{\partial q^+}{\partial t} = \frac{gb}{(P_b-P_t)}\,M_t N_{Aq}(P) \tag{19}$$

where $N_{Aq}(p)$ is the vertical moistening distribution function. Concluding that the most moistening should occur in the driest layers, he suggested the following form for $N_{Aq}(p)$

$$N_{Aq}(P) = \frac{(100\% - RH)q_s(T)}{\langle(100\% - RH)\,q_s(T)\rangle} \tag{20}$$

where $q_s(T)$ is the saturation mixing ratio at the environmental temperature T.

In order to close the cumulus parameterization scheme by using the above formulation, a cloud model is required to provide the mean cloud properties (ω_c, T_c, q_c and c^*) for computing the cloud transport terms and the vertical heating distribution function $N_{A\theta}(p)$. In this scheme, the vertical distribution of the latent heating is very sensitive to the radius of the mean cloud. How to determine the radius of the mean cloud is the major problem.

2.4 Krishnamurti et al. (1976)

Krishnamurti et al. modified Kuo's 1974 scheme and also proposed a hypothesis for computing b. First, they used the following form of the heat and moisture equations:

$$\frac{\partial \theta}{\partial t} + \vec{V}\cdot\nabla\theta = -\omega\frac{\partial\theta}{\partial p} + a_\theta\left[\omega\frac{\partial\theta}{\partial p} + \frac{\theta_c-\theta}{\Delta\tau}\right] \tag{21}$$

$$\frac{\partial q}{\partial s} + \vec{V}\cdot\nabla q = a_q\left[\frac{q_c-q}{\Delta\tau}\right] \tag{22}$$

They defined the available moisture supply as the vertically integrated vertical advection of mixing ratio:

$$M_t = I = -\frac{1}{g}\int_{P_t}^{P_b}\omega\frac{\partial q}{\partial P}\,dP \tag{23}$$

Furthermore, they defined Q_θ and Q_q as

$$a_\theta Q_\theta = \frac{a_\theta}{g}\int_{P_t}^{P_b}\frac{c_p}{L}\frac{T}{\theta}\left[\frac{\theta_c-\theta}{\Delta\tau} + \omega\frac{\partial\theta}{\partial P}\right]dp = (1-b)I \tag{24}$$

$$a_q Q_q = \frac{a_q}{g}\int_{P_t}^{P_b}(q_c-q)/\Delta\tau\;\;dP = bI \tag{25}$$

$$Q = Q_\theta + Q_q$$

where Q is a measure of the total moisture supply needed to cover a unit horizontal area with clouds, Q_θ is the moisture supply required to raise the temperature to the cloud temperature in this column and Q_q is the moisture

supply required to saturate the column at the cloud temperature. According to their argument, the inclusion of the second term on the righthand side of (24) provides a smooth transition between the convective heating in the conditionally unstable atmosphere and the large-scale condensational heating in the stable situation. The detailed description of the smooth transition when this term is retained can be seen in Krishnamurti et al. (1983). The cloud temperature and mixing ratio are computed from a moist adiabatic process so θ_c and q_c in (24) and (25) assume their saturated moist adiabatic values θ_s and q_s, respectively. The following hypothesis is made to close the system:

$$\frac{1}{g}\int_{P_t}^{P_b} \frac{c_p}{L}\frac{T}{\theta}\left(\frac{\partial\theta}{\partial t} + \vec{V}\cdot\nabla\theta\right) dP = \frac{1}{g}\int_{P_t}^{P_b}\left(\frac{\partial q}{\partial t} + \vec{V}\cdot\nabla q\right) dP \qquad (26)$$

The implication here is that in the cloud column the total change of θ and q due to both vertical advection and convection are proportional. This condition brings the θ and q values to the moist adiabatic values in near unison.

Substituting (21) and (22) into (26) and using A defined as

$$A = -\frac{1}{g}\int_{P_t}^{P_b} \frac{c_p}{L}\frac{T}{\theta}\,\omega\,\frac{\partial\theta}{\partial P}\,dP \quad , \qquad (27)$$

we can get

$$A + (1-b)I = bI,$$

$$b = \frac{A+I}{2I} \qquad (28)$$

Once b is determined, a_θ and a_q can be computed from (24) and (25). These values in turn can be used to compute the cumulus effect in (21) and (22). In notation similar to Kuo (1974), the convective heating profile can be expressed as

$$aQ_c = \frac{L}{c_p \pi} g(1-b) M_t \frac{N_{KR\theta}(P)}{(P_b - P_t)} \tag{29}$$

where the vertical heating distribution function is

$$N_{KR\theta}(P) = \left(\frac{\theta_c - \theta}{\Delta\tau} + \omega \frac{\partial\theta}{\partial P}\right) \Big/ \left\langle \frac{\theta_c - \theta}{\Delta\tau} + \omega \frac{\partial\theta}{\partial P} \right\rangle \tag{30}$$

The mixing ratio equation can be written as

$$\frac{\partial q}{\partial t} + V \cdot \nabla q = \frac{gbI}{(P_b - P_t)} \frac{(q_c - q)}{\langle q_c - q \rangle} \tag{31}$$

Basically the above approach is the extension of the Kuo (1974) scheme. The closure assumption is ad hoc and is not based on any valid theory.

2.5 Molinari (1982)

Based on the framework developed by Krishnamurti et al. (1976), an alternative closure was proposed by Molinari (1982) for the b parameter which more explicitly requires the warming and moistening of the cumulus column to produce a smooth change toward moist neutrality in both temperature and mixing ratio. The closure is written as

$$\int_{P_t}^{P_b} (T_s - T) dP \Big/ \left(\int_{P_t}^{P_b} \left(\frac{\partial T}{\partial t}\right)_{con} dP \right) = \int_{P_t}^{P_b} (q_s - q) dP \Big/ \left(\int_{P_t}^{P_b} \left(\frac{\partial q}{\partial t}\right)_{con} dP \right) \tag{32}$$

where

$$\left(\frac{\partial}{\partial t}\right)_{con} = \frac{\partial}{\partial t} + V\cdot\nabla$$

Substituting (21) and (22) into (32), yields

$$b = \frac{A+I}{I} \frac{\int_{P_t}^{P_b} (q_s - q)dP}{\int_{P_t}^{P_b} (q_s - q)dP + \int_{P_t}^{P_b} \frac{c_p}{L}\frac{T}{\theta}(\theta_c - \theta)dP} \tag{33}$$

This procedure forces the instantaneous time tendencies of θ and q to be such that they would reach their moist neutrality simultaneously.

This scheme is an extension of that of Krishnamurti et al. (1976). The only difference between these two schemes is the closure assumption. According to Molinari's (1982) results, the proposed closure produces a more accurate time variation of stability that approaches moist neutrality better than Krishnamurti et al. (1976). However, the closure assumption for b is still an ad hoc assumption.

2.6 Krishnamurti et al. (1983)

Following the previous work of Krishnamurti et al. (1976), they introduced an additional source of moisture supply, In, which may be considered a nonmeasurable mesoscale (or subgrid-scale) supply. The total supply of moisture is expressed by

$$I' = I(1+n) \tag{34}$$

and the rainfall rate R and moistening rate M are given by

$$R = I'(1-b) = I(1+\eta)(1-b) \tag{35}$$

$$M = I'b = I(1+\eta)b \tag{36}$$

In this formulation there are two unknown parameters, η and b, that need to be determined for the closure of the cumulus parameterization scheme. They proposed that η and b be expressed as functions of pairs of known large-scale variables such as the vertically averaged large-scale vertical velocity w and the 700 mb relative vorticity ξ . Based on the multiple regression analysis, they get

$$b = \frac{a_1\xi + b_1\bar{w} + c_1}{(a_1+a_2)\xi + (b_1+b_2)\bar{w} + (c_1+c_2)} \tag{37}$$

$$\eta = [(a_1+a_2)\xi + (b_1+b_2)\,\bar{w} + (c_1+c_2)] - 1 \tag{38}$$

where a_i, b_i, and c_i are regression coefficients. Therefore,

$$aQ_c = \frac{L}{c_p\pi}\, g(1-b)(1+\eta)I\, N_{KR\theta}(P)/(P_b-P_t) \tag{39}$$

$$\frac{\partial q}{\partial t} + V\cdot\nabla q = \frac{gbI(1+\eta)}{(P_b-P_t)}\,\frac{(q_c-q)}{\langle q_c-q\rangle} \tag{40}$$

They have tested the above scheme to determine the vertical distributions of the heating, moistening, and rainfall rates for the entire GATE (Global Atmospheric Research Program's Atlantic Tropical Experiment) Phase III data. The results of these calculations are in good agreement with the

observed estimates. However, they did not mention whether the regression coefficients are universal constants or not. Those constants may change with different time periods or locations.

3. Semiprognostic Test of the Kuo Scheme

Imperfectly represented cloud processes in cumulus parameterization schemes may interact with the large-scale flow in unrealistic ways. For this reason, any proposed parameterization scheme must be verified with observed data. Generally speaking, two approaches have been taken to test a cumulus parameterization scheme against observations. The first approach may be categorized as a semiprognostic approach because it is a one time-step prediction of cumulus-produced heating and drying profiles and rainfall rate. The other approach is to incorporate the parameterization schemes into a large-scale prediction model, such as a regional, hemispherical or global model.

In this section we will focus on a semiprognostic test of the Kuo scheme using GATE B-scale data. The apparent heat source Q_1 and the apparent moisture sink Q_2 are defined by the following equations:

$$Q_1 = \frac{1}{\pi}\left(\frac{\partial \bar{\theta}}{\partial t} + \bar{\vec{V}}\cdot\nabla\bar{\theta} + \bar{\omega}\frac{\partial \bar{\theta}}{\partial P}\right) = -\frac{1}{\pi}\left(\frac{\partial \overline{\omega'\theta'}}{\partial P}\right) + \frac{L}{c_p}\bar{c}^* + Q_R \tag{41}$$

$$Q_2 = -\frac{L}{c_p}\left(\frac{\partial \bar{q}}{\partial t} + \bar{\vec{V}}\cdot\nabla\bar{q} + \bar{w}\frac{\partial \bar{q}}{\partial P}\right) = \frac{L}{c_p}\left(\bar{c}^* + \frac{\partial \overline{\omega'q'}}{\partial P}\right) \tag{42}$$

Here the overbar denotes the average over the GATE B-scale area and the prime denotes the cloud scale. Q_1-Q_R represents the cloud heating effect and Q_2 represents the cloud drying effect. Dr. Y.-L. Chen of the University

of Hawaii has diagnostically estimated Q_1 and Q_2 for the entire GATE Phase III (30 August - 18 September) B-scale area by computing the terms between the equal signs in (41) and (42). We will use his data and refer to his Q_1 and Q_2 values as the observation values. The vertical resolution of the data is 38 uneven levels from the surface to 92.5 mb. The area average is over 2.5° in radius and the time resolution is every 3 hours. The radiational heating (or cooling) rates Q_R that we used in this study are taken from Krishnamurti et al. (1983). Table 1 lists the 6-hourly net radiational heating rates averaged over the entire phase III period. In this data, significant changes in the magnitude of Q_R are evident between the night and daytime hours.

In the semiprognostic approach, the cumulus heating and drying effects, i.e., those terms on the righthand side of (41) and (42) excluding Q_R, are calculated from the parameterization schemes (thereafter referred to as the calculated values) and compared with the observation values of Q_1-Q_R and Q_2. The advantage of this approach is that a prediction can be made without using a large-scale prediction model. Moreover, since this is only a one time-step integration, the predicted results are free from numerical nonlinear errors and complicated physical feedback effects. Any successful parameterization scheme has to first achieve a good score on this semiprognostic test.

The method used to parameterize the cumulus effects in this test is a combination of Kuo's 1965 and 1974 schemes. They can be summarized as follows:

(a) The moisture supply is computed from the vertically integrated moisture convergence and surface evaporation.

Table 1. Six-hourly total radiative heating rate (C/day) averaged over the entire Phase III of the GATE period.

Pressure level(mb)	0000-0600	0600-1200	1200-1800	1800-2400
100	-0.78	-0.09	-0.10	-0.74
175	-0.93	-0.14	-0.15	-0.92
250	-1.52	-0.31	-0.34	-1.55
325	-2.02	-0.29	-0.36	-2.14
400	-2.34	-0.40	-0.47	-2.43
475	-2.55	-0.58	-0.59	-2.52
550	-2.70	-0.76	-0.70	-2.56
625	-2.36	-0.79	-0.72	-2.24
700	-2.08	-0.89	-0.83	-2.01
775	-1.81	-0.93	-0.89	-1.79
850	-1.46	-0.80	-0.79	-1.46
925	-1.04	-0.49	-0.48	-1.03
1000	-0.10	-0.10	-0.12	-0.12

(b) A fraction (1-b) of the moisture supply is used to heat the atmosphere and a fraction b of the moisture supply is used to moisten the atmosphere.

(c) The calculated (Q_1-Q_R)(<u>total</u> cloud heating) profile is computed using (11).

(d) The <u>cloud moistening effect</u> (including the large-scale advection and surface evaporation) is computed from

$$\frac{\partial q}{\partial t} = \frac{gbM_t}{(P_b-P_t)} \frac{(q_c-q)}{\langle q_c-q \rangle}$$

(e) The calculated Q_2 profile is computed by subtracting the large-scale advection and surface evaporating terms from the above equation.

The partition of the moisture supply is based on Kuo's 1974 scheme. Once this partition is determined, the Q_1-Q_R and Q_2 profiles are computed based on Kuo's 1965 scheme.

As mentioned in Section 2.2, Kuo proposed that the parameter b in his 1974 scheme is very small. Several methods to compute b have been proposed (see Section 2) but no verification has been made. However, Krishnamurti et al. (1980) compared the observed rainfall to that predicted from Kuo's scheme with small b ($b \approx 0$) and found extremely good agreement. Therefore, in this semiprognostic test we have set b equal to zero. For simplicity, the entrainment effect on cloud temperature and mixing ratio is not included.

Figs. 1 and 2 are the calculated and observed $Q_1 - Q_R$ for September 1-18, 1974 shown on pressure-time sections. The large observed heating occurred on the following dates: 2, 4, 5, 12, 13, 14, 15, 16, and 17. There is general agreement between the calculated and the observed values. To examine the results closely, Fig. 3 shows the comparison of the calculated $Q_1 - Q_R$ profiles with those obtained from observations during periods of heavy rainfall on 2(1200, 1800GMT), 4(1200, 1800GMT), 5(1200, 1800GMT), 12(1200GMT), 15(0000GMT), 16(1200GMT), and 17(1200GMT). The maximum value of heating lies between 10 and 15°C/day, in good agreement with the observed heating values.

Fig. 4 shows the comparison of calculated and observed $Q_1 - Q_R$ during periods of weak convection period on 2(0600GMT), 3(1800GMT), 9(0000GMT), 10(1800GMT), 11(1200GMT), 12(0000GMT), 13(1200GMT), 14(1800GMT), and 16(0600, 1800GMT). The observed maximum heating is located below 550 mb; however, the calculated maximum heating is above 550 mb. The cloud heating rate has been consistently overestimated above 500 mb and underestimated at the lower levels.

In general, the observed vertical distributions of convective heating are highly variable; but the vertical profiles of the cloud-environment temperature difference computed from rising, undiluted surface parcels (T_c - T) are less variable (Song and Frank, 1983). Since the cloud heating profile was based on the profile of T_c - T and no entrainment was considered, the poor agreement between the calculated and observed cloud heating profiles during weak convective conditions is not surprising. On the other hand, during strong convection the cloud heating profile does match the undiluted T_c - T profile well.

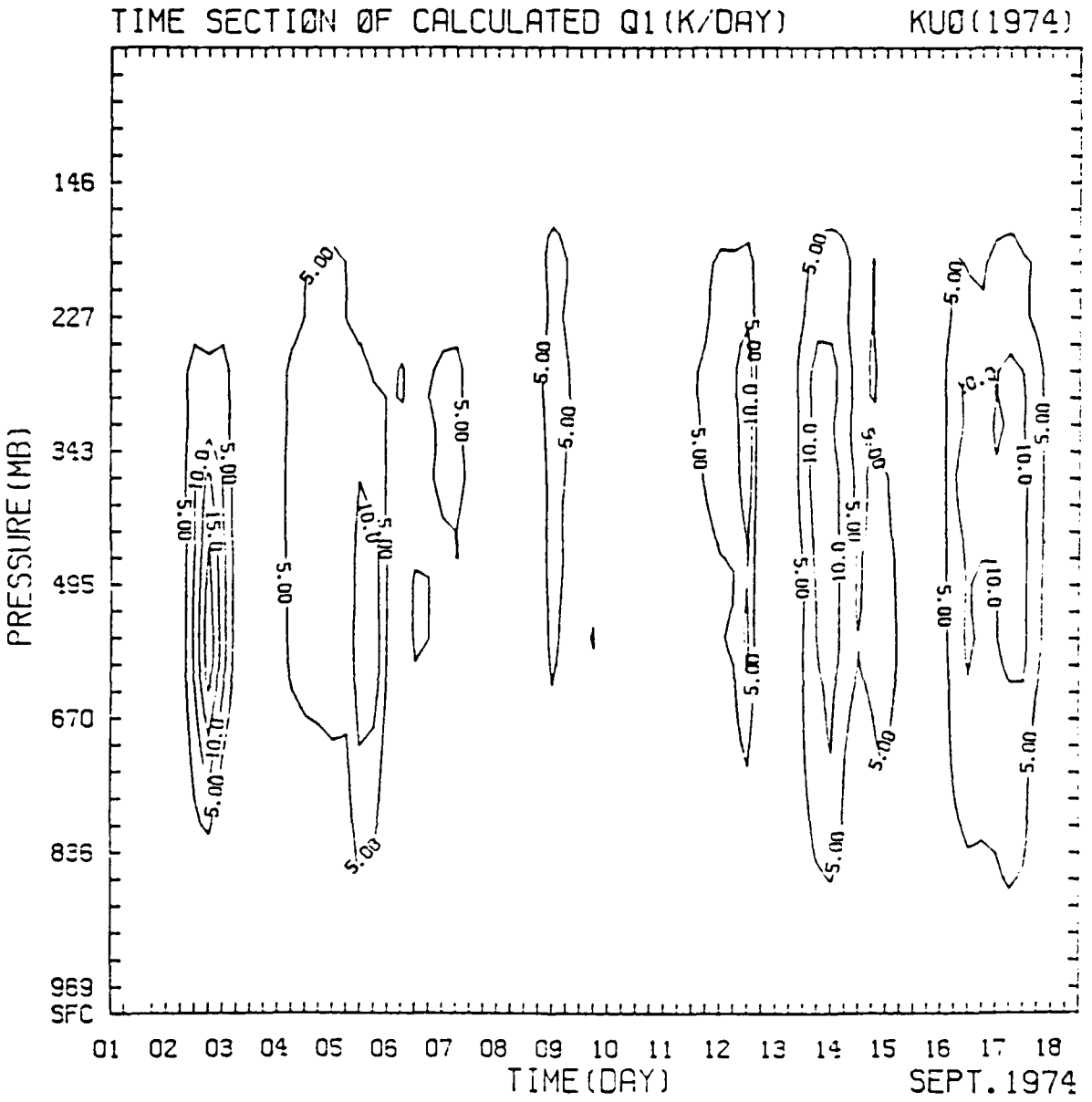

Fig. 1. Vertical cross section of the calculated cloud heating effect (Q_1-Q_R) for the Kuo scheme. Abscissa denotes dates during the Phase III of GATE. The vertical coordinate is pressure.

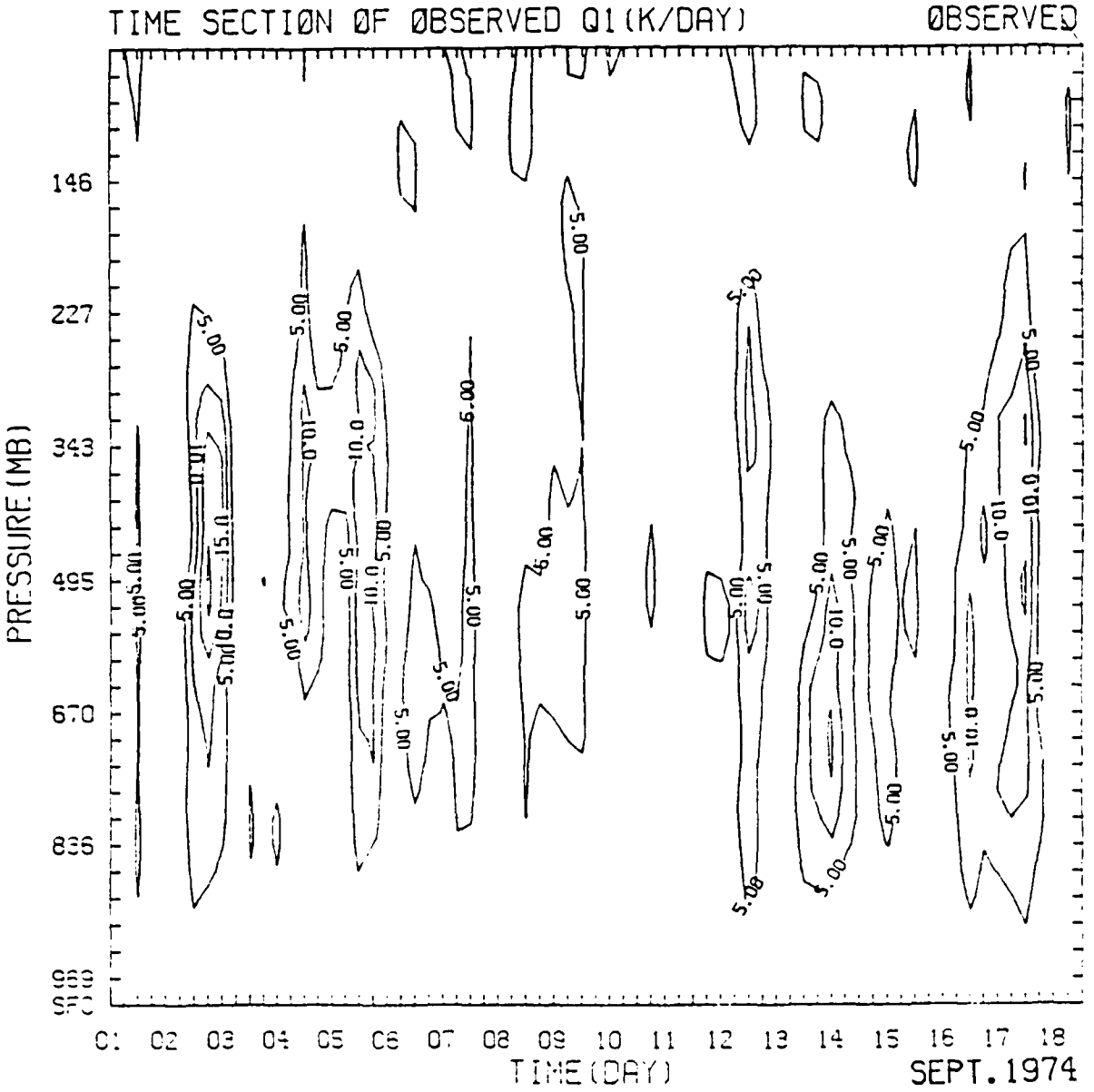

Fig. 2. As in Fig. 1 except for the observed cloud heating effect.

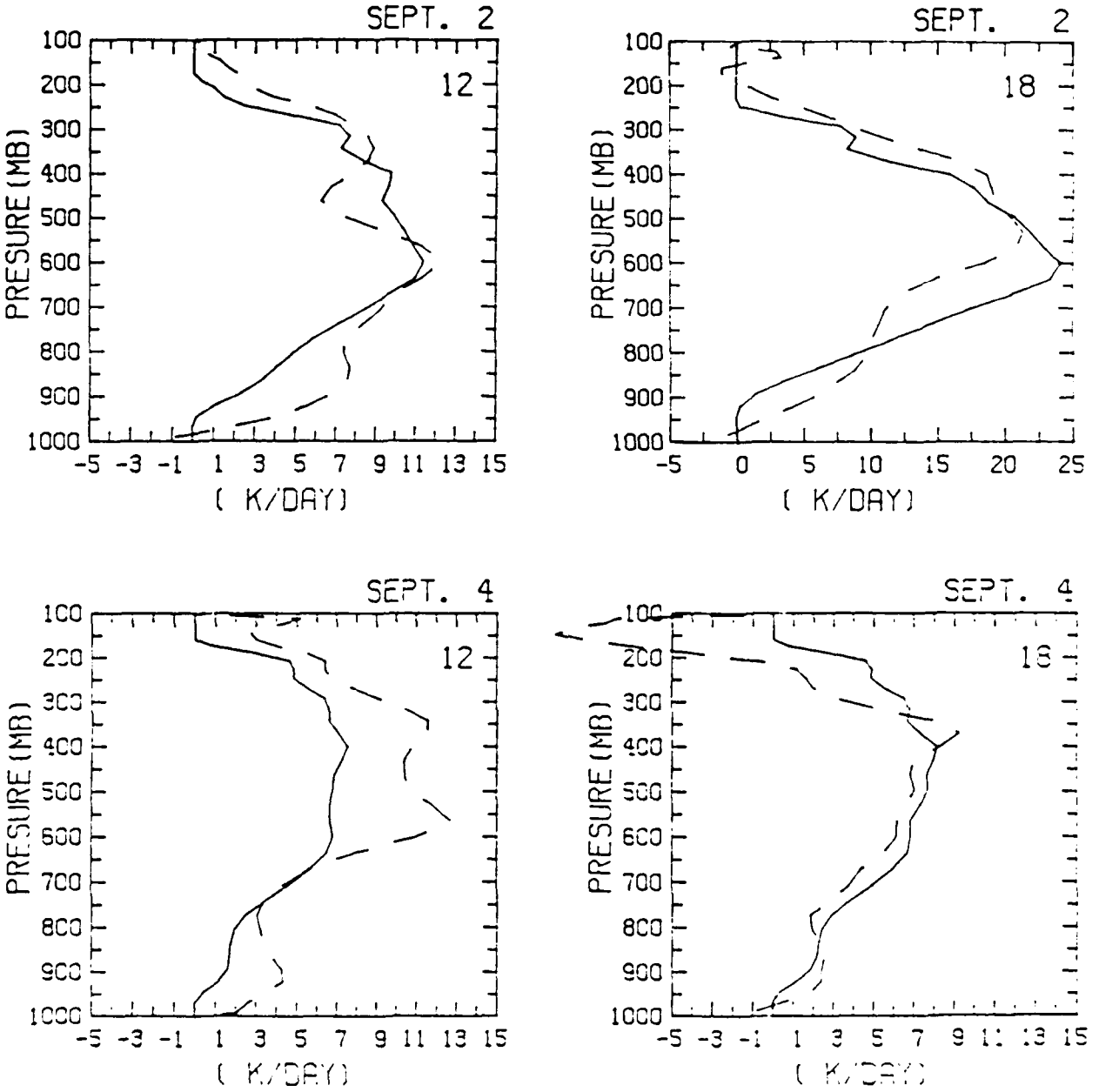

Fig. 3. The cloud heating profiles (Q_1-Q_R) on 2(12, 18GMT), 4(12, 18GMT), 5(12, 18GMT), 12(12GMT), 15(00GMT), 16(12GMT), and 17(12GMT) of September, 1974. The calculated values from the Kuo scheme are indicated by solid lines and the observed values are indicated by dashed lines.

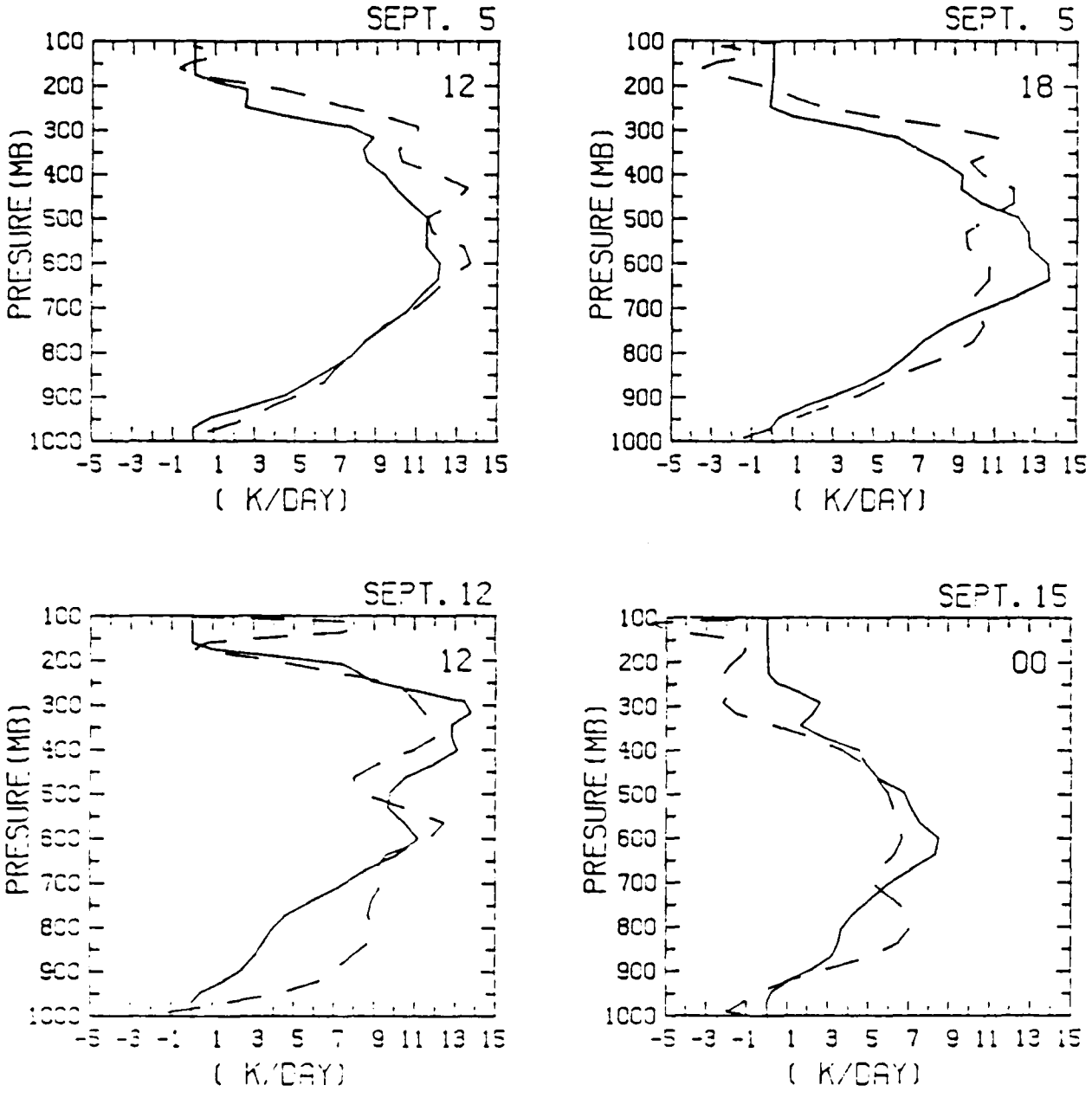

Fig. 3. (continued)

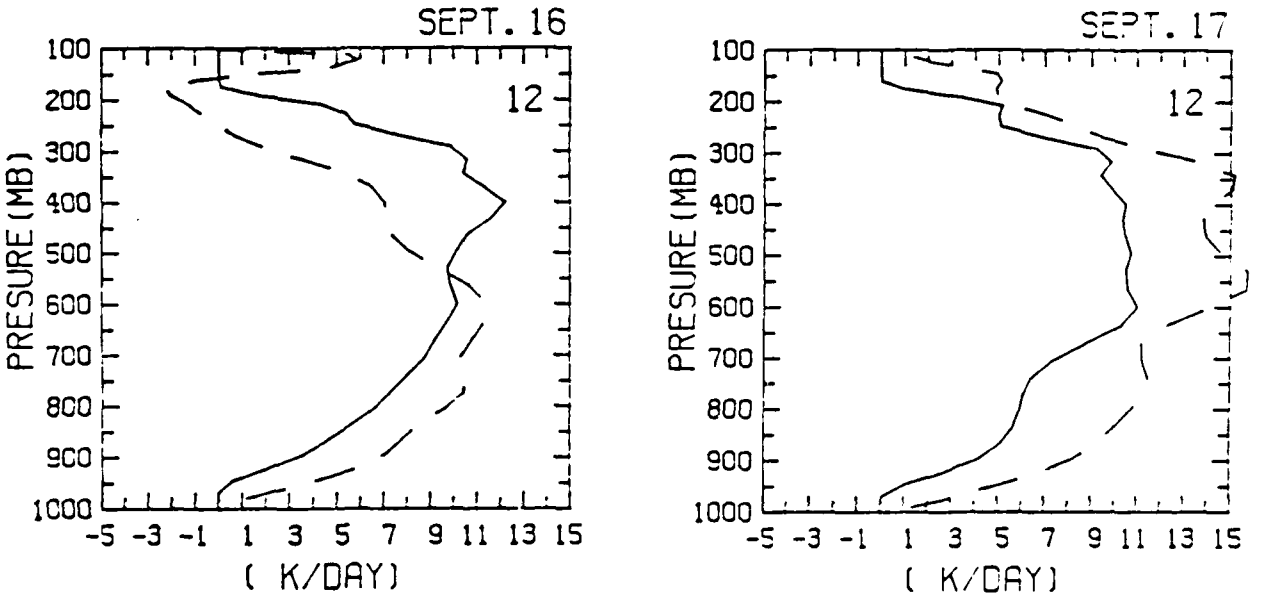

Fig. 3. (continued)

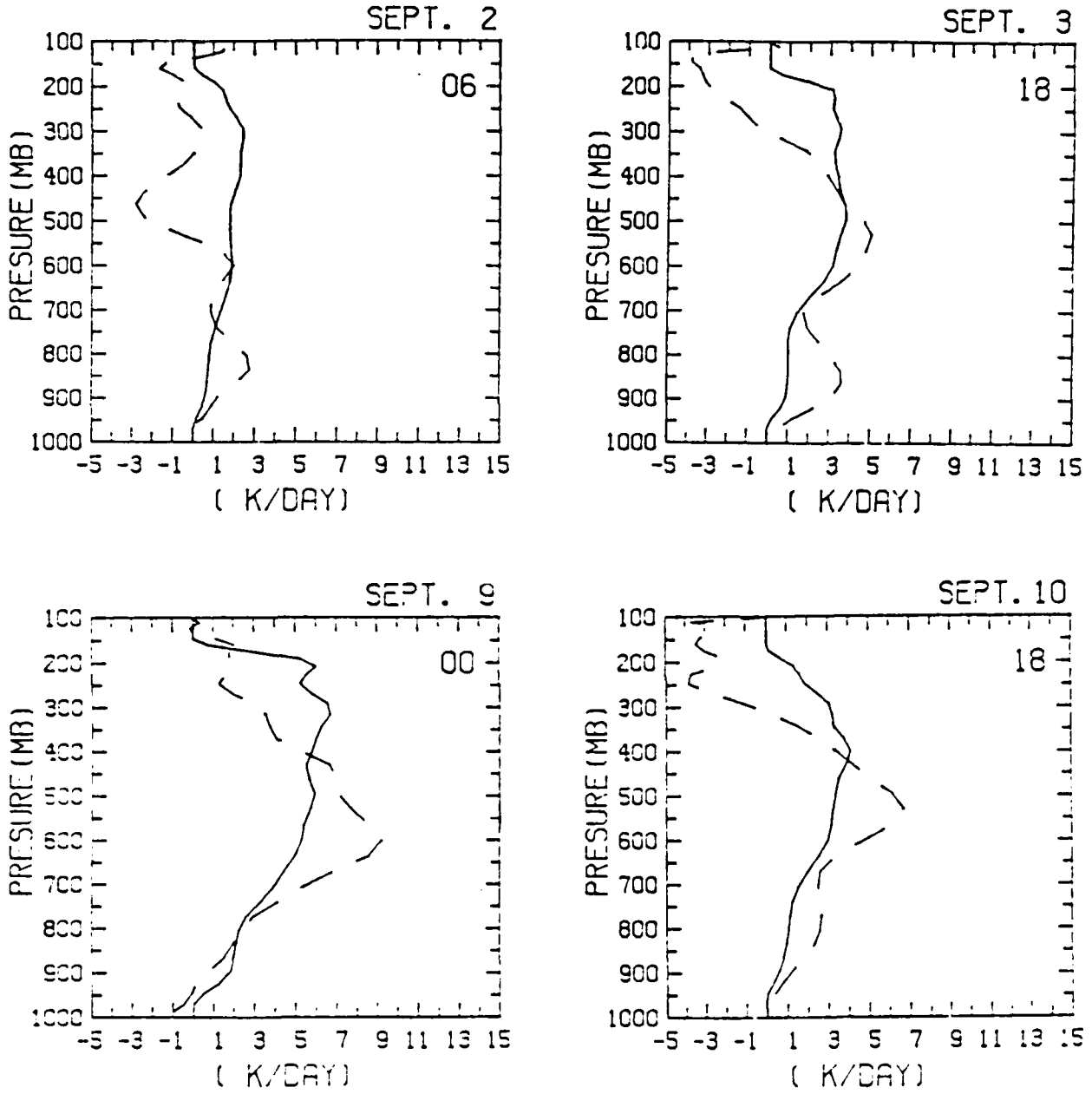

Fig. 4. As in Fig. 3 except on 2(06GMT), 3(18GMT), 9(00GMT), 10(18GMT), 11(12GMT), 12(00GMT), 13(12GMT), 14(18GMT), and 16(06, 18GMT) of September, 1974.

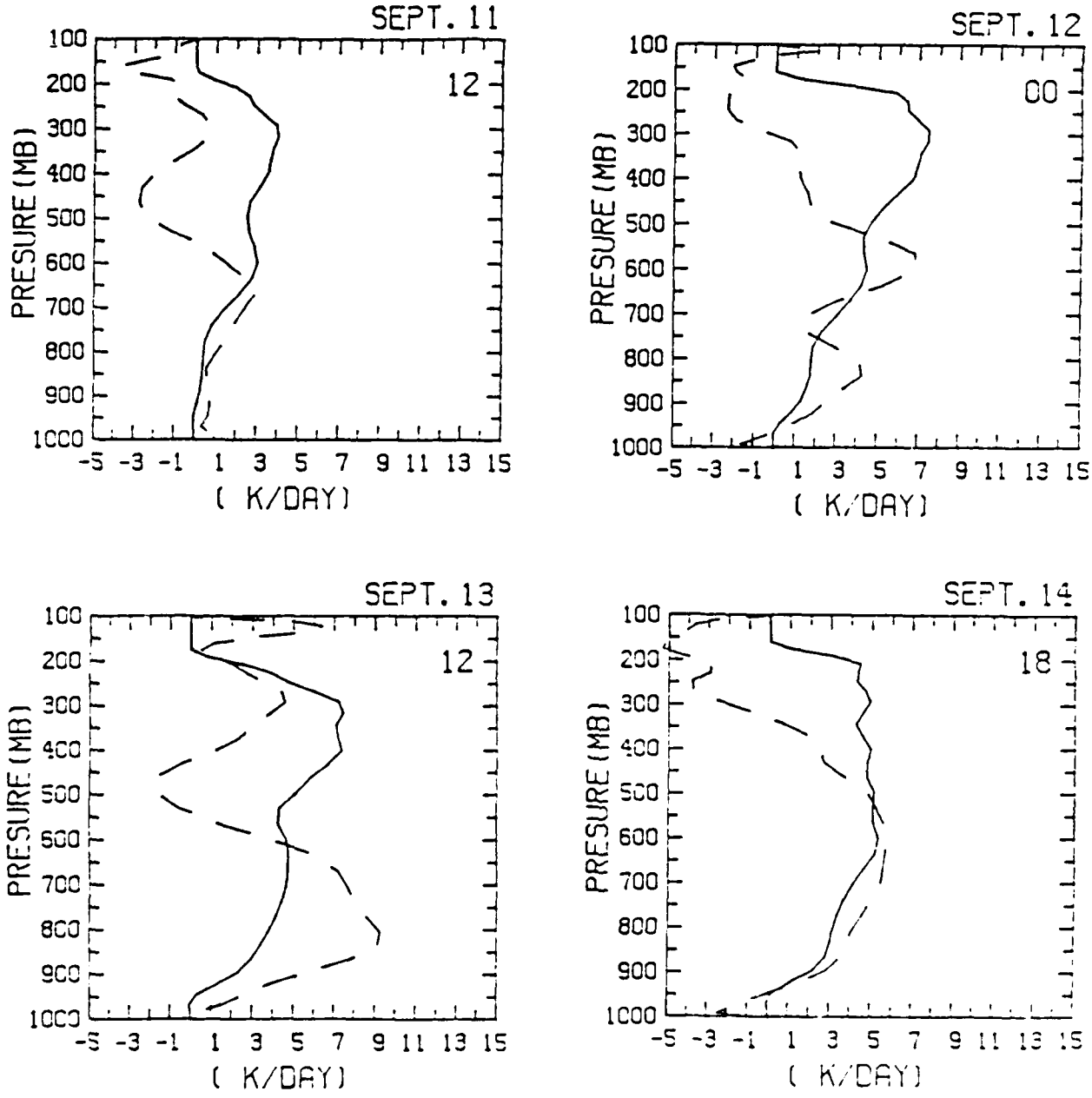

Fig. 4. (continued)

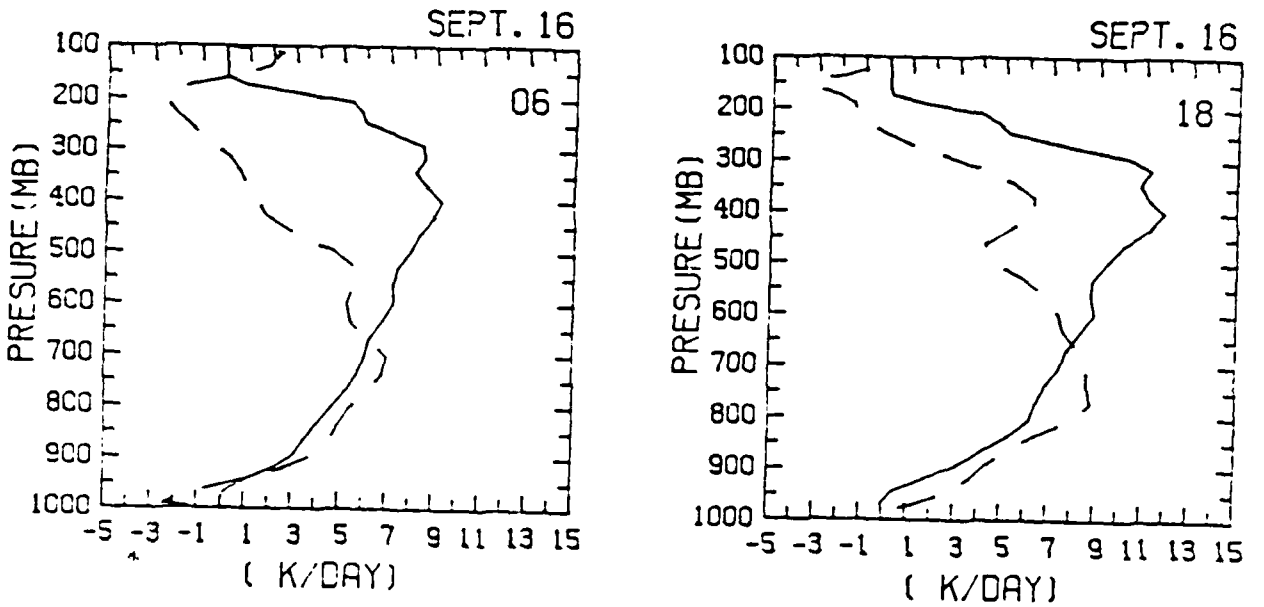

Fig. 4. (continued)

The time-averaged (for the entire GATE Phase III) vertical profiles of Q_1-Q_R are shown in Fig. 5. Again, the calculated $Q_1 - Q_R$ was overestimated above 700 mb and underestimated under 700 mb. The maximum difference between them is about 2.5°C/day.

4. Present Approach

The results from the above semiprognostic tests indicate that Kuo's scheme would produce good results during periods of deep clouds and heavy precipitation. However, it also indicates the need to include the entrainment according to convective activity in computing the cloud heating profile. The entrainment should have a minimal effect on the profiles of $T_c - T$ during strong convection; but it will significantly alter the $T_c - T$ profiles and lower the level of maximum cloud heating during weak convection, as indicated by observations.

When Kuo proposed his 1974 scheme, he actually formulated the effect of entrainment on cloud heating profiles [see (14)]. This part of his scheme has received little attention since it requires that two additional constants be specified. Otherwise, his entrainment consideration is straightforward and easy to apply. Our improvement of Kuo's scheme includes the adoption of the entrainment formulation based on Kuo's method, the details of which will be discussed later.

Other than entrainment, Kuo's 1974 scheme requires the computation of the parameter b, the fraction of moisture convergence used to moisten the atmosphere. The value of 1-b is the fraction of moisture convergence producing precipitation. Sui and Yanai (1984) found a remarkable similarity between the time variations of the percentage coverage of deep clouds with tops above the 300 mb level and the rainfall rate. The rainfall rate can

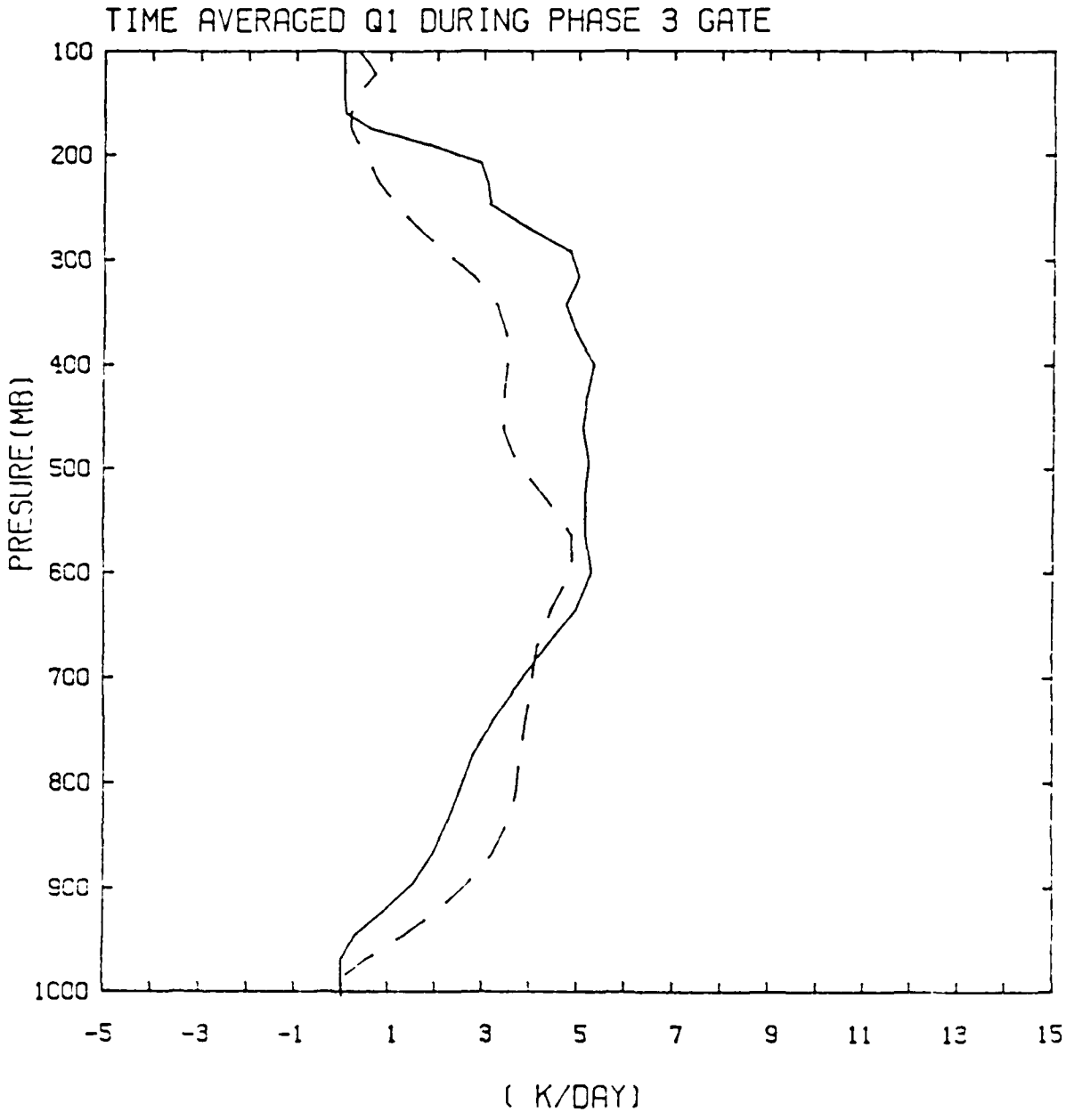

Fig. 5. Time-averaged vertical distributions of the cloud heating profiles (Q_1-Q_R). The observed values (dashed line) are compared with those calculated from the Kuo scheme (solid line).

therefore be considered proportional to the activity of deep cumulus clouds. Chao et al. (1979) also pointed out that the cloud tops were substantially higher during the disturbed period than during the undisturbed period. Song and Frank (1983) suggested "an area for future research would be to determine whether a relationship exists between the area-averaged rainfall rate and mean cloud entrainment rate which would bring profiles of $T_c - T$ and net convective heating into closer agreement". These papers indicated that (1-b) could be used as an indicator of cloud activity and the entrainment effect on the model cloud. We have used the GATE Phase III data to calculate the b value according to (28) and (33). The results indicate that the b value from these two equations are almost identical and that their values are very reasonable in comparison with precipitation observations. Therefore, (28) will be used to determine the b value.

In order to use (14), as Kuo proposed for considering the influence of entrainment, the value of α_j and γ_j has to be predetermined. At this moment, we assume that only one particular type of cumulus cloud exists at each time step. Therefore, only α_1 and γ_1 need to be determined before (14) is used. Since, according to Kuo, the value of γ_1 is most likely greater than 2, the value of γ_1 in this study is set empirically to 2.2. Because α_1 is used to determine the vertical extent of the cumulus cloud, we need to define the level of cloud top, P_T, where the cloud heating equals zero. From several tests, we found that the best equation to estimate the vertical extent of the cumulus cloud is

$$P_T = 900 \times \mathrm{EXP}\left\{-1.5(1-b)^2\right\} \tag{43}$$

For periods of strong convection (b = 0), P_T = 200 mb while for periods of extremely weak convection (b = 1), P_T = 900 mb. Once P_T is determined for the particular cumulus cloud under consideration, α_1 is computed using (14) by setting $T_c - T = 0$ at the cloud top, P_T. This computation leads to

$$\alpha_1 = \frac{T_s - T}{T(1-P_T/P_o)^{2.2}} \tag{44}$$

The $T_c - T$ profile can then be computed as:

$$T_c - T = T_s - T - [\alpha_1(1-P/P_o)^{2.2}]T \tag{45}$$

Let us consider two cases, each with the same M_t and $N_{k\theta}(p)$. In one case, the atmosphere is stable and $T_c - T$ is small. In the other case, the atmosphere is unstable and $T_c - T$ is large. From (11) and (12), the two cases should produce the same cloud heating profile, which is not realistic since the stability is not considered in the determination of the cumulus activity. Song and Frank (1983) found that the net conditional instability (CI) seldom dropped below 1°C during the convection, where CI was defined as

$$CI = \int_{P_T}^{P_b} (\theta_c - \theta) dP/(P_b - P_T) \tag{46}$$

For this reason, we set a critical CI value (CI_{cr}) as 1°C. If $CI > CI_{cr}$, there is no cloud heating. The entire procedure of this cumulus parameterization scheme is presented in Fig. 6 in flow-chart form.

$$M_t = -\frac{1}{g}\int_o^{P_s} (\nabla\cdot\vec{V}\, q)dP + \rho_o c_D V_o (q_g - q_o)$$

$$I = -\frac{1}{g}\int_{P_t}^{P_b} \omega \frac{\partial q}{\partial P}\, dP$$

$$A = -\frac{1}{g}\int_{P_t}^{P_b} \frac{c_p}{L}\frac{T}{\theta}\,\omega\frac{\partial\theta}{\partial P}\, dP$$

$$b = \frac{A+I}{2I}$$

↓

$$P_T = 900 \times \mathrm{EXP}\left\{-1.5(1-b)^2\right\}$$

↓

$$\alpha_1 = T_s - T \,/\left[T(1-P_T/P_o)^{2.2}\right]$$

↓

$$T_c - T = T_s - T - T\left[\alpha_1(1-P/P_o)^{2.2}\right] = 0$$

↓

$$CI = \int_{P_T}^{P_b} (\theta_c - \theta)dP/(P_b - P_T)$$

→ $\leq 1.0°C$ $\quad aQ_c = 0$

$\quad \frac{\partial q}{\partial t}^{+} = 0$

↓ $> 1.0°C$

$$aQ_c = \frac{L}{c_p \pi}\,\frac{g(1-b)M_t}{(P_b - P_T)}\,\frac{(\theta_c-\theta)}{\langle\theta_c-\theta\rangle}$$

$$\frac{\partial q}{\partial t} = \frac{gbM_t}{(P_b-P_t)}\,\frac{(q_c-q)}{\langle q_c - q\rangle}$$

Fig. 6. Present Scheme

5. Semiprognostic Test of the Present Scheme

Using the present cumulus parameterization scheme, we again calculated $Q_1 - Q_R$ profiles for the entire GATE Phase III period. During periods of strong convection, the results are no different than the previous computation. This can be expected since the entrainment effect is small for deep convection. Fig. 7 shows the cloud heating profiles using the present scheme and observed $Q_1 - Q_R$ during selected periods of moderate to weak convection, as in the last section. We can see a significant improvement compared to Fig. 4. The level of maximum heating has shifted from the upper troposphere to a lower level. The cloud tops vary with convective activity and can be as low as 500 mb. In general, the calculated maximum heating in the present scheme is about the same as in the observations.

Fig. 8 shows the pressure-time sections of the calculated $Q_1 - Q_R$ fi ld for September 1-18, 1974 in the GATE Phase III period. A comparison of Fig. 8 with Fig. 1 shows the following features: on 6 September the maximum heating has increased to 6°C/day and was around 575 mb; on 12 September the maximum heating shifted from above 400 mb to below 500 mb; and on 16-17 September the maximum heating was around 500 mb instead of 400 mb, as in Fig. 1. A comparison of Fig. 8 with Fig. 2 shows that the results from the present scheme agree well with the observations. Overall, the heating distribution from the present scheme is quite impressive.

Figs. 9 and 10 show the pressure-time sections of the calculated and observed apparent moisture sink Q_2 field. The observed field of Q_2 exhibits large drying ($Q_2 > 0$) on the following dates, 2, 4, 5, 12, 13, 14, 16, and 17. The maximum intensity of this drying occurs around and below 700 mb.

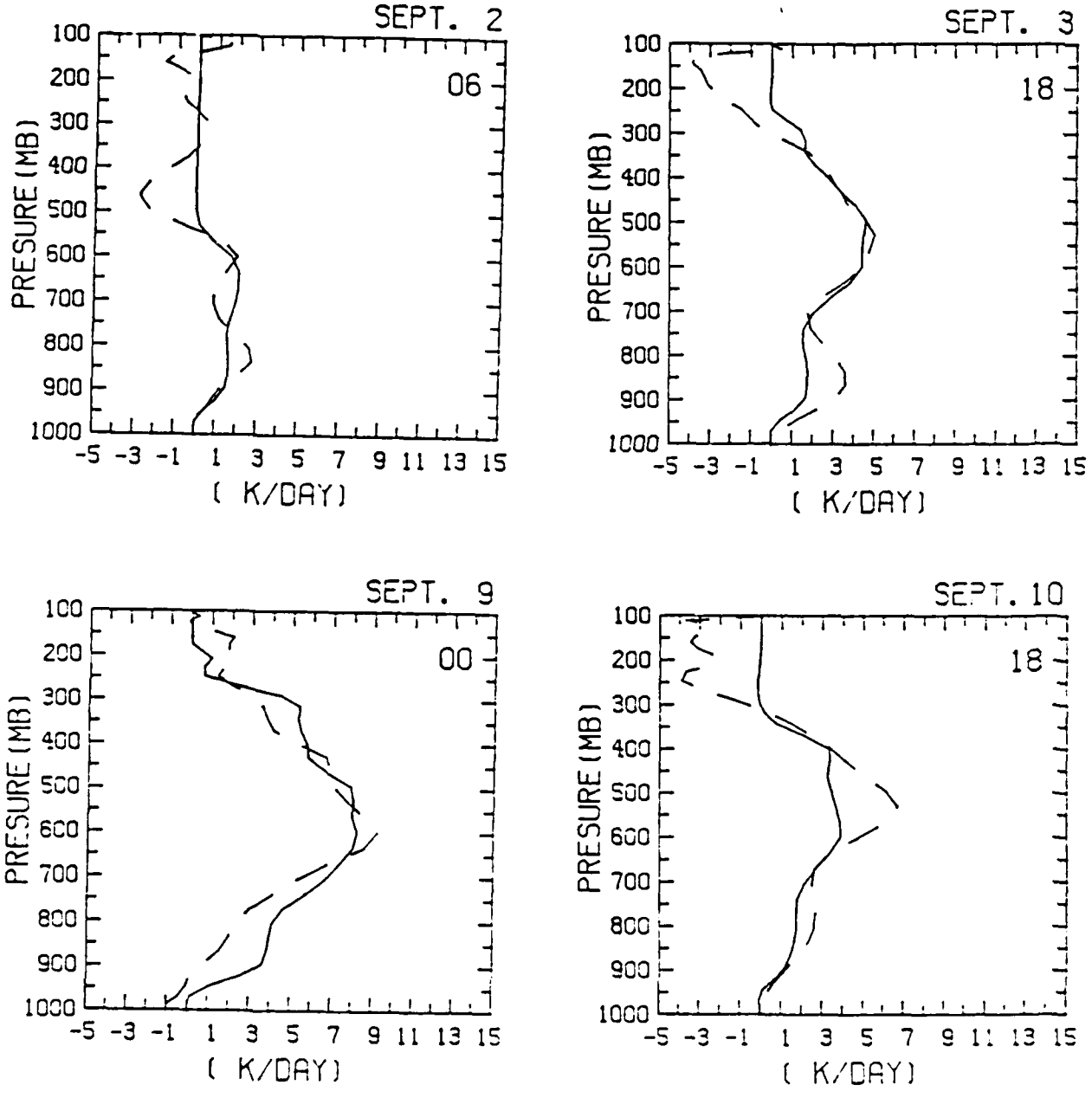

Fig. 7. As in Fig. 4 except for the present scheme.

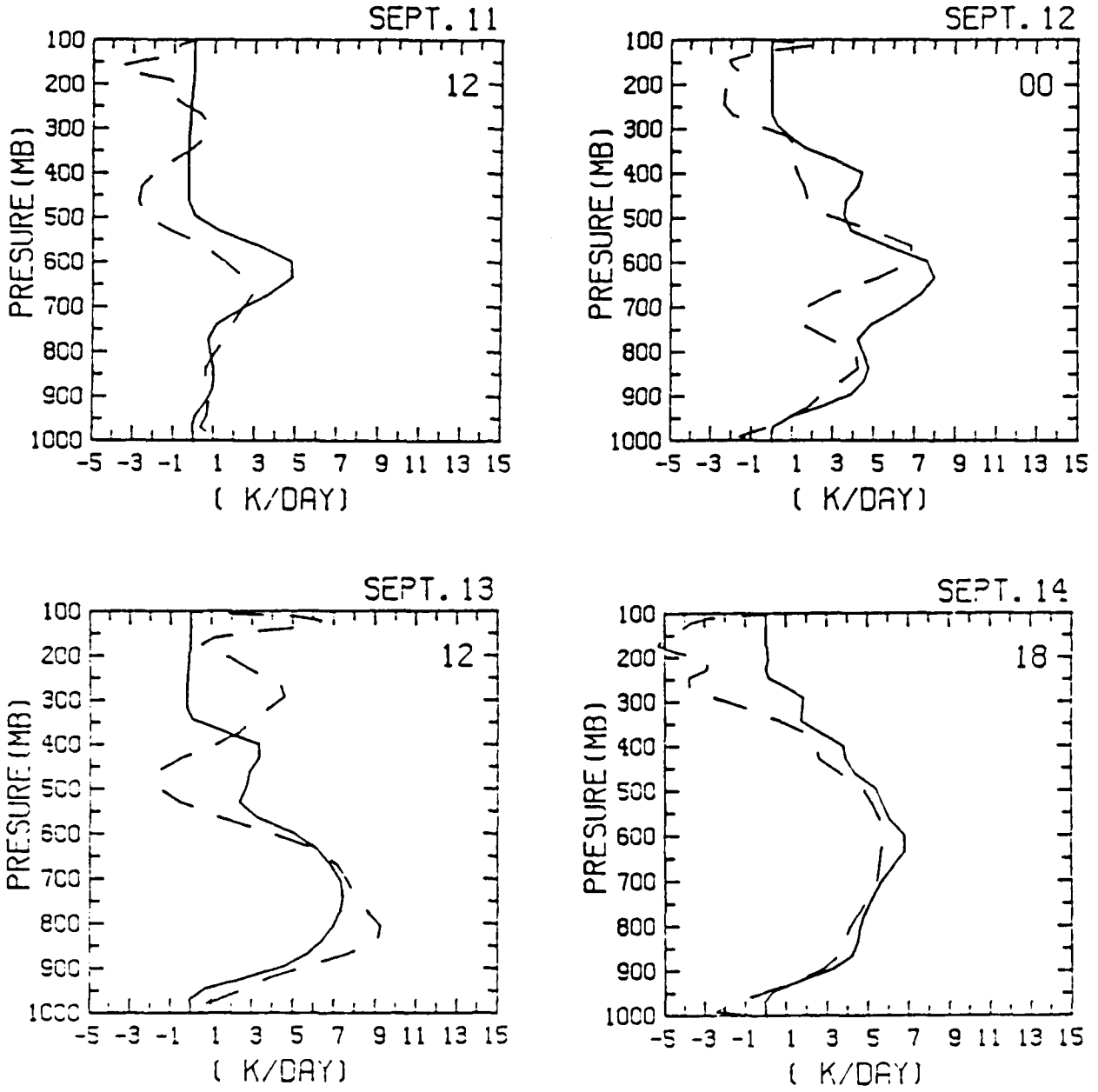

Fig. 7. (continued)

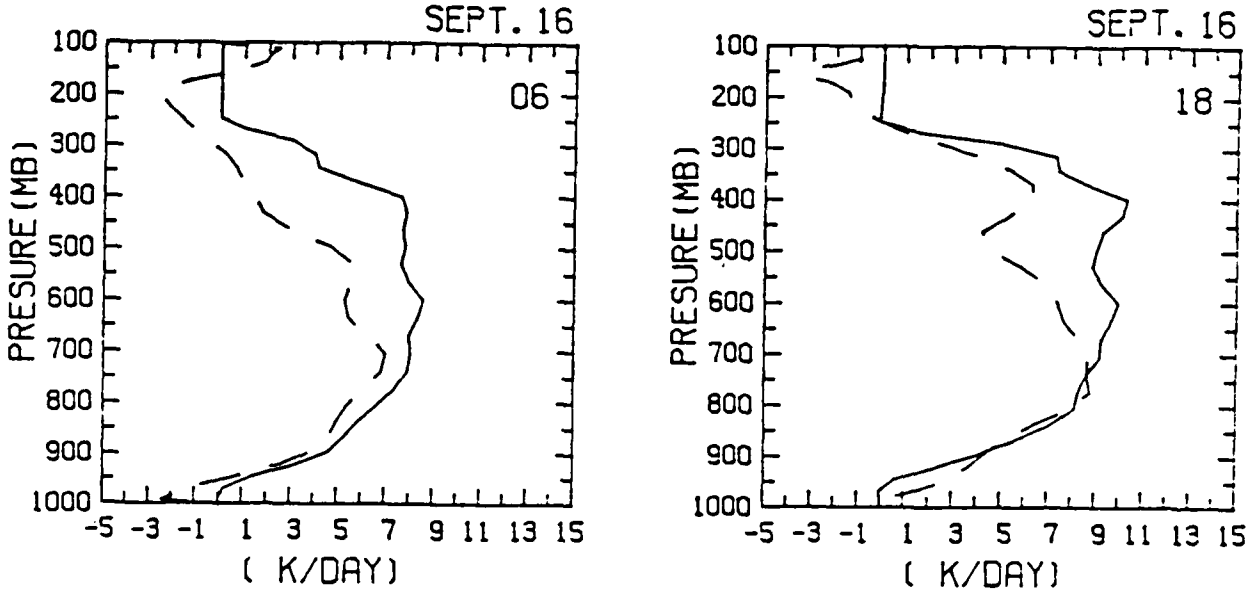

Fig. 7. (continued)

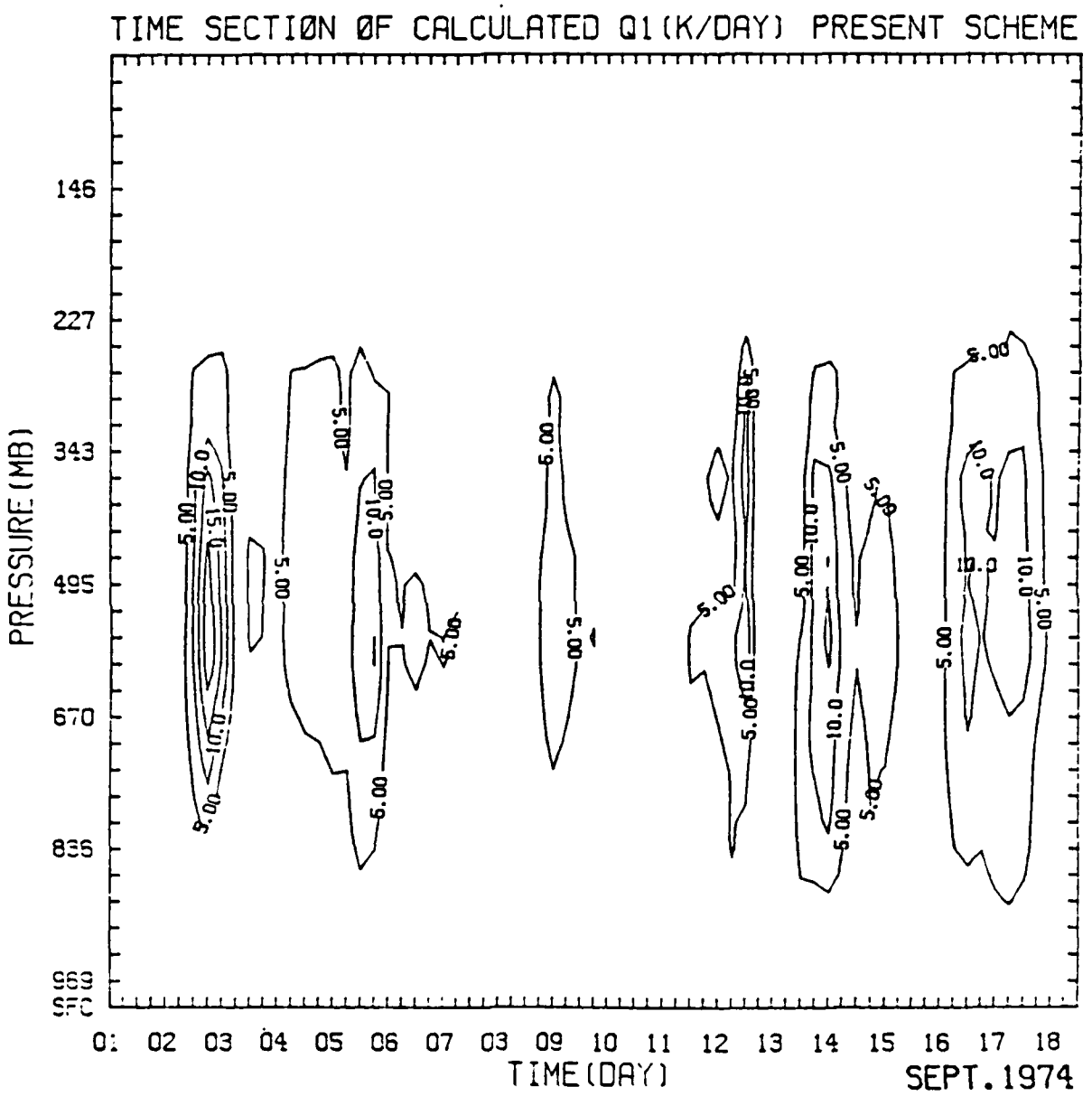

Fig. 8. As in Fig. 1 except for the present scheme.

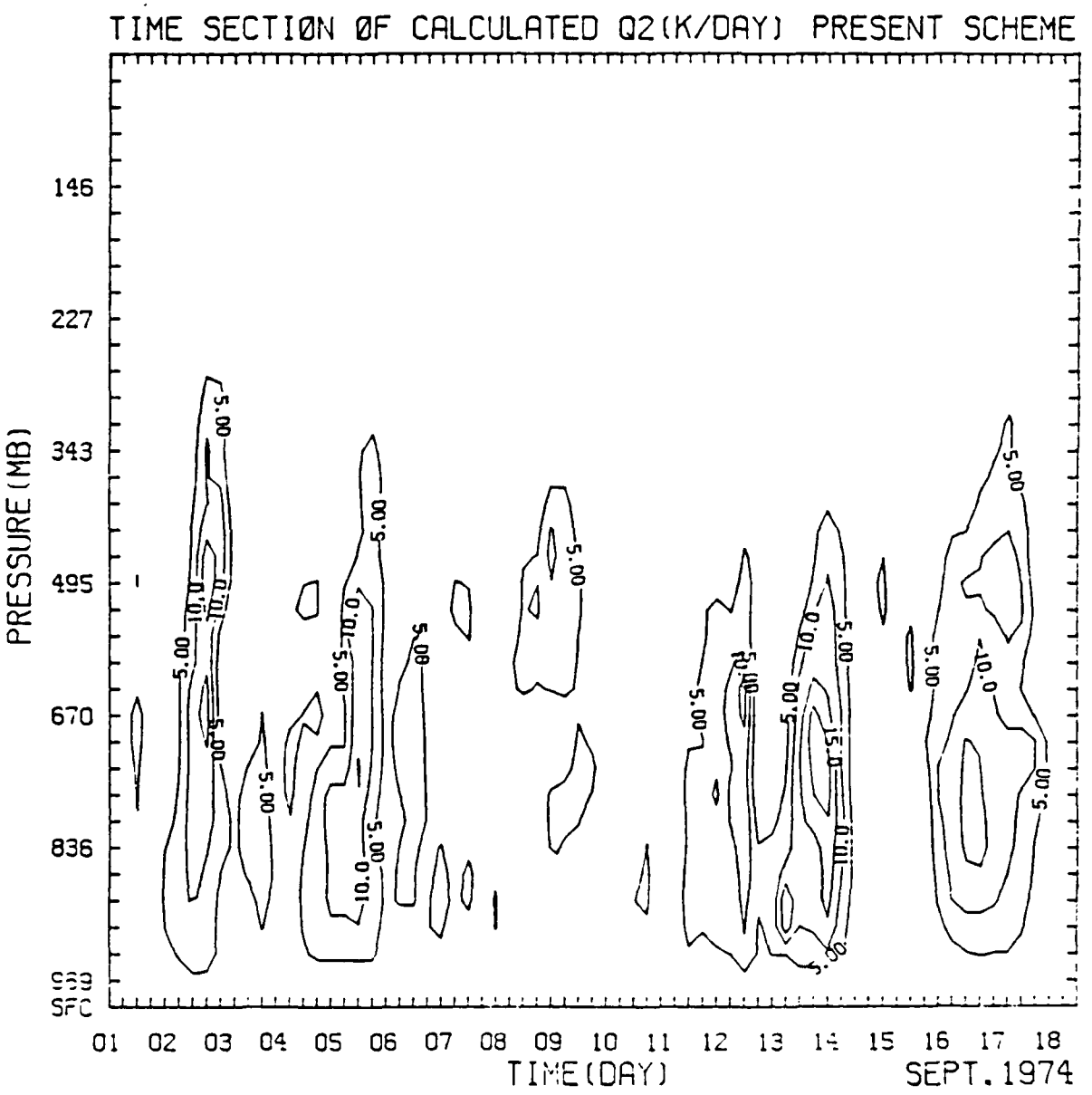

Fig. 9. Vertical cross section of the calculated cloud drying effect (Q_2) for the present scheme.

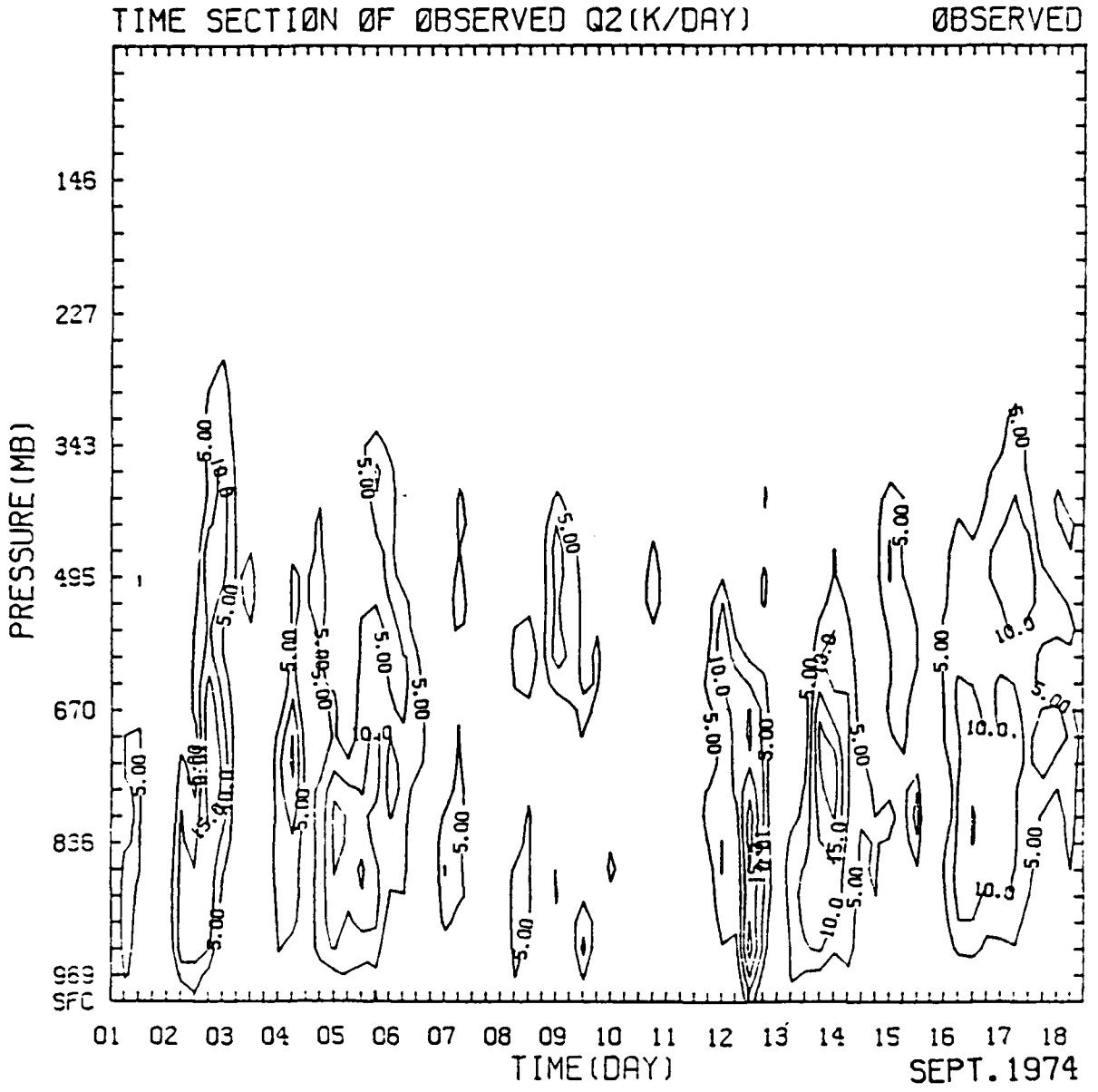

Fig. 10. As in Fig. 9 except for the observed values.

Occasionally, it extends to very high levels. The periods of strong drying usually coincide with the periods of strong cloud heating. In general, the present scheme essentially captures all of the observed features of Q_2.

The time averaged vertical profiles of calculated $Q_1 - Q_R$ and Q_2 are very similar to the observed profiles (see Figs. 11 and 12). The maximum heating level is around 600 mb in both profiles, with the maximum difference between them being less than 1.1°C/day. The calculated Q_2 profile is almost coincident with the observed profile. For a comparison, Fig. 13 shows the same vertical profiles of $Q_1 - Q_R$ and Q_2 as calculated by Krishnamurti et al. (1983).

Fig. 14 is a time series of rainfall rates (mm/day) from 1-18 September 1974 as estimated by the present scheme, as well as those from the moisture budget and the radar measurements. The estimated rainfall from the moisture budget R_{bu} is calculated from:

$$R_{bu} = \int_0^{P_s} \frac{c_p Q_2}{L} \frac{dP}{g} + E_g \tag{47}$$

where E_g is the estimated surface evaporation rate calculated using the bulk aerodynamic formula:

$$E_g = \rho_o C_D V_o (q_g - q_o) \tag{48}$$

where q_g is the surface mixing ratio calculated based on the sea surface temperature given by Wuchnitz et al. (1977). The calculated rainfall rate agrees closely with the two independent estimates from the moisture budget and from radar measurements. The peak calculated rainfall values on 2, 14, and 16 September are almost identical to the observed values. There are some

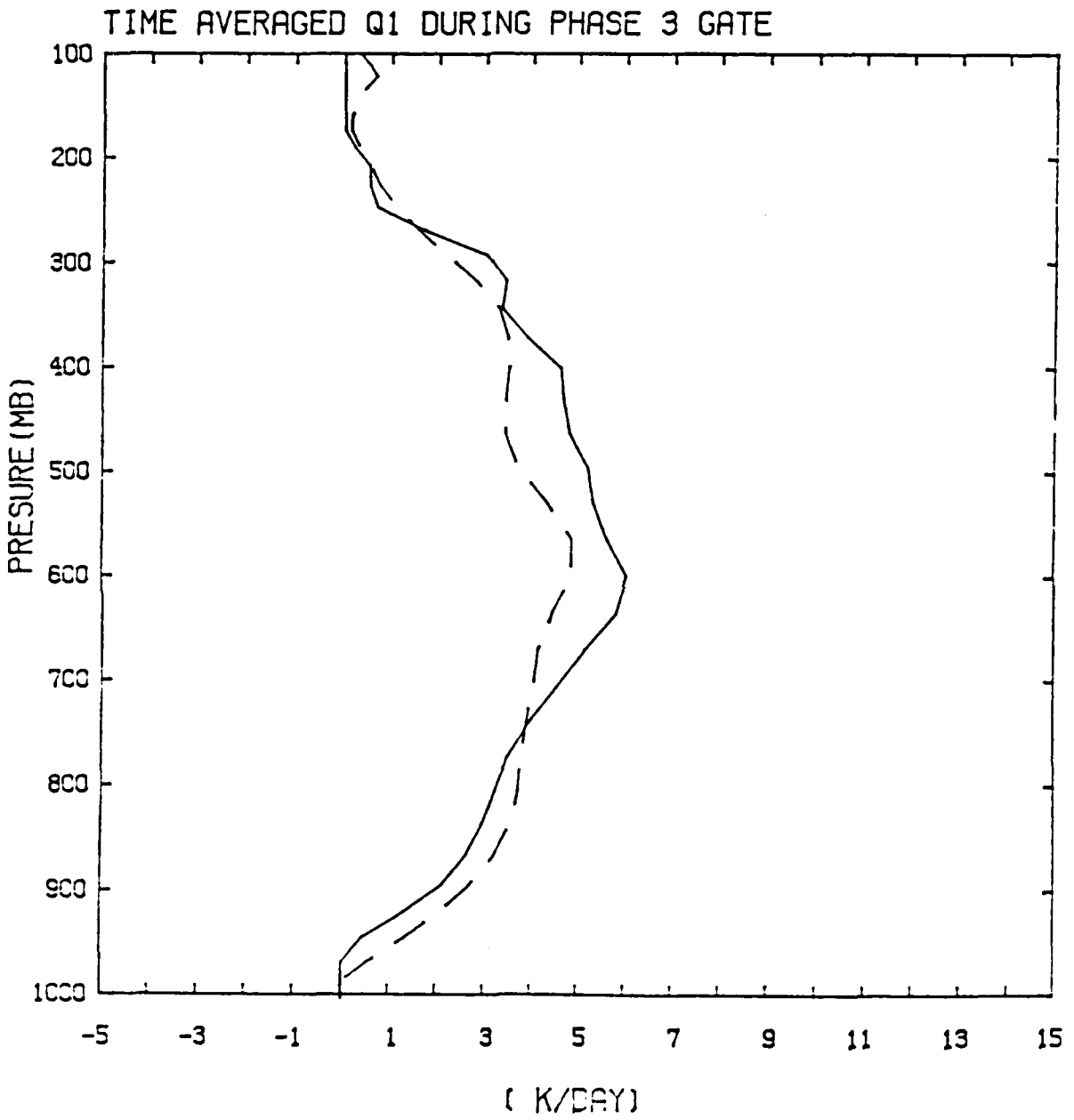

Fig. 11. Time-averaged vertical distribution of the cloud heating profiles (Q_1-Q_R). The observed value (dashed line) is compared with those calculated from the present scheme (solid line).

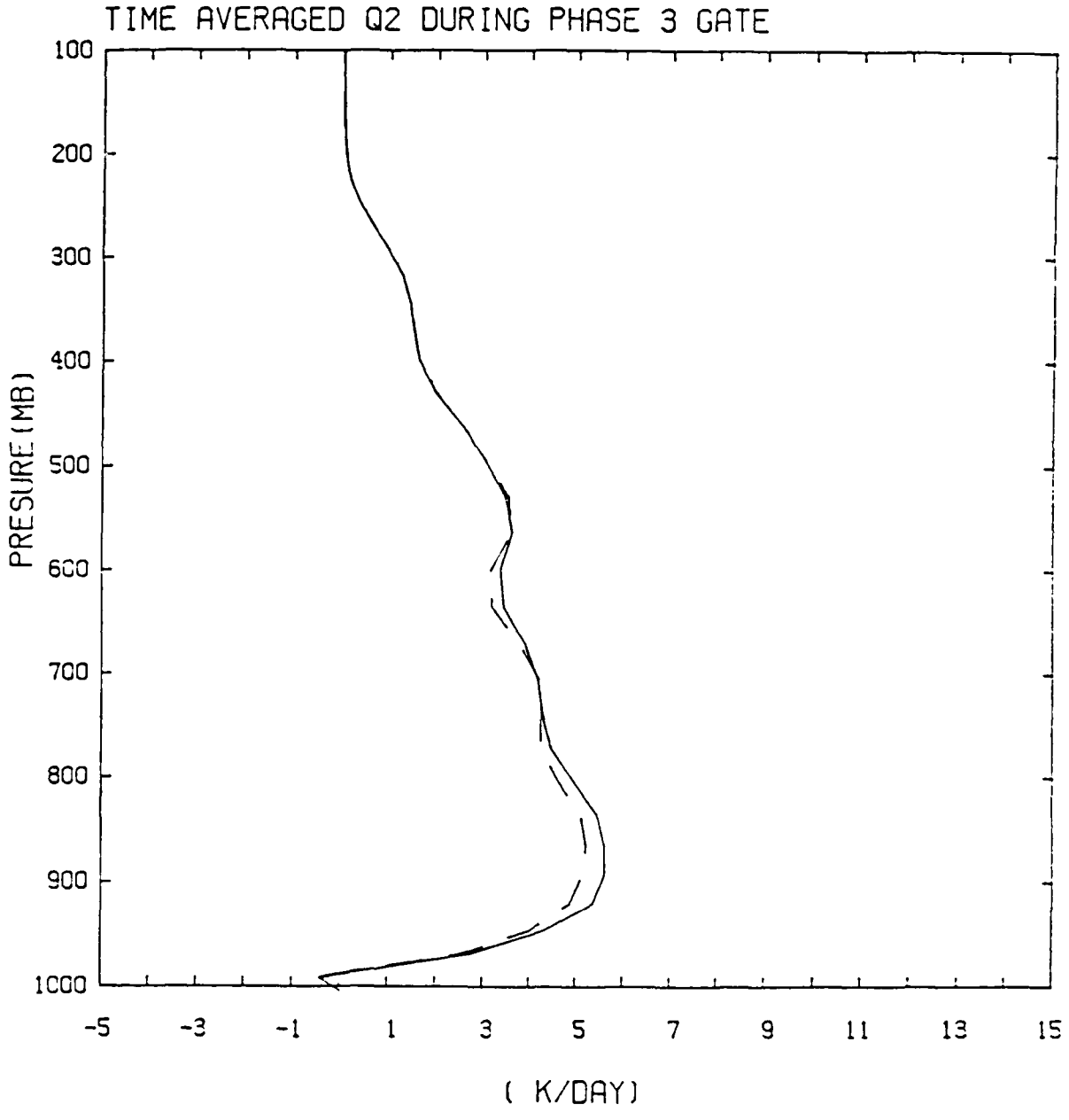

Fig. 12. Time-averaged vertical distribution of the cloud drying profiles (Q_2). The observed valued (dashed line) is compared with those calculated from the present scheme (solid line).

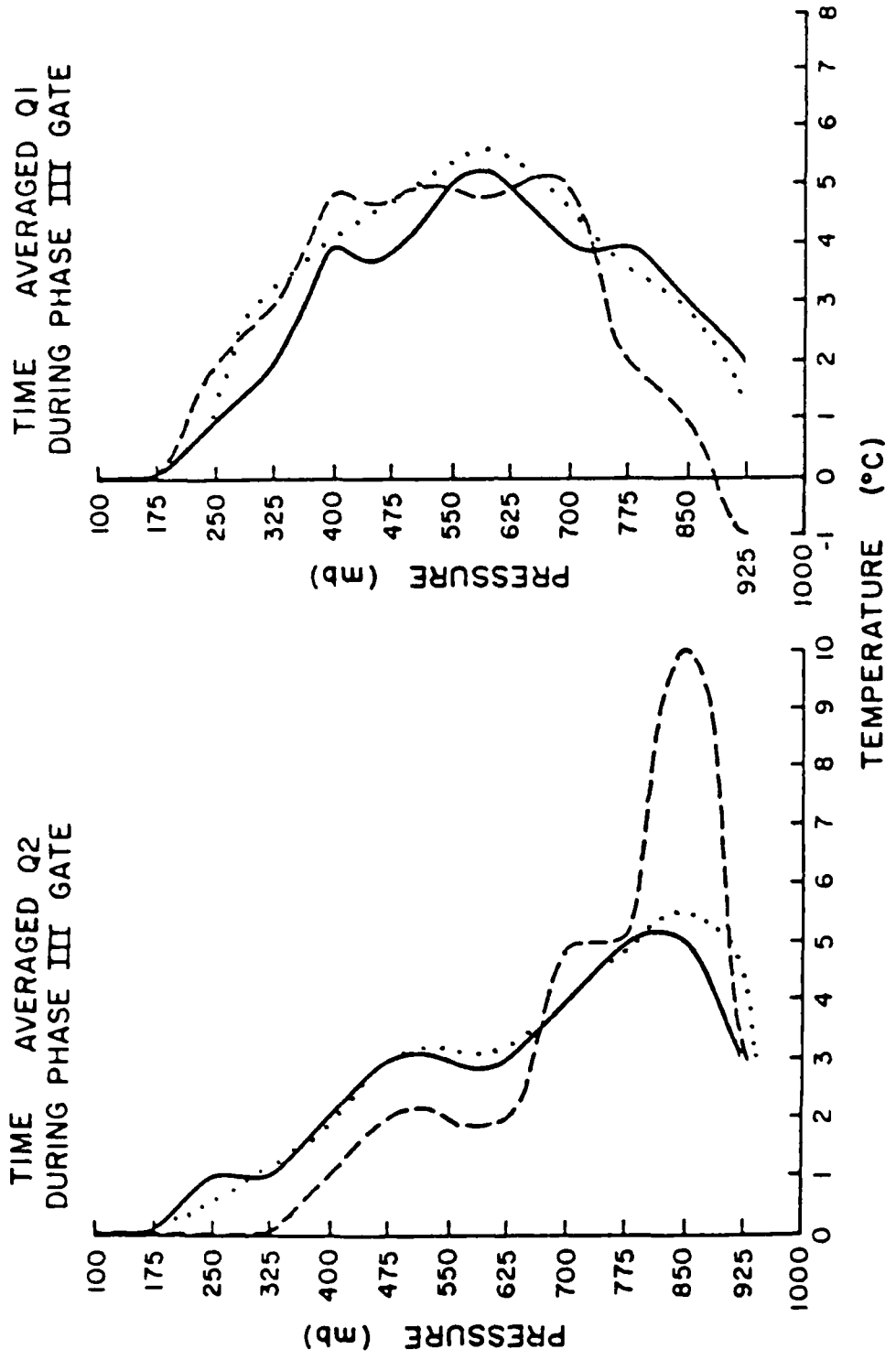

Fig. 13. Time-averaged vertical distributions of cloud drying profiles (Q_2) and cloud heating profiles (Q_1-Q_R). (Adopted from Krishnamurti et al., 1983. Solid lines are from observation, dashed lines are calculated by Krishnamurti et al. (1983), and dotted lines are calculated from the present scheme.)

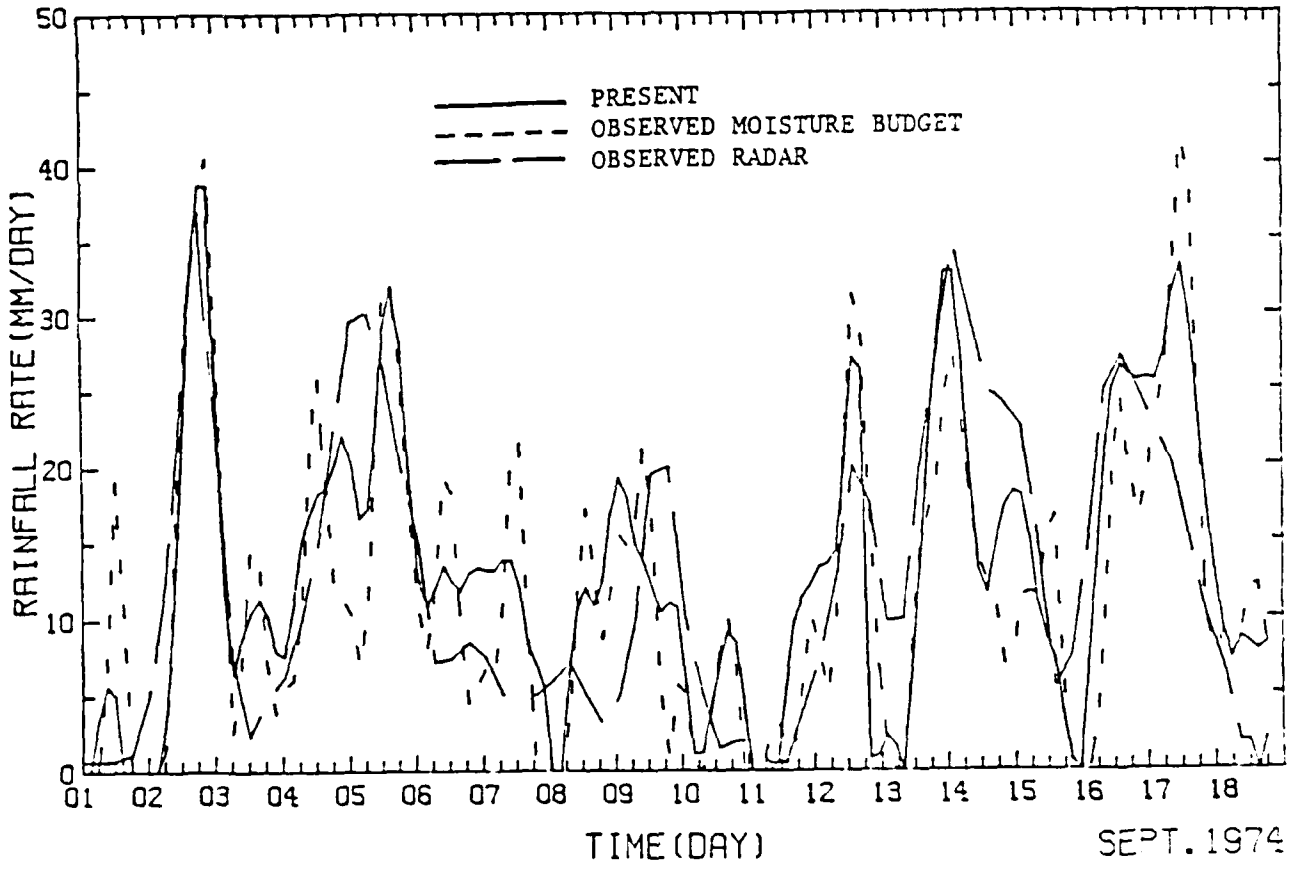

Fig. 14. A time series of rainfall rates from 1-18 September estimated by the present scheme, the moisture budget and the radar measurements.

differences in the time of maximum calculated rainfall rate and the observed maximum by the radar during the periods of 5-6 and 9-10 September. No conclusive explanation can be made with the limited amount of data.

In order to examine the general behavior of the present scheme in various conditions in the tropics, the composite easterly wave data in Phase III were also used in this semiprognostic study. The observed Q_1 values were provided by Dr. Chen of the University of Hawaii. Fig. 15 shows the calculated and observed $Q_1 - Q_R$ fields for the composite wave in the GATE B-scale area at latitude 8.5°N. The waves are separated into 8 categories with category 4 representing the trough area and category 8 representing the ridge area. We can see that the level of the maximum heating rate varies with the wave category. The comparisons between observed and calculated $Q_1 - Q_R$ curves are reasonably good.

6. An Evaluation of Kuo's Cumulus Parameterization Scheme Using a Two-Dimensional Cloud Cluster Model

As stated previously, it is necessary for a good cumulus parameterization scheme to produce cloud heating and drying effects and precipitation rates in agreement with diagnostic results in a semiprognostic test. However, this agreement does not imply that these schemes will have prognostic value. This point is clear since a 'scheme' requiring no change in the large-scale temperature and moisture fields will give good verification in the semi-prognostic approach but cannot be used in a large-scale prediction model.

In this step of the work, a cloud cluster model will be used to evaluate the cumulus parameterization scheme in a fully prognostic sense. The cloud cluster model with a fine grid has been used to simulate the development of clouds and a cloud cluster under a weak low-level lifting condition

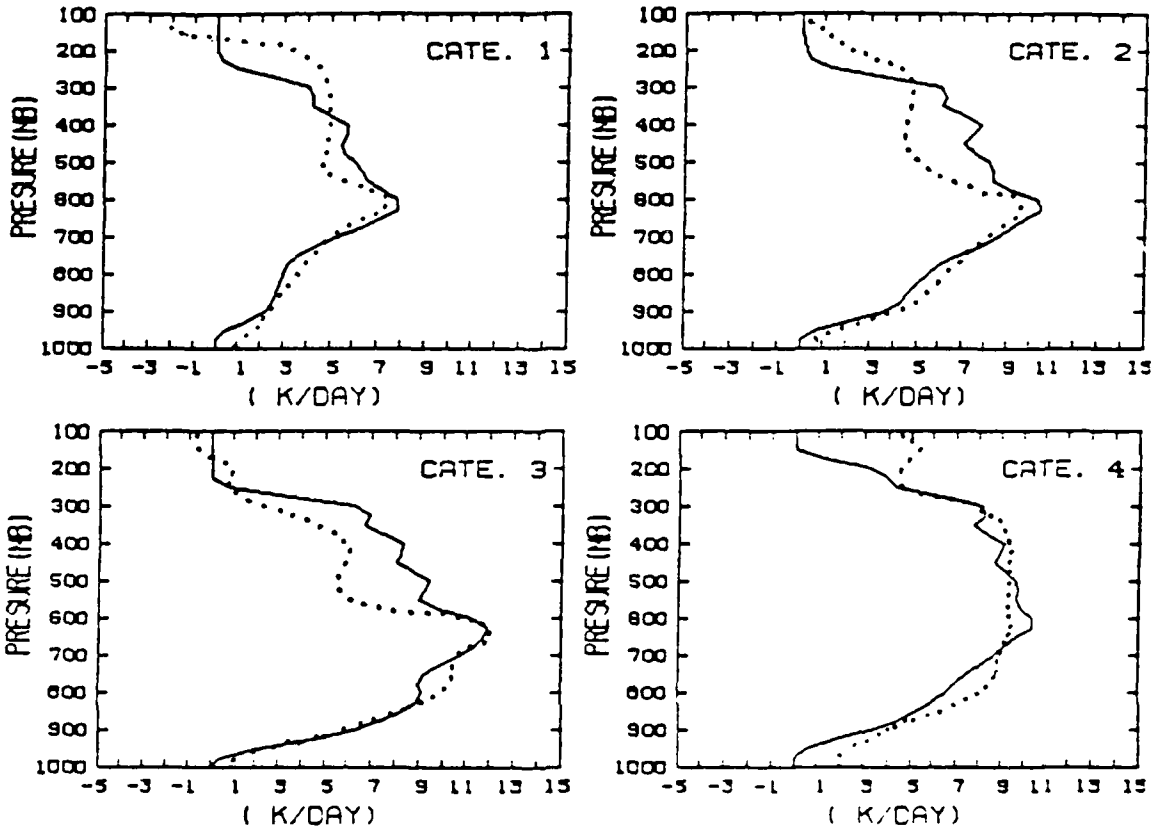

Fig. 15. The vertical distributions of the cloud heating profiles (Q_1-Q_R) for the composite waves during GATE Phase III period. The calculated values are indicated by solid lines and the observed values are indicated by dashed lines.

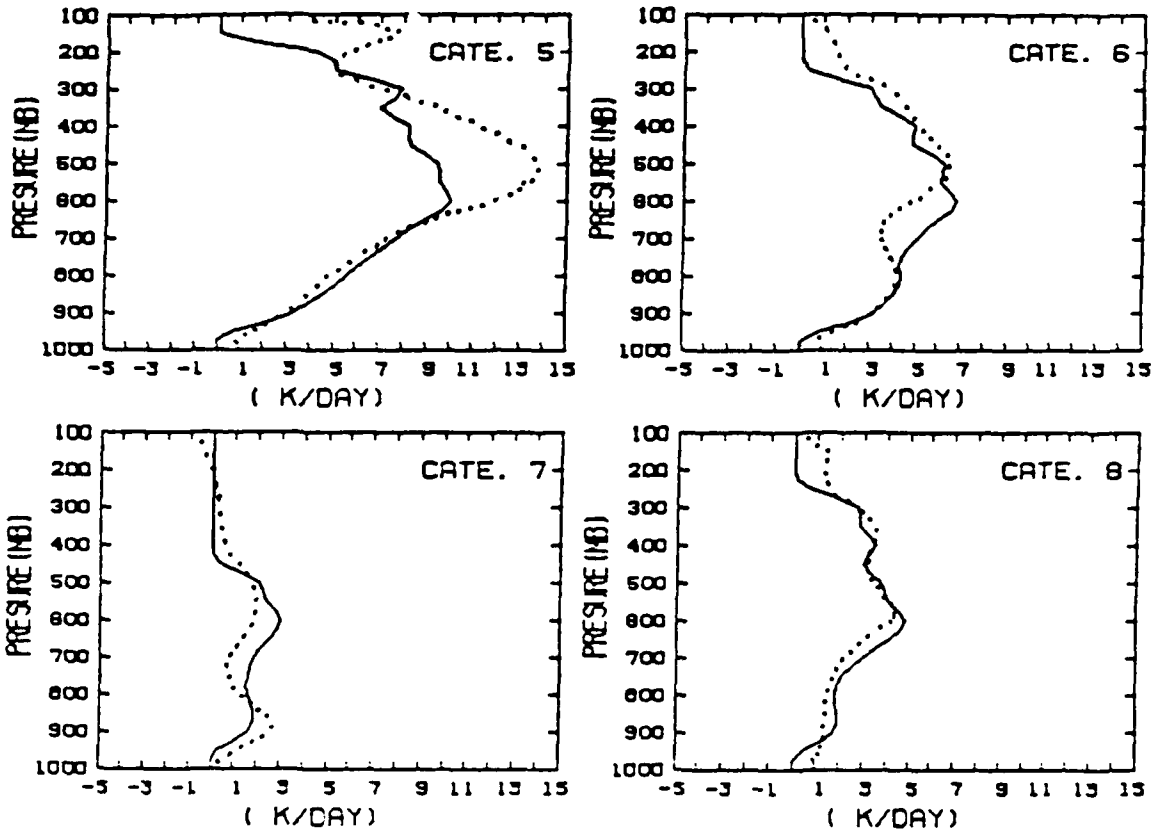

Fig. 15. (continued)

in the GATE environment (Soong and Ogura, 1982). The model also provides the cloud heating and drying effects in the cloud cluster region as well as the large-scale lifting generated by the cloud effects at each integration time step. This model is modified to use a coarse grid and the hydrostatic system of equations. The cloud dynamics and physical processes are eliminated and the present scheme of cumulus parameterization is incorporated under the same weak low-level lifting condition.

6.1. Model equations

The momentum equations of this two-dimensional hydrostatic cloud cluster model in the x-z slab symmetric domain are:

$$\frac{\partial u}{\partial t} = - u \frac{\partial u}{\partial x} - w \frac{\partial u}{\partial z} + fv - c_p \theta \frac{\partial \pi}{\partial x} \tag{49}$$

$$\frac{\partial v}{\partial t} = - u \frac{\partial v}{\partial x} - w \frac{\partial v}{\partial z} - f(u-u_g) \tag{50}$$

where θ is the potential temperature, f is the Coriolis parameter, u_g is the x-component geostrophic wind, and π is the nondimensional pressure, which is defined as:

$$\pi = (P/P_o)^{R/C_p} \tag{51}$$

where P is pressure, P_o is the reference pressure of 1000 mb, R is the gas constant of dry air and C_p is the specific heat of dry air at constant pressure.

The hydrostatic equation is:

$$C_p \theta_v \frac{\partial \pi}{\partial z} = - g \tag{52}$$

where g is gravity and θ_v is the virtual potential temperature defined by

$$\theta_v = \theta(1 + 0.61q) \tag{53}$$

The thermodynamic and moisture equations are:

$$\frac{\partial \theta}{\partial t} = - u \frac{\partial \theta}{\partial x} - w \frac{\partial \theta}{\partial z} + Q_c \tag{54}$$

and

$$\frac{\partial q}{\partial t} = - u \frac{\partial q}{\partial x} - w \frac{\partial q}{\partial z} + P_r \tag{55}$$

where Q_c is the adiabatic heating rate due to clouds and P_r is the production rate of water vapor due to clouds. The radiation effects are neglected in the thermodynamic equation.

The mass continuity equation is expressed in the anelastic form:

$$\frac{\partial u}{\partial x} + \frac{1}{\rho} \frac{\partial \rho w}{\partial z} = 0 , \tag{56}$$

where ρ is the density and is a function of height only.

Now consider a variable A(A = π, θ, or q) separated into the horizontal mean and the departure as:

$$A(x,z,t) = \overline{A}(z,t) + A'(x,z,t) . \tag{57}$$

The horizontal average variables represent the large-scale conditions and are functions of time and height only. The primed variables define the cloud-scale system. Substituting (57) into (49), (50), (52), (54), and (55) with the use of (56), one can obtain a set of governing equations in flux form as follows:

$$\frac{\partial u}{\partial t} = - \frac{\partial}{\partial x} u^2 - \frac{1}{\rho} \frac{1}{\partial z} (\rho uw) + fv - c_p \overline{\theta} \frac{\partial \pi'}{\partial x} \tag{58}$$

$$\frac{\partial v}{\partial t} = - \frac{\partial uv}{\partial x} - \frac{1}{\rho} \frac{\partial}{\partial z} (\rho vw) - f(u-u_g) \tag{59}$$

$$c_p \overline{\theta}_v \frac{\partial \pi'}{\partial z} = g \left(\frac{\theta'}{\overline{\theta}} + 0.61 q' \right) \tag{60}$$

$$\frac{\partial \theta}{\partial t} = - \frac{\partial}{\partial x} (u\theta') - \frac{1}{\rho} \frac{\partial}{\partial z} (\rho w\theta') - (w_o + w) \frac{\partial \overline{\theta}}{\partial z} + Q_c \tag{61}$$

$$\frac{\partial q}{\partial t} = - \frac{\partial}{\partial x} (uq') - \frac{1}{\rho} \frac{\partial}{\partial z} (\rho wq') - (w_o + w) \frac{\partial \overline{q}}{\partial z} + R_r \tag{62}$$

In deriving (60) it was assumed that the horizontal means satisfy the hydrostatic relation:

$$c_p \overline{\theta}_v \frac{\partial \overline{\pi}}{\partial z} = - g \tag{63}$$

and θ_v was approximated by $\overline{\theta}_v$. In the derivation of (58), the θ in front of the pressure gradient term was approximated by $\overline{\theta}$. The variable w_o is the large-scale low-level lifting imposed on the model based on observation. As discussed by Ogura et al. (1979) and Soong and Tao (1980), large-scale low-level lifting usually preceeds the development of deep clouds. It will destabilize the atmosphere and provide the moisture supply for clouds.

6.2. Numerical technique, boundary and initial conditions

As shown in Fig. 16, this model has a horizontal domain of 1280 km, with 600 km of grids at the center part of the domain (cloud cluster area). On each side of the cloud cluster area, there is an environment area. The horizontal domain has 64 uniform gridpoints with a grid distance equal to 20 km. It has 16 grid intervals in the vertical with an even grid spacing of 900 m such that the top of the domain is at the level of 14.4 km, which is around 140 mb in the P-coordinate.

A staggered grid arrangement [the same one used by Soong and Ogura (1973)], shown in Fig. 17, is used in this model. A leapfrog time integration and a second-order-centered space difference scheme is applied with a time step of 60 s. A time-smoothing scheme formulated by Robert (1966) is adopted in the integration with a smoothing coefficient of 0.1 to avoid the time splitting. This model also includes a horizontal second-order numerical smoother which is applied to all the prognostic fields. This horizontal smoother reduces the growth of nonlinear instabilities and filters out very short waves.

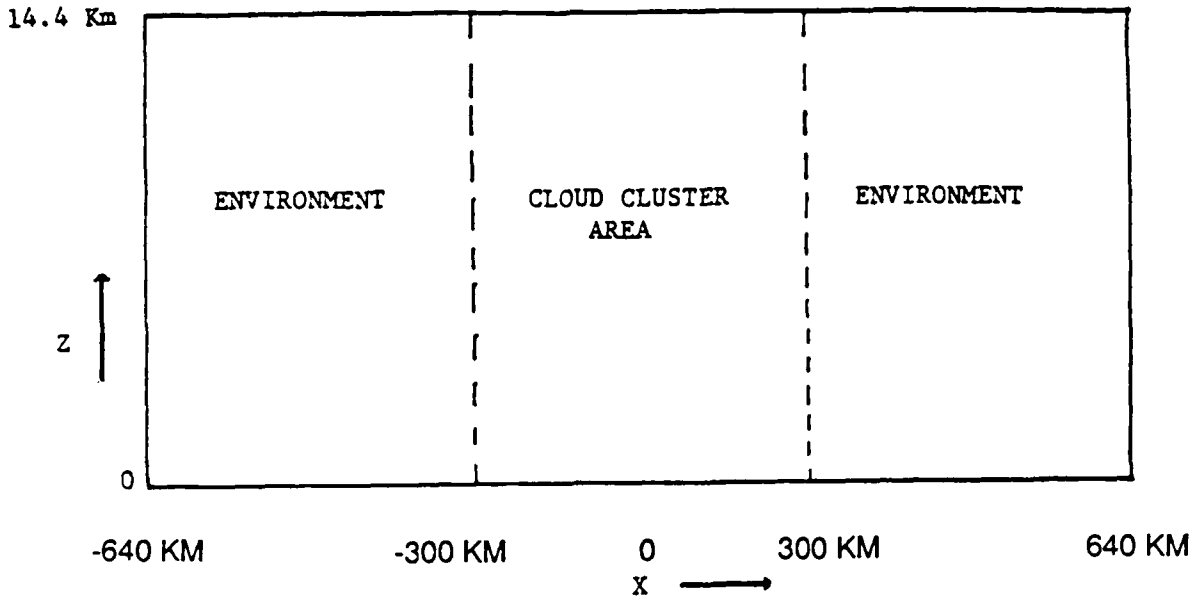

Fig. 16. The schematic diagram of the model design.

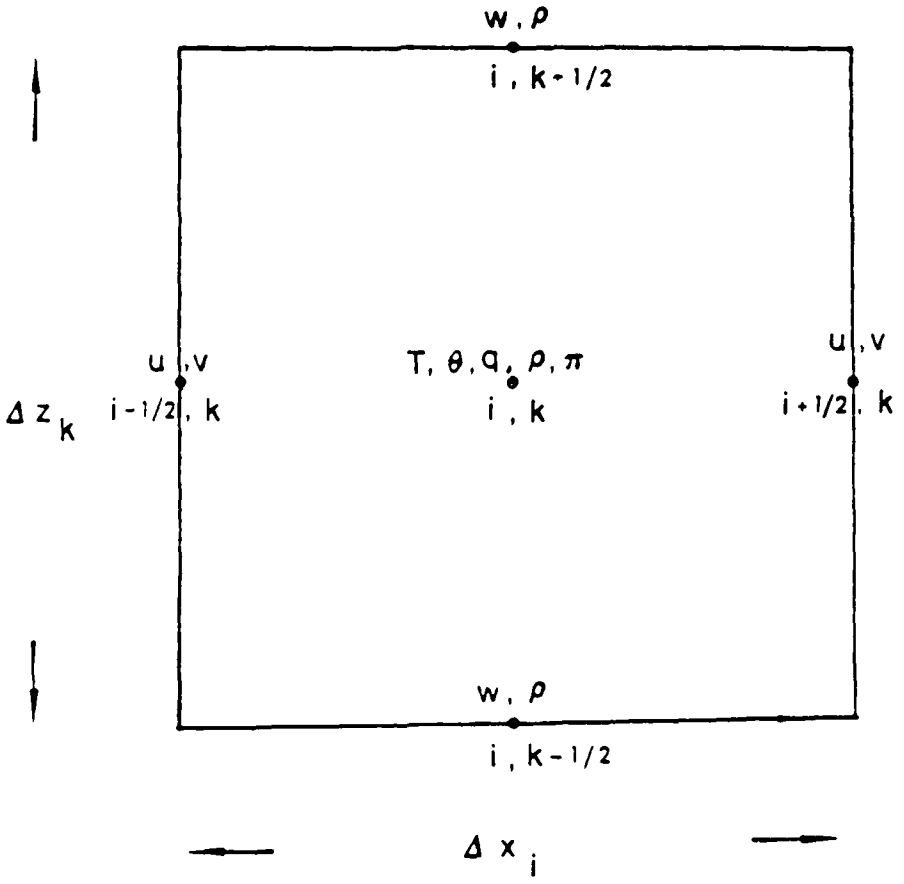

Fig. 17. The arrangement of the model variables.

At the upper and lower boundaries, a free-slip boundary condition is used for u and a fixed boundary condition with zero velocity is used for w. No fluxes of θ and q are allowed across these boundaries. The lateral boundaries are open (see Klemp and Wilhelmson, 1978). The values of u and v at the lateral boundaries are determined by advecting corresponding values at the adjacent interior gridpoints outward with the gravity wave speed. As for θ and q, zero horizontal gradient is assumed at the lateral boundaries. The boundary conditions can be summarized as

$$w = 0 \qquad \text{at upper and lower boundaries}$$

and

$$\frac{\partial u}{\partial t} = - c_g \frac{\partial u}{\partial x}$$

$$\frac{\partial v}{\partial t} = - c_g \frac{\partial v}{\partial x} \qquad \text{at left and right boundaries} \tag{64}$$

$$\frac{\partial \theta}{\partial x} = \frac{\partial q}{\partial x} = 0$$

where C_g represents the outward-propagating gravity wave speed. Under the GATE environment, the estimated gravity wave speed is 36 m s^{-1} and this value is used for C_g.

At time $t = 0$, T and q are horizontally uniform and their profiles are shown in Fig. 18. These are GATE soundings taken from the ship Researcher at 00 GMT 12 August 1974. A computed low-level vertical velocity at 00 GMT 12 August 1974 within an ITCZ rainband (Ogura et al., 1979) using GATE A/B scale data is given in Fig. 19. It is seen that the maximum magnitude is about 1.7 cm s^{-1} around 850 mb. A sinusoidal function was used with values of 3.4 cm s^{-1} at the center of the domain and zero at the boundaries of the cloud cluster area to obtain the imposed vertical velocity w_o in (61) and (62). The average w_o in the cloud cluster area will therefore be

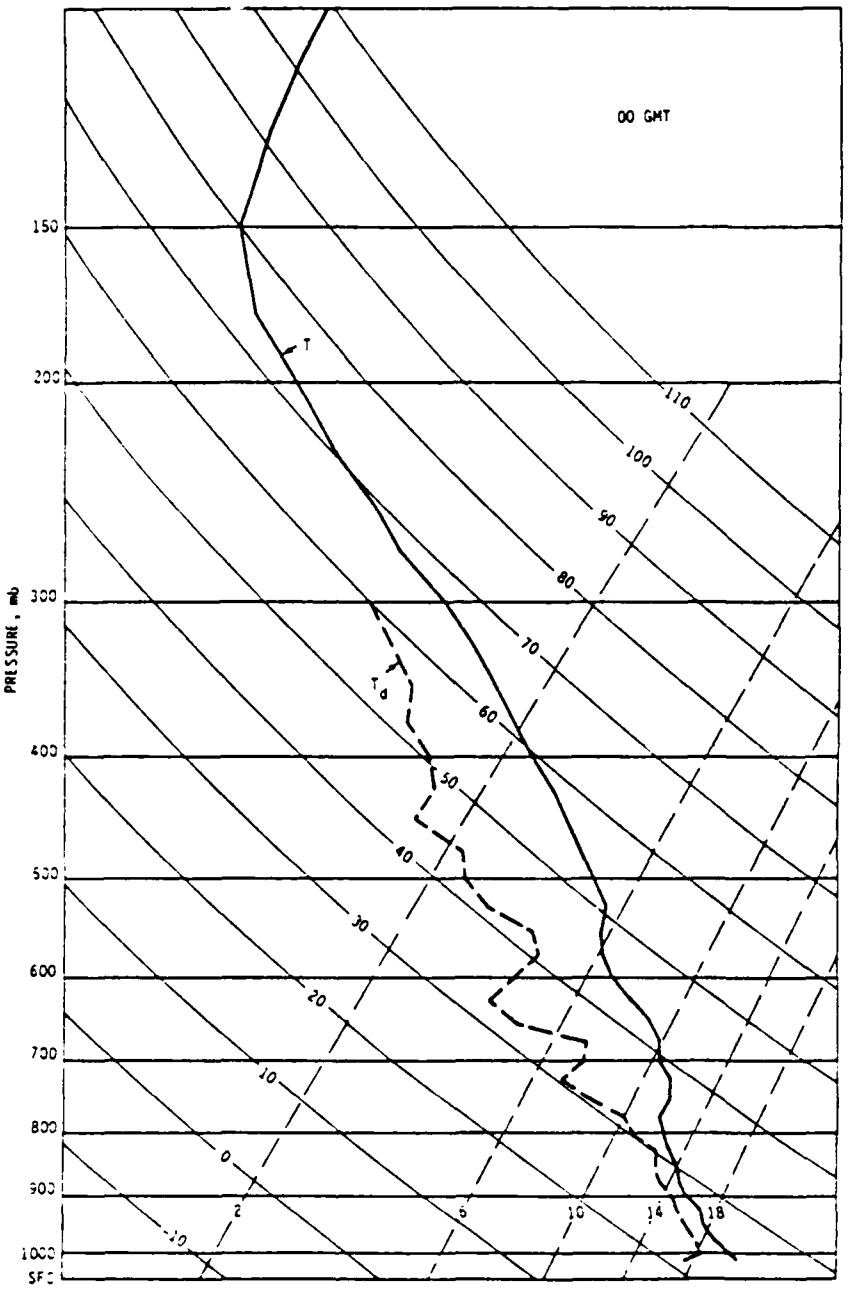

Fig. 18. The atmospheric sounding taken from the ship Researcher at 00GMT 12 August 1974.

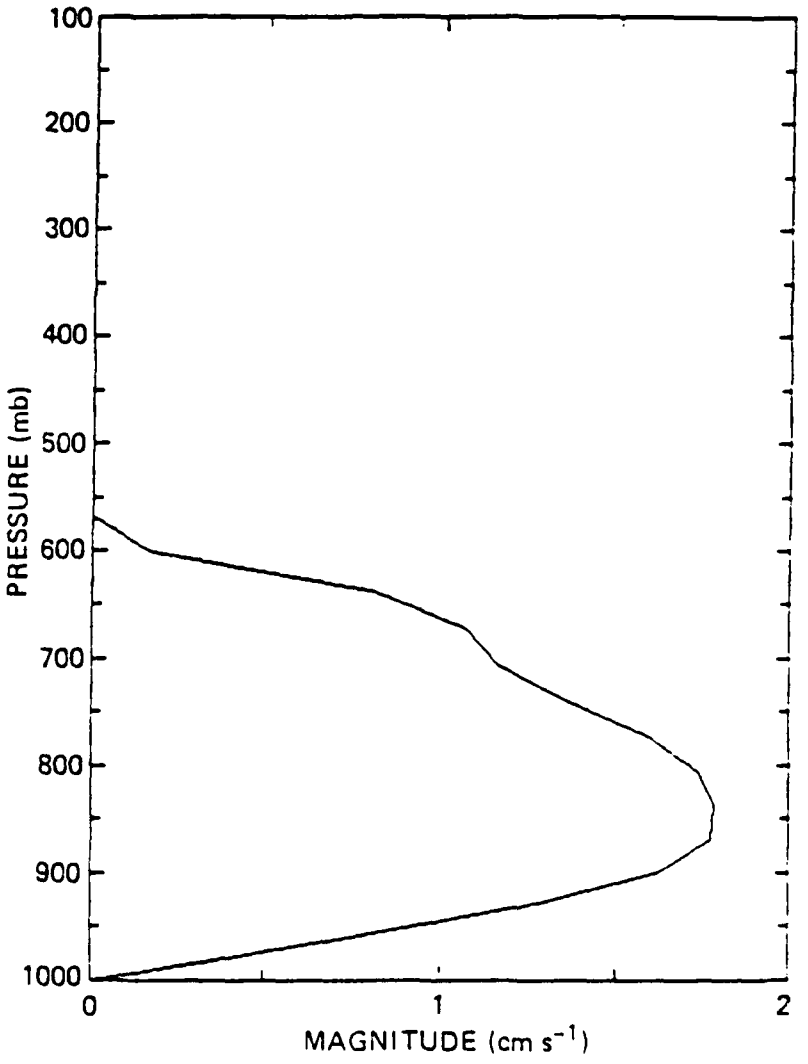

Fig. 19. The computed low-level vertical velocity at 00GMT 12 August 1974 at the ship Researcher.

1.7 cm s^{-1} as observed. There is no horizontal wind initially. Fig. 20, adopted from Ogura et al. (1979), shows the surface wind and divergence calculated at the initiation stage of the cloud band at 00 GMT 12 August 1974. It is evident that convective cells started developing in the area of the maximum surface convergence. Almost symmetric decreases of surface convergence are present on both sides of the cloud. This indicates that our imposed circulation w_o described above is fairly justifiable.

6.3. A 24-hour integration

In this section, the results of the response of the tropical mesoscale cloud band to the large-scale, low-level lifting process through the application of the present cumulus parameterization scheme will be illustrated in terms of the following "circulation descriptors", as defined by Kreitzberg and Perky (1977): (1) the intensity of the mesoscale vertical motion, (2) the life-cycle of the development of the mesoscale circulation and (3) the horizontal width scale of the cloud band and its associated precipitation area. For verification purposes, the model results will be compared with the observed values deduced from data analysis.

The initial conditions, shown in Fig. 18, are conditionally unstable except for a stable layer around 700 mb. There is no initial motion field in the model except the externally imposed, time-independent, large-scale, low-level lifting w_o . Since the model is symmetric about the center axis of the domain, hereafter all of the model results are presented only in the right half of the domain. Also, all of the w fields presented in this section do not include the imposed large-scale w_o .

During the first six hours of simulation, it is observed that no convective activity is present, primarily because the large-scale moisture convergence has not reached the minimum critical value for convection to

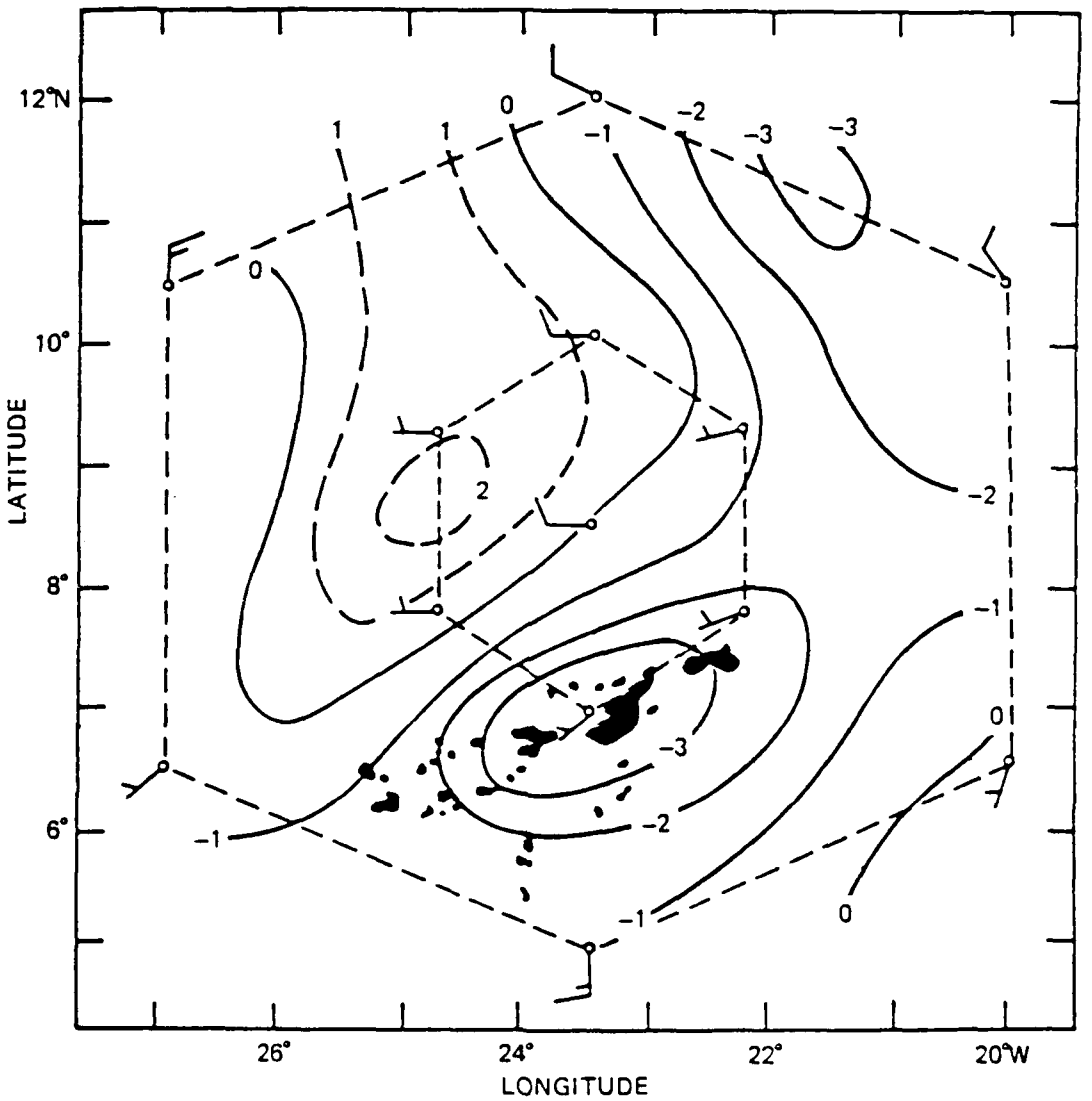

Fig. 20. The surface wind and divergence (in the units of 10^{-5} s^{-1}) along with radar echoes observed at 00GMT 12 August 1974. The outer hexagon indicates the GATE A/B scale ship array and the inner hexagon the B scale ship array. The full barb for wind is 5 m s^{-1}. (Adapted from Ogura et al., 1979).

occur. [Here, the minimum critical value is set to 5×10^{-7} Δt s^{-1} as in Phillips (1979).] Fig. 21 shows the evolution of the mesoscale circulation in the vector field of [u,w] (the magnitude of w has been enlarged by 10 times because of the scale difference between u and w) at 9, 13, 15, and 23 hrs. At 9 hr, the flow pattern has inflows at low levels, upward motion at the central portion of the domain, and outflows at the middle level. The upper levels have almost no motion. The circulation system is located within 160 km of the center. At this time, we can categorize this mesoscale circulation as the developing stage. As the convection continues to develop, the magnitude of the upward motion becomes larger and the upward motion area also expands and extends to higher levels. At 13 and 15 hr, inflow is still from low levels, upward motion is around the center and the outflow is at upper levels. The whole circulation system is much larger than at the developing stage. This is the mature stage. Then as the convection continues, this circulation system begins to split and the intensity of the upward motion decreases rapidly. At 23 hr, a reverse circulation is present at the low levels, categorizing it as the decaying stage.

The reasons for the above evolution of the mesoscale circulation were previously explained by Yamasaki (1984): (1) If the outflow is not very strong or the inflow is relatively strong, the updraft is maintained or intensified at almost the same location; (2) if the outflow of the downdraft air is strong enough for a new updraft to occur at some distance from the old cloud, the cloud has a short lifetime and the new updraft may contribute to the formation of another cloud system.

Now we will look into the intensity of this mesoscale vertical motion at the developing, mature, and decaying stages. Fig. 22 shows the evolution of the vertical velocity at different stages. It is seen that at 9 hr the

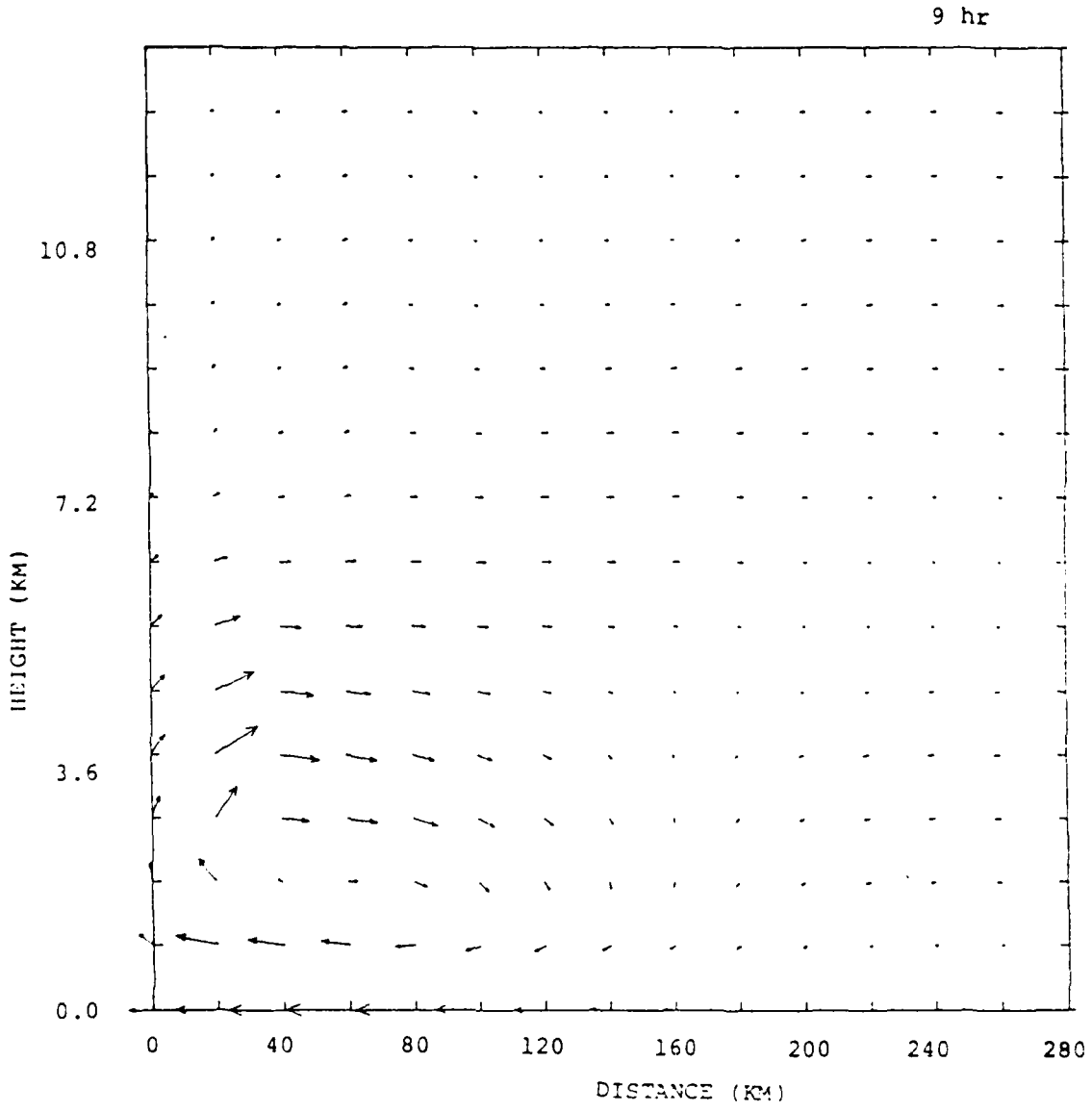

Fig. 21. Cross sections of the predicted vector field of [u,w] at 9, 13, 15, and 23 hours.

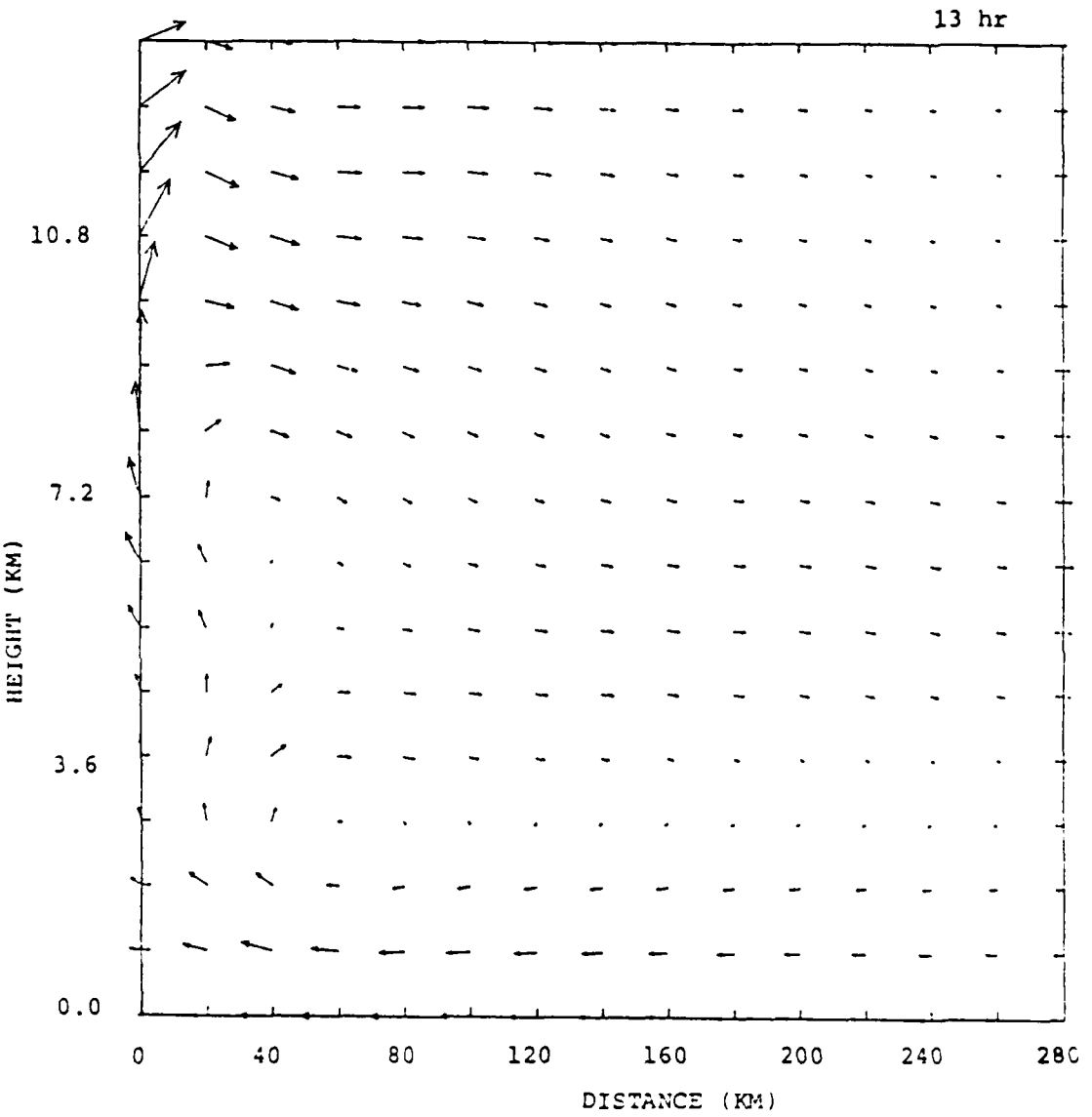

Fig. 21. (continued)

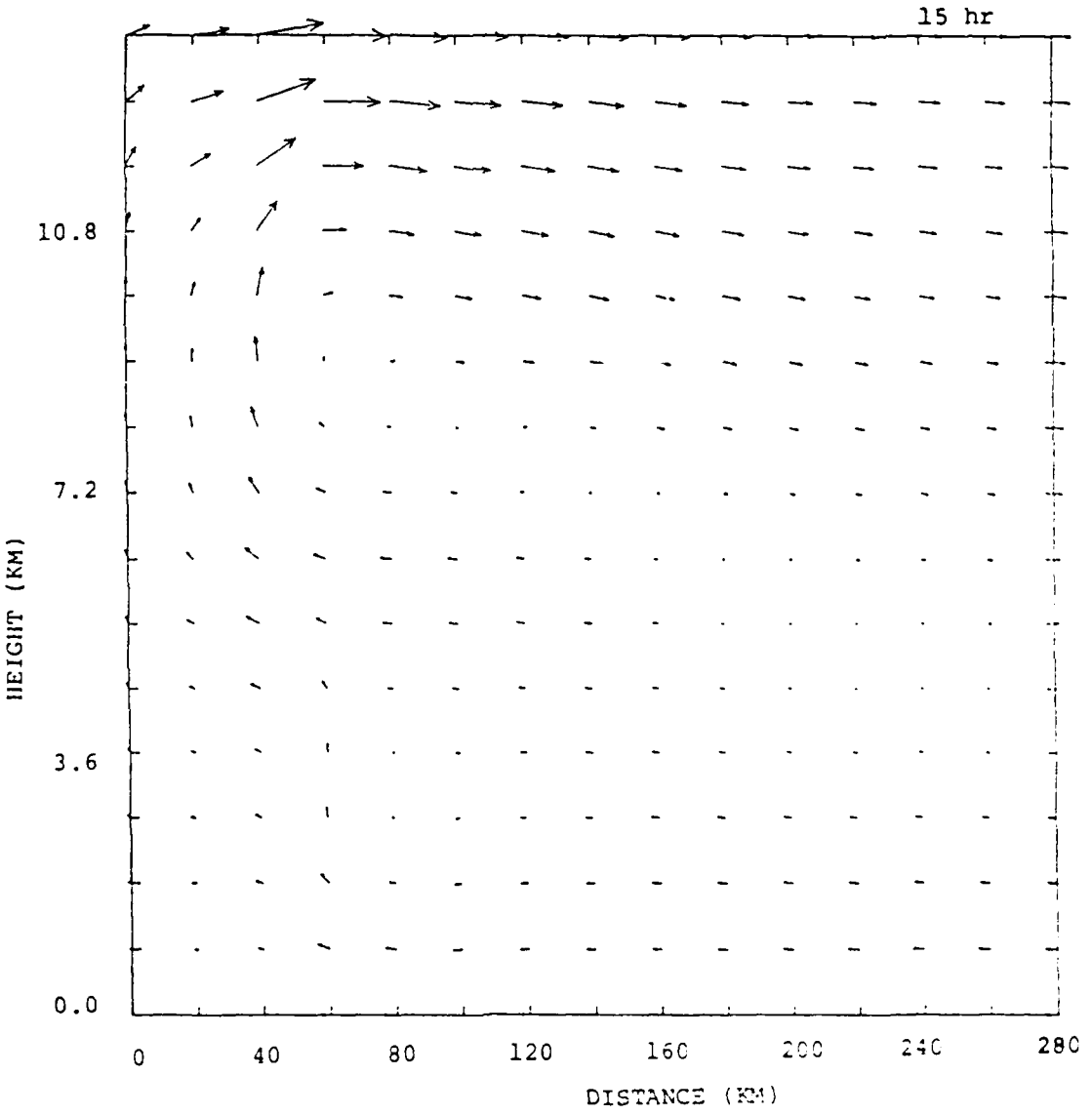

Fig. 21. (continued)

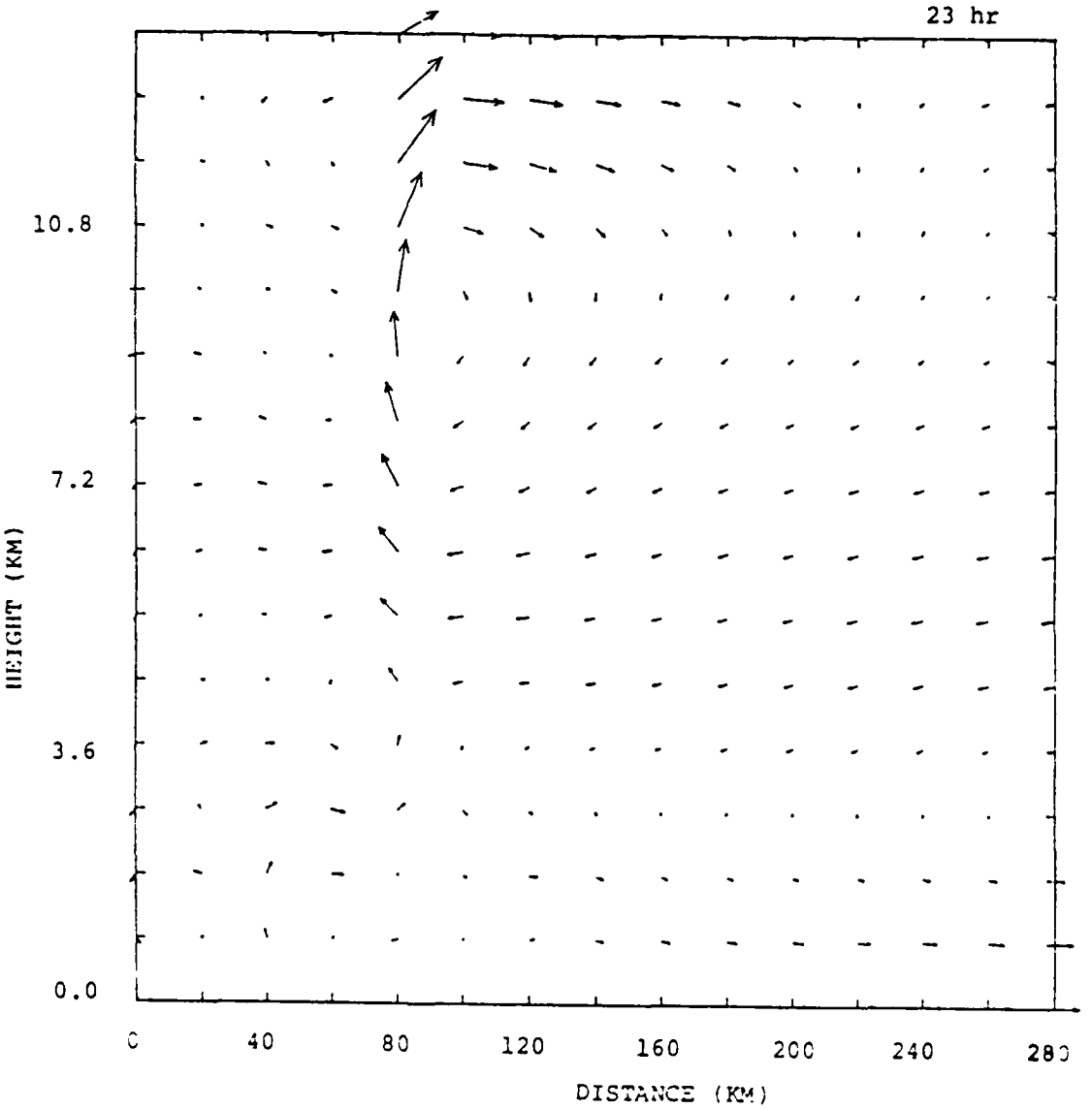

Fig. 21. (continued)

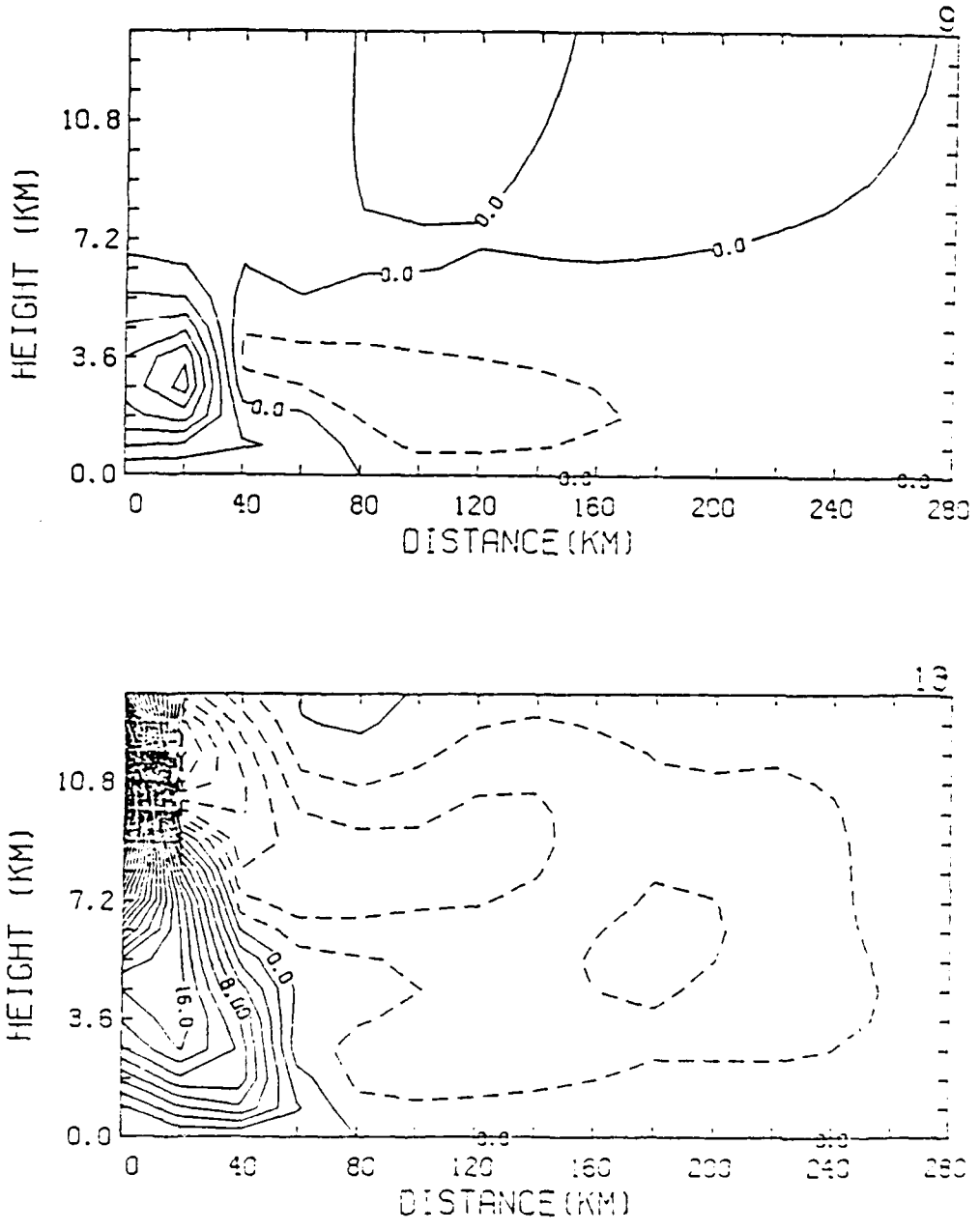

Fig. 22. Cross sections of the predicted vertical velocity at 9, 13, 15, and 23 hours with a contour interval of 2 cm/sec.

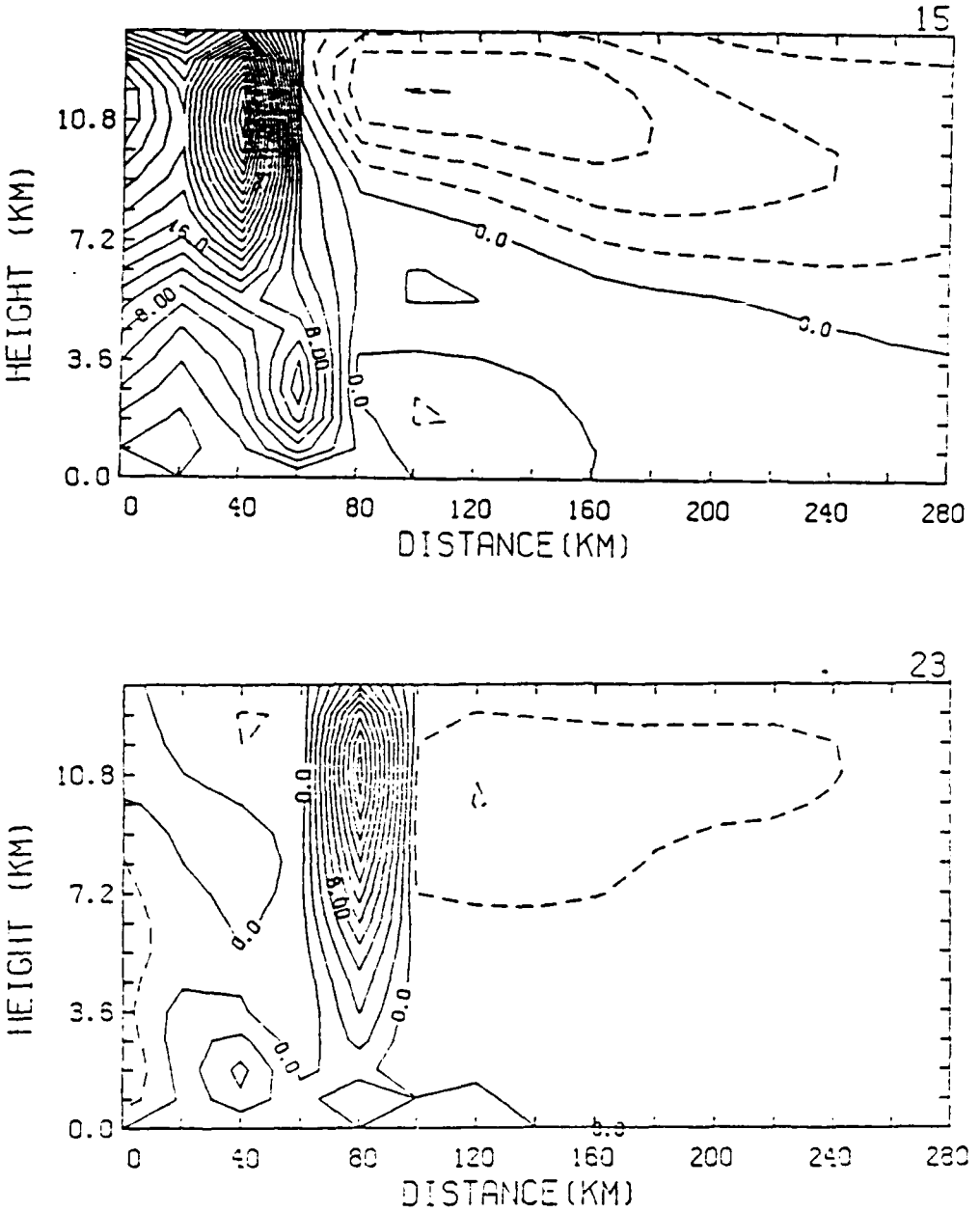

Fig. 22. (continued)

upward motion is around the center. Significant downward motion with a magnitude of about 2 to 3 cm/s is adjacent to an upward motion area. The level of maximum vertical velocity is located at around 2.7 km. Above the 7.2 km height, the upward motion is close to zero. At this stage the convection is dominated by middle and shallow clouds. This is due to the formulation we have in (43) to (45): when the convection is weak or moderate, the entrainment effect will be important; therefore, the cloud top level is not located at a higher level. At 13 and 15 hr, the intensity of upward motion has increased and both the upward motion area and the downward motion area are more broad, with the level of maximum vertical velocity at around 10.8 km. During these stages the convection is dominated by deep clouds. At 23 hr, two features are noted: one is the downward motion appearing in the central portion of the domain, while another is the secondary maximum of the upward motion area located at high levels some distance from the center. As mentioned earlier, if the outflow of the downdraft air is strong enough for a new updraft to occur at some distance from the old cloud, the new updraft may contribute to the formation of another cloud system with this secondary upward motion becoming the new updraft. This secondary upward motion consumes most of the moisture supply so it tends to reduce the original convection around the center. On the other hand, this secondary upward motion area cannot develop into a well-defined convective system because the magnitude of the imposed w_o in this area is small. Therefore, the low-level mass convergence is insufficient for the new cloud to maintain itself.

Fig. 23 shows the predicted cloud heating at the same time periods as Fig. 22. Basically, the cloud heating area coincides with the upward motion area in Fig. 22. At 9 hr, the heating area is located around the center of

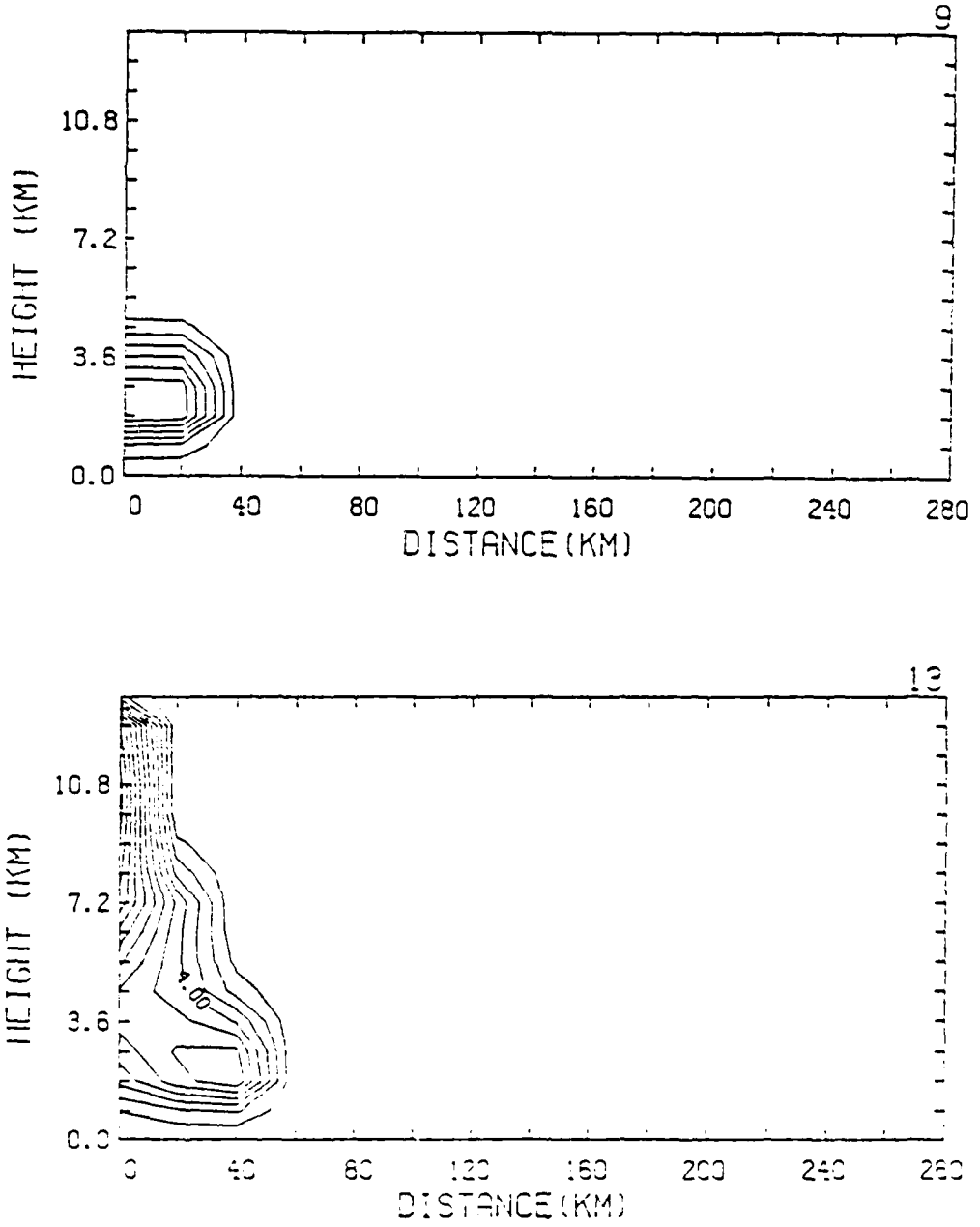

Fig. 23. Cross section of the predicted cloud heating rates at 9, 13, 15, and 23 hours with a contour interval of 1 °C/hr.

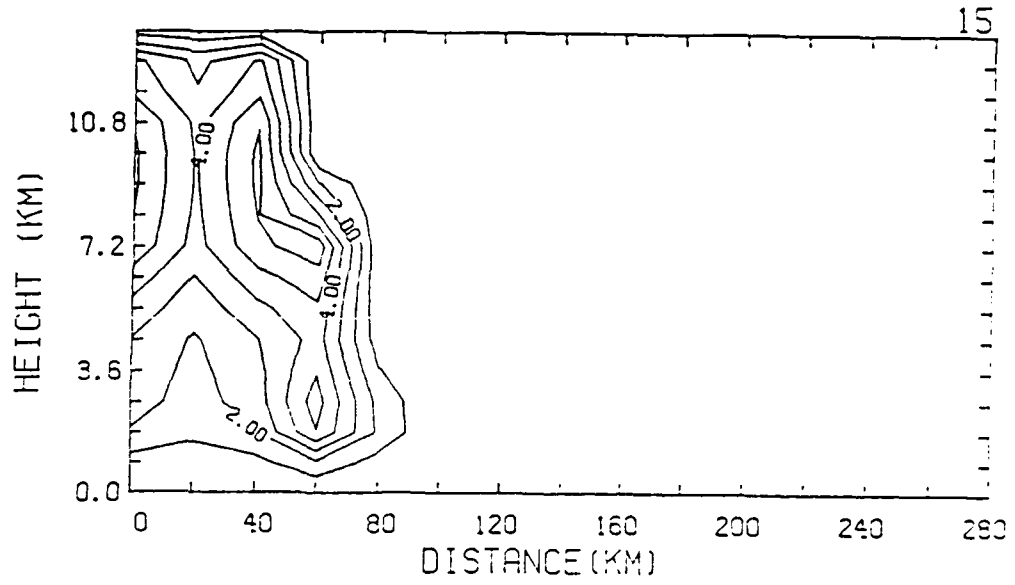

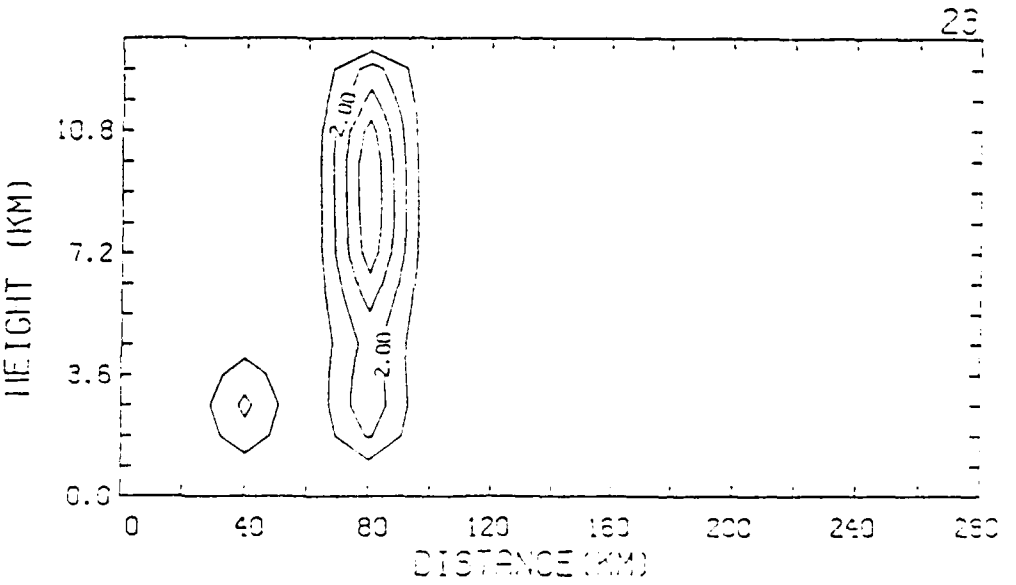

Fig. 23. (continued)

the domain and stays at low levels. At 13 and 15 hrs, the level of maximum heating has shifted to high levels and the heating area has become more broad. At 23 hr, the heating area has moved away from the center.

6.4. Comparison with observation

Fig. 24 shows the observed vertical velocity (adopted from Ogura et al., 1979) at the center of the cloud band as a function of time and height, as determined by wind data from the GATE B-Scale observational network. It is evident from this figure that prior to and during the initiation stage low-level upward motion was present with weak subsidence at middle and upper levels. As convection developed, w increased in intensity and the area of upward motion increased greatly in vertical extent. The local maximum w was located around the 400-mb level during the mature stage of the cloud band at 15 GMT. The decaying stage was characterized by the rapid decrease in upward motion at low levels followed by the development of descending motion, while significant ascending motion remained at upper levels.

Fig. 25 shows the evolution of the model-predicted w field averaged horizontally over 160 km of the central portion of the domain, which is considered the width of the cloud band simulated by the model. As mentioned in the previous section, there is no convection present initially. The convection started around the 7th hr when the area-averaged w started to increase in intensity. The level of maximum w remained at the 2.7 km level until 12 hr. After 12 hr, the area-averaged w rapidly increased its magnitude and the level of maximum w shifted to a higher altitude. At 16 hr, the upward velocity reached its maximum value of around 10 cm/sec at 9.9 km height. Around 18 hr, the averaged w rapidly decreased in intensity and

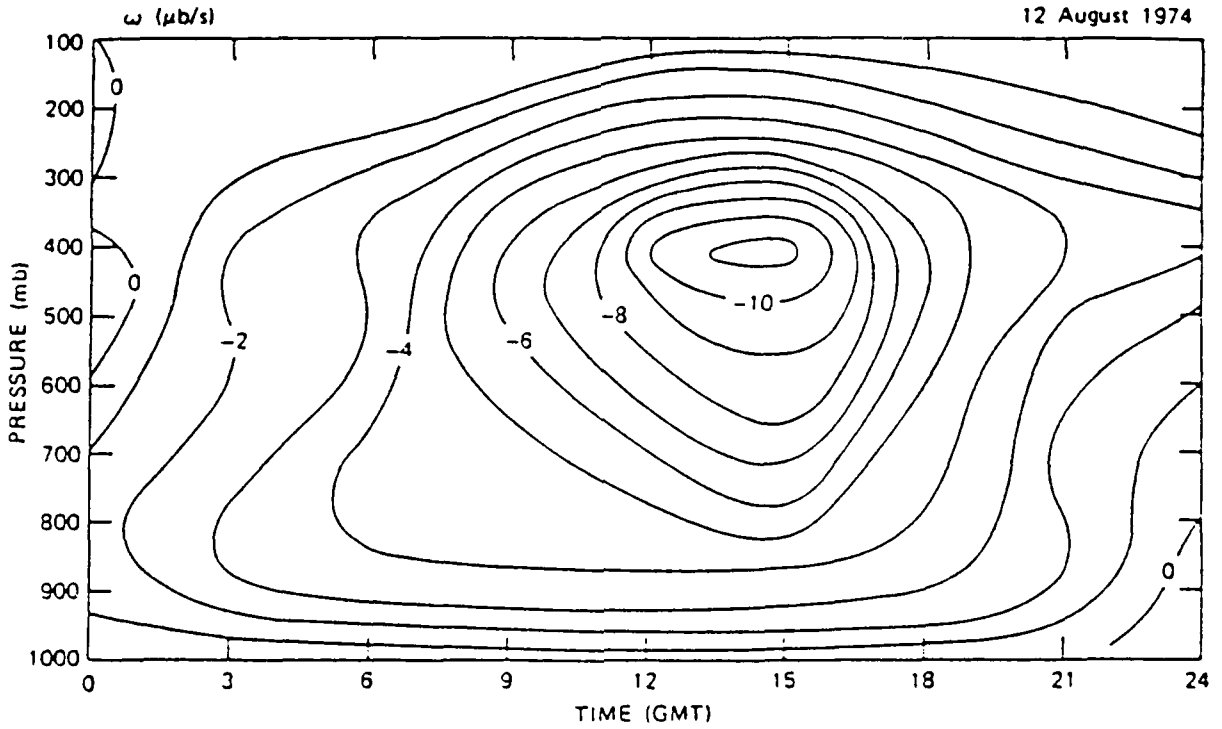

Fig. 24. Time-pressure section of the vertical P-velocity (ω) at the center of the cloud band in units of μb/sec.

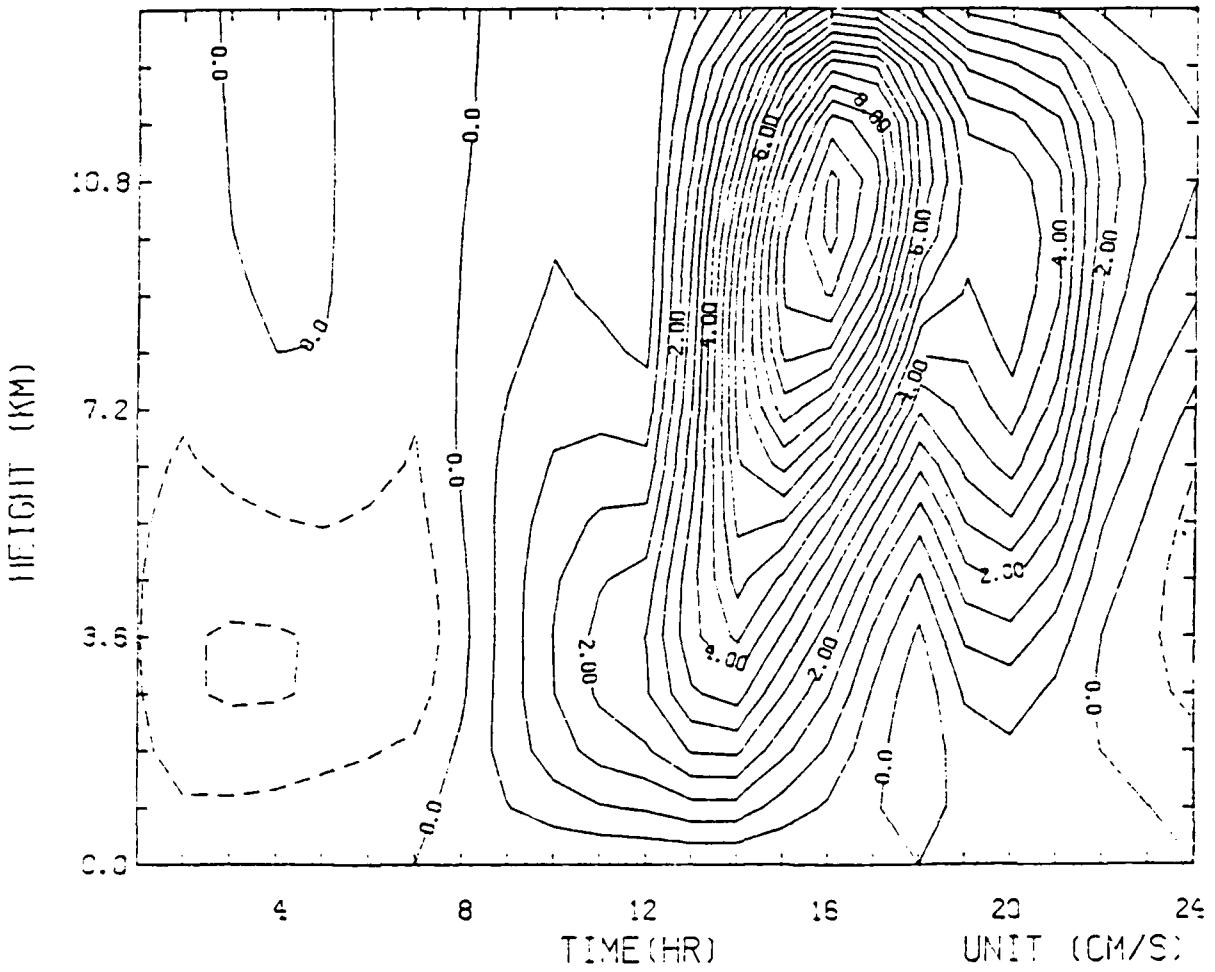

Fig. 25. Time-height section of the model-predicted vertical velocity averaged over the central 160 km of the model domain with a contour interval of 0.5 cm/sec.

low-level downward motion was observed. Then the whole system gradually started decaying. At 24 hr, the lower half of the domain was dominated by downward motion.

Comparing the simulated w field with observations, one can see that the model results agree well with the observations in that (1) the area-averaged w increases in intensity with time, (2) prior to the mature stage the level of maximum w is located at low levels; then as the convection developed the location of maximum w is shifted to a higher altitude, i.e., the height of the local maximum of w increases with time, and (3) after the mature stage the intensity of upward motion at low levels decreases rapidly and then becomes downward motion.

Fig. 26 shows the model-predicted surface precipitation as a function of time and distance from the center. The width and distribution of precipitation almost coincide with those of the predicted upward motion. Fig. 27 shows the observed precipitation accumulation for the cloud band from 12 to 18 GMT 12 August 1974. The observed average rainfall accumulation in the center of the cloud band (8.5 to 10 N and 23.5 to 22 W) is around 11.8 mm from 12 to 18 GMT. The area-averaged rainfall from our simulation during the same period is 11.9 mm, which is very close to the observation.

For comparison, Fig. 28 shows the time-height section of the the predicted vertical velocity averaged over the central 160 km of the model domain with the use of a combination of Kuo's 1965 and 1974 schemes (see Section 3) with the value of b set to zero. A comparison of this figure with Fig. 20 shows that as the convection started the level of maximum upward motion immediately shifted to a higher level and then remained at the same level. At 13 hr, the area-averaged vertical velocity w of the simulated system reached its maximum value of around 12 cm/sec. After 16 hr,

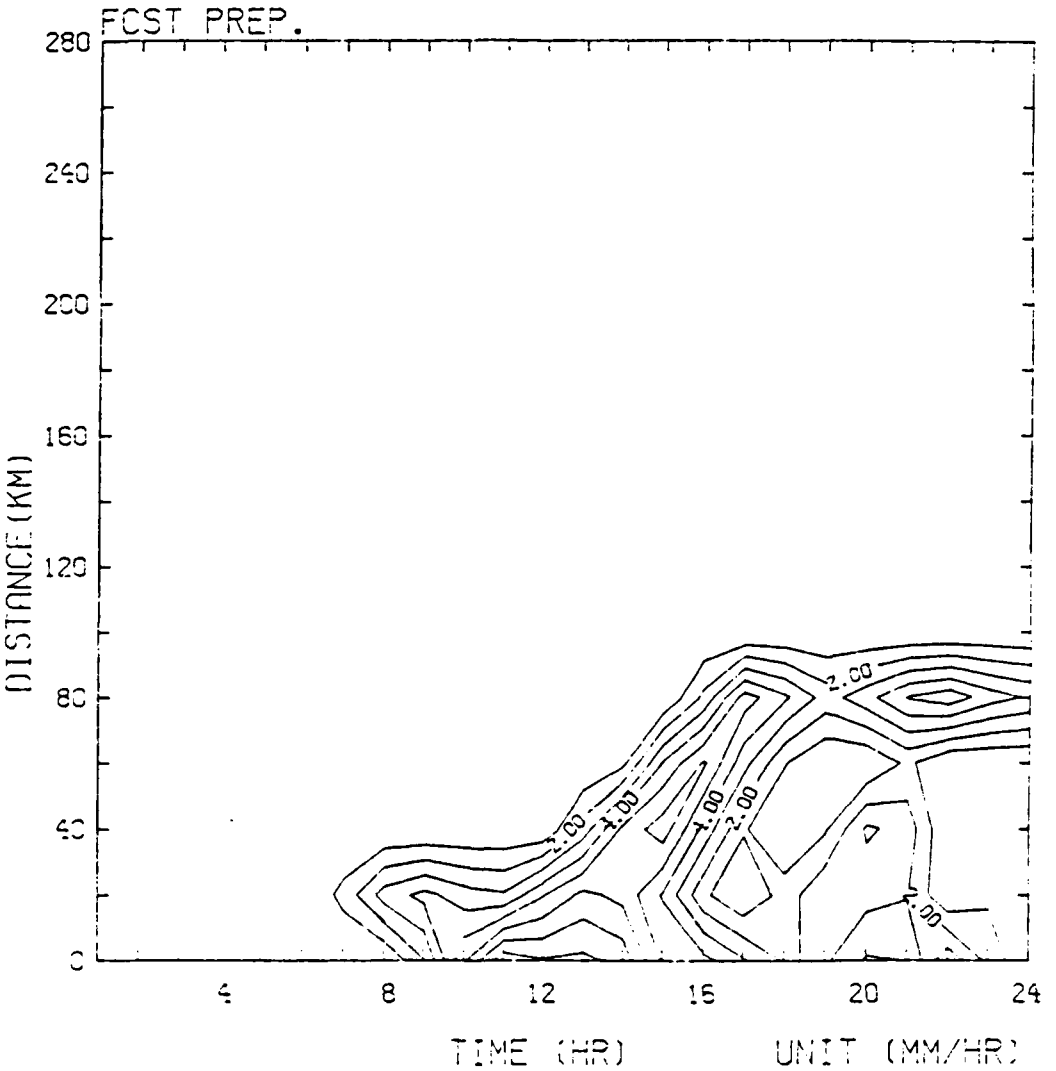

Fig. 26. Model-predicted rainfall accumulation as a function of time and distance from the center in units of mm/hr with a contour interval of 1 mm/hr.

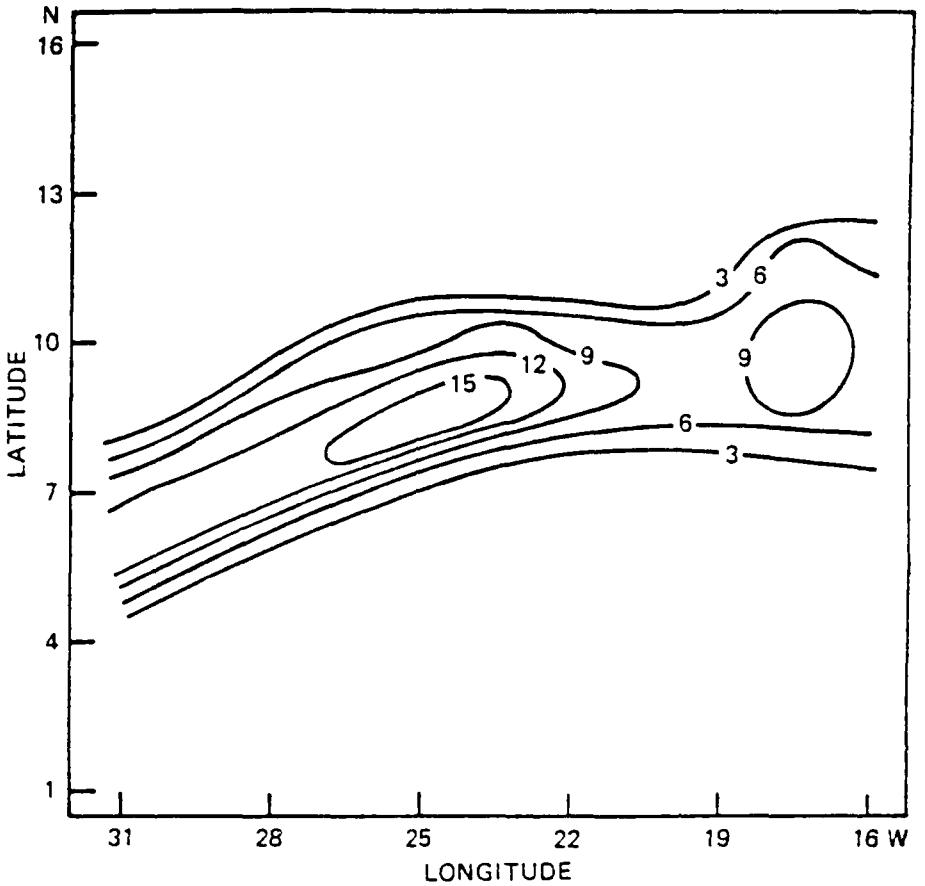

Fig. 27. The observed rainfall accumulation for the period from 12GMT to 18GMT 12 August 1974 in units of mm.

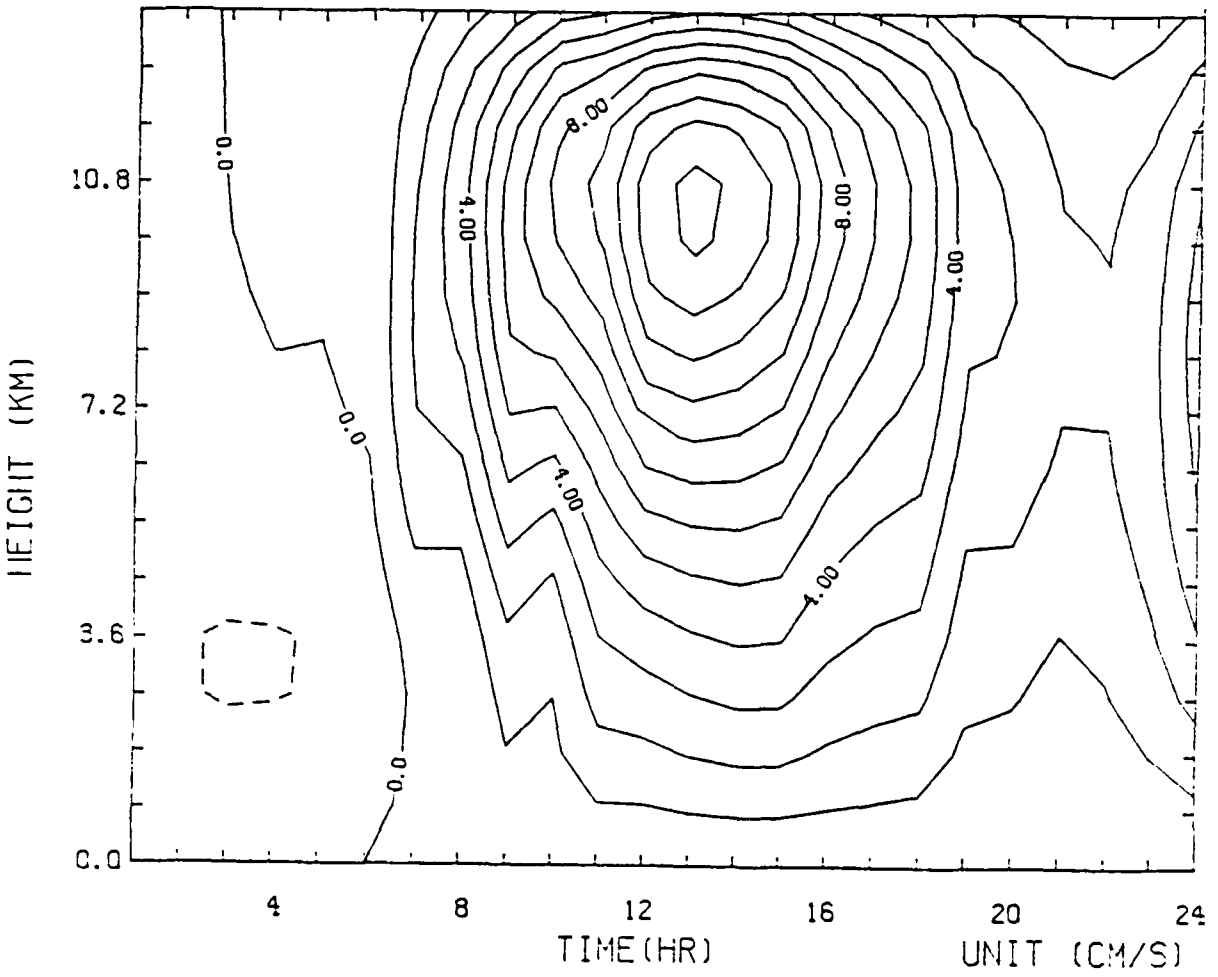

Fig. 28. Time-height section of the model-predicted vertical velocity from the Kuo scheme averaged over the central 160 km of the model domain with a contour interval of 1 cm/sec.

the intensity of w decreased rapidly; however, no downward motion was observed. At 23 hr, the averaged w started to increase its intensity instead of entering the decaying stage. In this simulation, one can see that (1) the height of the local maximum w did not increase with time, and (2) the downward motion did not appear at low levels during the decaying stage.

7. Concluding Remarks

The determination of the vertical distributions of heating and moistening by the cumulus-scale motions and the estimation of reasonable rainfall rates are some of the major problems related to the parameterization of cumulus convection. Kuo has proposed that both the amount and the vertical distribution of convective heating by convergence-controlled cumulus convection can be calculated by using the moisture convergence M_t and the temperature difference $(T_c - T)$ between the cloud and the environment. In this report, a combination of Kuo's 1965 and 1974 schemes were first applied using a semiprognostic approach without considering the entrainment to the GATE Phase III data. It was found that the vertical heating profiles are in good agreement with observations during periods of strong convective conditions. However, they are in poor agreement during periods of weak convection. This problem can be resolved by considering the vertical extent of the cumulus cloud (entrainment effect) and the vertical profiles of heating based on different convective conditions. This led to the present scheme. Comparisons between the present scheme and Kuo's scheme without entrainment were then made using semiprognostic tests, showing that the present scheme produces a drastic improvement in cloud heating profiles during periods of

weak convection. Generally, the present scheme can reproduce the observed rainfall and heating-drying profiles quite well in the semiprognostic tests using the GATE Phase III data.

A prognostic application of the present modified Kuo scheme was made by incorporating the scheme into a two-dimensional, cloud cluster model to simulate a tropical cloud band under the influence of a low-level, large-scale lifting. A realistic life cycle behavior was simulated and the model results from our present scheme bear considerable resemblance to many aspects of the observations including (1) the evolution of an area-averaged vertical velocity, (2) the intensity and distribution of precipitation, and (3) the development of low-level downward motion during the decaying state. The results indicate that (1) linking rainfall to a fraction of the large-scale moisture supply is reasonable in mesoscale tropical cloud band simulation, and (2) the incorporation of the entrainment effect into Kuo's approach appears to be essential to reproduce the evolution of the area-averaged vertical velocity and the life cycle of the convective system.

PART II

An Evaluation of the Cumulus Parameterization Scheme using the Air Force Geophysics Laboratory Global Moist Forecast Model

1. Introduction

A good cumulus parameterization scheme should be based on understanding cloud-environment interactions. These interactions include (a) the controlling influence of environmental conditions on the development and intensity of an ensemble of cumulus clouds and (b) the physical processes through which this cumulus ensemble modifies its environment. The verification of a cumulus parameterization scheme should also be based on its ability to realistically represent the heating and drying effects of cumulus clouds and predict accurately the cumulus precipitation. In Scientific Report No. 1 (Kao and Ogura, 1985), we evaluated the Arakawa-Schubert (A-S) scheme of cumulus parameterization. In Part One of this report, we evaluated the Kuo scheme. Two methods were used in these evaluation processes. One is the semi-prognostic approach, in which the parameterized cumulus heating and drying profiles and precipitation are compared with the values diagnostically determined from the heat and moisture budget equations. The second approach is to incorporate the cumulus parameterization schemes into a fully prognostic cloud cluster model. The ability of cumulus parameterization schemes to simulate the cloud-environment interaction processes and to reproduce the life cycle of a cloud cluster can be evaluated. Through these studies, an improved algorithm to implement the A-S scheme and an improved Kuo's scheme including the entrainment effect were developed.

The ultimate test of any cumulus parameterization scheme is to actually incorporate that scheme into a large-scale prediction model. The advantage

of this approach is obviously that the predicted cloud coverage and precipitation amount can be compared with actual observations. The drawback is that when the prediction is incorrect, it is not certain whether the fault rests on a poor cumulus parameterization scheme or on the large-scale prediction model itself. In spite of these shortcomings, this test is necessary for the improvement of numerical weather prediction. This part of the report presents the results of applying the Kuo scheme and the A-S scheme of cumulus parameterization to the AFGL Global Moist Forecast Model. Section 2 provides a brief description of the AFGL model. Section 3 presents the prediction results, followed by the discussion of the results in Section 4.

2. The AFGL Global Moist Forecast Model

The equations and framework of the AFGL Global Moist Forecast Model are described in Brenner et al. (1982). A brief description will be provided here as background. The AFGL Global Moist Forecast Model is a spectral model with 12 layers and rhomboidal 30 waves. The prognostic equations are vorticity, divergence, temperature, specific humidity, and the logarithm of the surface pressure (continuity equation). The vorticity and divergence are given conventionally as Laplacians of a streamfunction and velocity potential respectively. The velocity components and geopotential are obtained diagnostically with the aid of the hydrostatic relation. The vertical coordinate of the model is $\sigma = 1 - P/p_*$, defined by Phillips (1959), with a specification of layer locations described by Brown (1974) and Phillips (1975). The numerical methods in the model include spectral representation in the horizontal, the Arakawa quadratic conserving finite differencing in the vertical, and the semi-implicit time integration scheme. The physical effects included in the model are the influences of orography,

position-dependent surface friction, moisture physics, and subscale horizontal dissipation, parameterized by diffusion. Evaporation and sensible heat flux from the oceans are also included. The application of the moisture physics consists of a sequence of three steps to adjust the temperature and specific humidity. Each step possesses a characteristic spatial scale: (1) cumulus convection in conditionally unstable, generally unsaturated large-scale flow, (2) large-scale condensation in stable, saturated large-scale flow, and (3) dry convection in unstable, unsaturated large-scale flow. The adjustments are applied after the provisional values of the dynamic variables at a new time step are obtained through time integration. Large-scale condensation produces nonconvective and stratiform precipitation. The effects of the cumulus clouds are parameterized using Kuo's modified 1965 scheme. The highlights of this scheme consist of computing vertically integrated moisture convergence in the seven lowest layers of each column. If the computed amounts exceed 10^{-7} s^{-1}, and the atmosphere is unstable, then cumulus clouds will be allowed to develop. An unstable region is defined as extending from the bottom to the first layer, which is warmer than a moist adiabatically lifted parcel. If such an unstable column is found, the following sums are computed from the bottom layer to the top of the unstable part of the column:

$$Q_{11} = \Sigma(q_c - q_k) \cdot \Delta\sigma_k$$

$$Q_{22} = \frac{c_p}{L} \Sigma(T_c - T_k) \cdot \Delta\sigma_k$$

$$Q_{eff} = \text{WATER}/(Q_{11}+Q_{22})$$

$$\text{DTKUO}_k = Q_{eff} \cdot (T_c - T_k)$$

$$\text{DQKUO}_k = Q_{eff} \cdot (q_c - q_k)$$

where the term "WATER" in the expression for Q_{eff} is the moisture convergence in the unstable column, q_c and T_c are the cloud mixing ration and temperature calculated from the lifted parcel values, and L is the latent heat. $DTKUO_k$ represents the latent heat release of convective precipitation and is added to the temperature forecast before cumulus parameterization. $DQKUO_k$ represents the change in specific humidity by cumulus parameterization and is added to the value at the previous time step. In this version of the Kuo scheme, the condensed water is also allowed to evaporate while falling into the lower layers. Fig. 29 contains the flow chart of Kuo's cumulus parameterization scheme in the AFGL spectral model.

3. Results

The experiments consist of 3 cases, each case consisting of 4 integrations of the AFGL spectral model for 24-hour simulations and starting from identical conditions. Integration 1 uses Kuo's parameterization in the original AFGL spectral model, as described above. Integration 2 uses the same Kuo scheme, but the condensed water is not allowed to evaporate. Integration 3 uses the present modified Kuo scheme reported in Part One of the report, and Integration 4 uses the A-S (Arakawa-Schubert) cumulus parameterization scheme. A detailed description of the A-S scheme is given in Scientific Report No. 1. The initial data used for the global test forecasts consisted of FGGE Level III-B on 1, 4, and 9 April 1979. Since the rainfall distribution is the major feature that needs to be simulated accurately by a "good" formulation of parameterization, only the rainfall prediction will be addressed in this report. In view of the limited observed precipitation data available, the discussion of forecast results will be limited to the area of the U.S. where the observed hourly precipitation data are available through the National Center for Atmospheric Research.

KUO (1965)-Type Convection

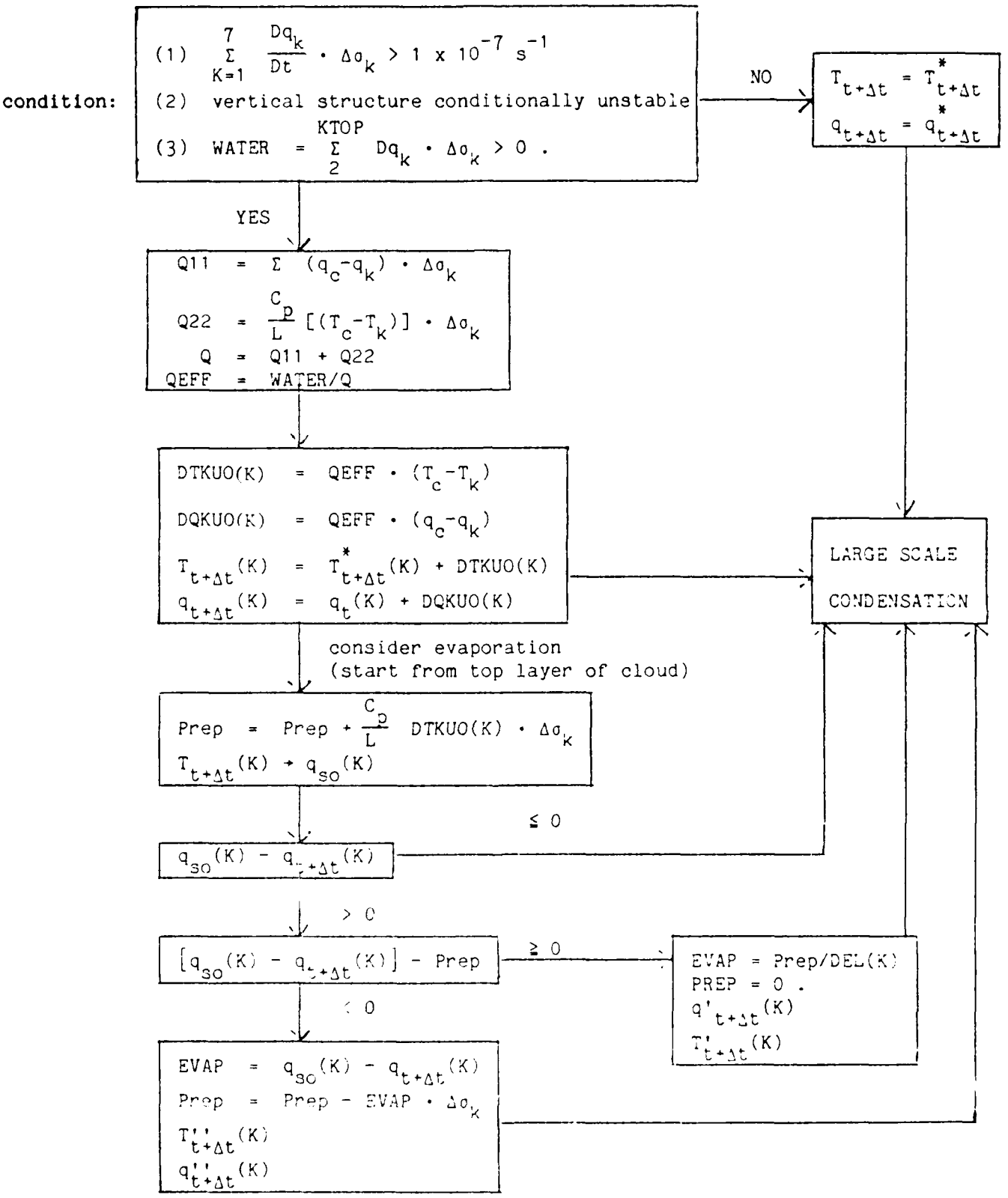

Fig. 29. The schematic diagram of the computational procedure of the Kuo-type (1965) scheme in the AFGL model.

3.1. The April 1, 1979 case

Starting with an initial condition from the FGGE Level III-B data at 00 GMT April 1, 1979, a 24-hour simulation was undertaken with four different versions of cumulus parameterization. In the first few hours of the simulation, any adjustments to the initial data may cause unrealistic rainfall patterns. Therefore, the comparison between the predicted rainfall and observations will be made only for the second 12 hours.

Fig. 30 shows the surface synoptic conditions at 1200 GMT 1 April 1979. The major features included a low-pressure system centered around the Texas-Oklahoma border. A cold front associated with this low was located at the southern end of this low center and extended to Texas. A stationary front was located at the northeastern end of this low center and extended to the East Coast. Also there was a cold front lying across North Dakota, South Dakota, Nebraska, and Wyoming. During the time between 1200 and 2400 GMT, the low pressure system moved northeastward to the Arkansas-Missouri border, while the associated cold front followed the movement of this low and gradually became a stationary front. Also, a squall line system developed to the east. Heavy convective precipitation occurred with this frontal system from Kentucky southwest to Arkansas and Louisiana during this 12-hr period, as shown in the radar summary in Fig. 31. The stationary front northeast of this low center also moved along with this low and produced moderate rainfall from Massachusetts southwest to Kentucky. The cold front around Nebraska and Wyoming contributed some light rainfall over Montana, Wyoming, Colorado, Kansas, and Nebraska.

Fig. 32 shows the observed 12-hr accumulated rainfall ending at 24 GMT 1 April 1979 over the U.S. No data is available over the oceans and Canada; therefore, the contour lines over these areas are produced by interpolation

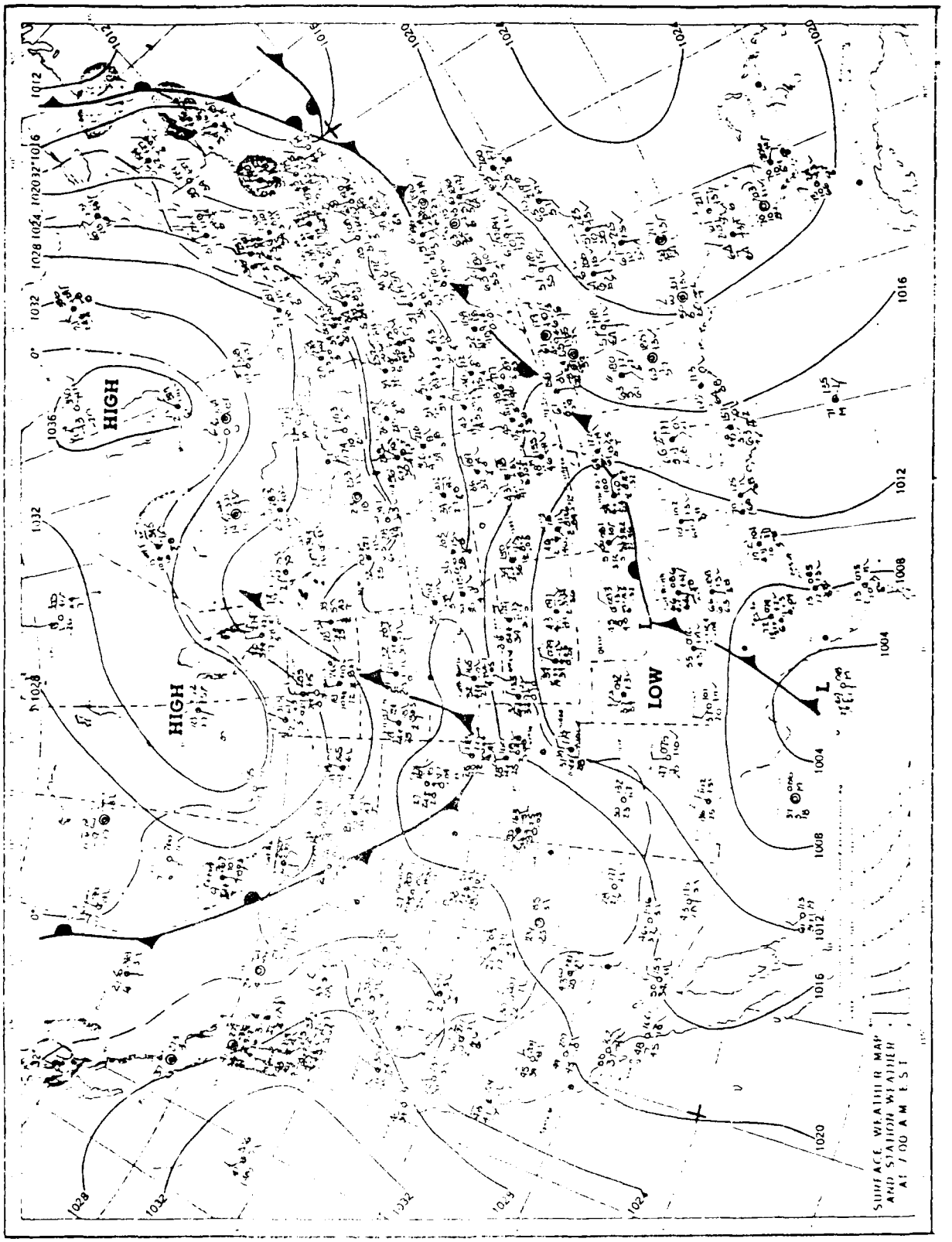

Fig. 30. Surface synoptic chart for 1200 GMT 1 April 1979.

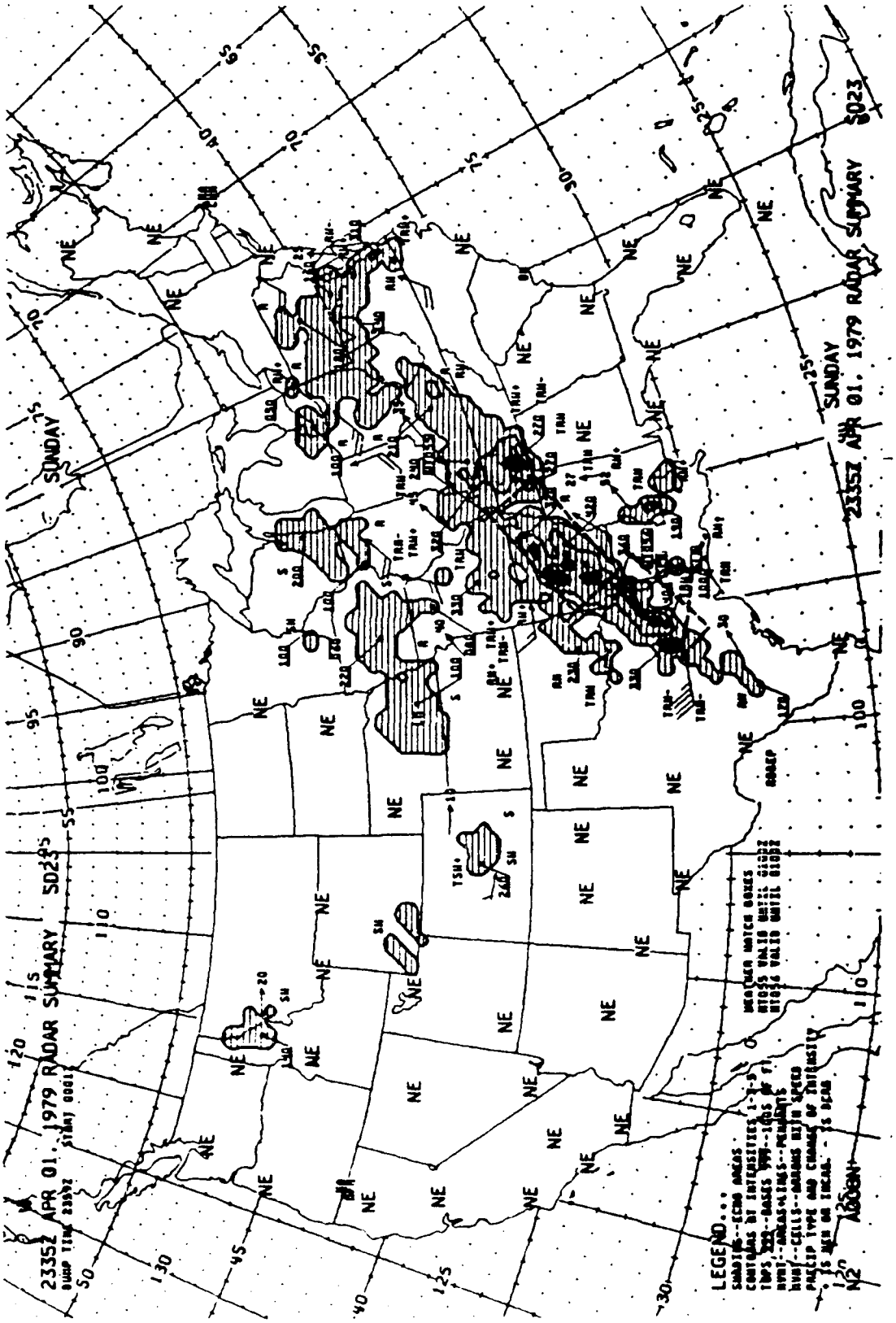

Fig. 31. Radar summary chart at 2335 GMT 1 April 1979.

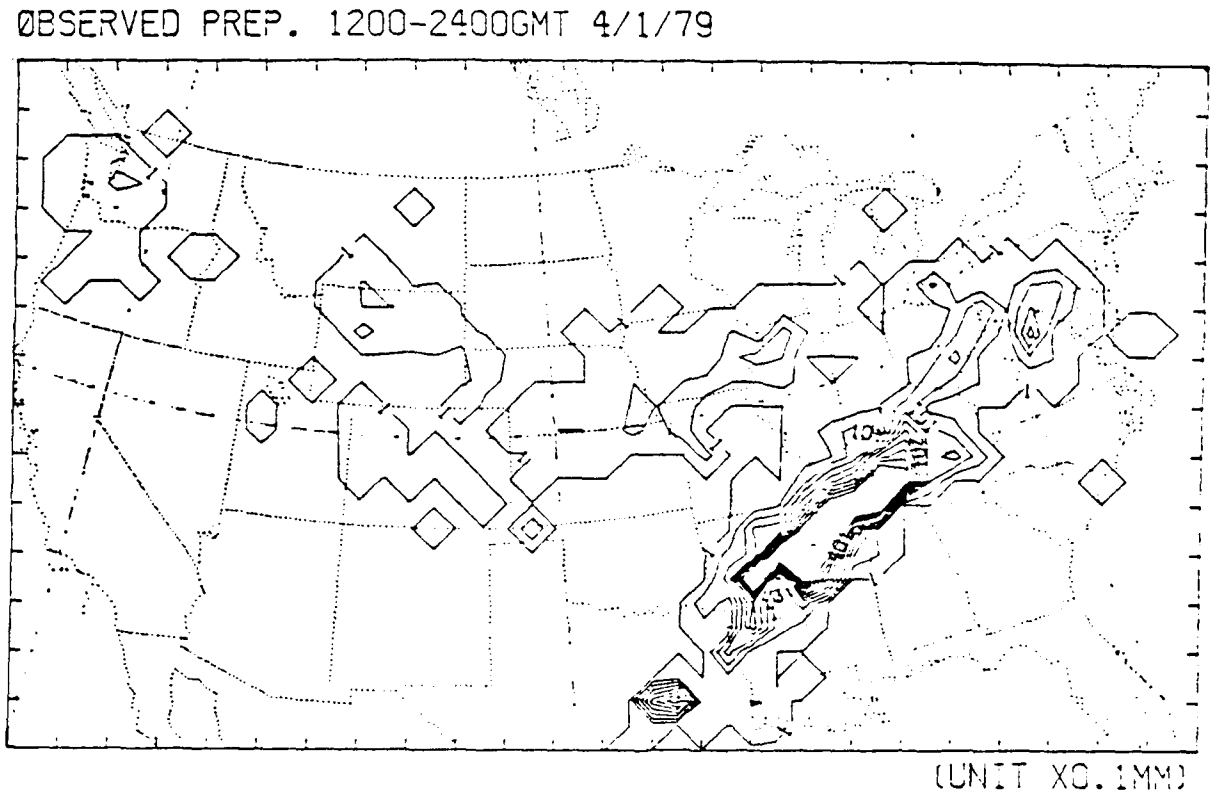

Fig. 32. Observed 12-hr precipitation ending at 2400 GMT 1 April 1979 over the U.S.

and are not meaningful. This figure shows a large amount of accumulated rainfall from Massachusetts southwestward to Texas and some light rainfall over Colorado, Wyoming, and Montana. The rainfall areas coincide with the areas of radar echoes in Fig. 31.

Fig. 33 is the predicted 12-hr accumulated total rainfall from Integration 1. The display area is chosen to be the same as in Fig. 32. The forecast total precipitation includes the convective and large-scale precipitation. In this integration, the forecast rainfall area is from Massachusetts west to Wyoming and Colorado with heavy precipitation over Indiana and Illinois. A small area of light rainfall is predicted over Washington and Oregon. This predicted light rainfall area agrees in general with the observation; but heavy precipitation is not predicted over Arkansas and Louisiana, as observed. The predicted rainfall in this integration is almost totally contributed by large-scale condensation. The convective rainfall (not shown) is very small, i.e., not over 0.1 mm during this period. Fig. 34 is the predicted rainfall from Integration 2. Fig. 34a is the predicted total precipitation. The forecast rainfall area is essentially the same as that from Integration 1 except the rainfall area is slightly bigger. The predicted convective rainfall (Fig. 34b), is located from the East Coast to Missouri and Arkansas in the broad area of observed heavy precipitation. However, the amount is still very small compared with that from the large scale condensation. Fig. 35 is from Integration 3. Comparing Fig. 35a with Fig. 32, one can see that the predicted rainfall area, especially the rainfall associated with the cold front, agrees much better with the observation. Fig. 35b shows that the rainfall area from Kentucky to Louisiana is produced purely by convective rainfall. This convective rainfall area almost coincides with the intense radar echo area in Fig. 31;

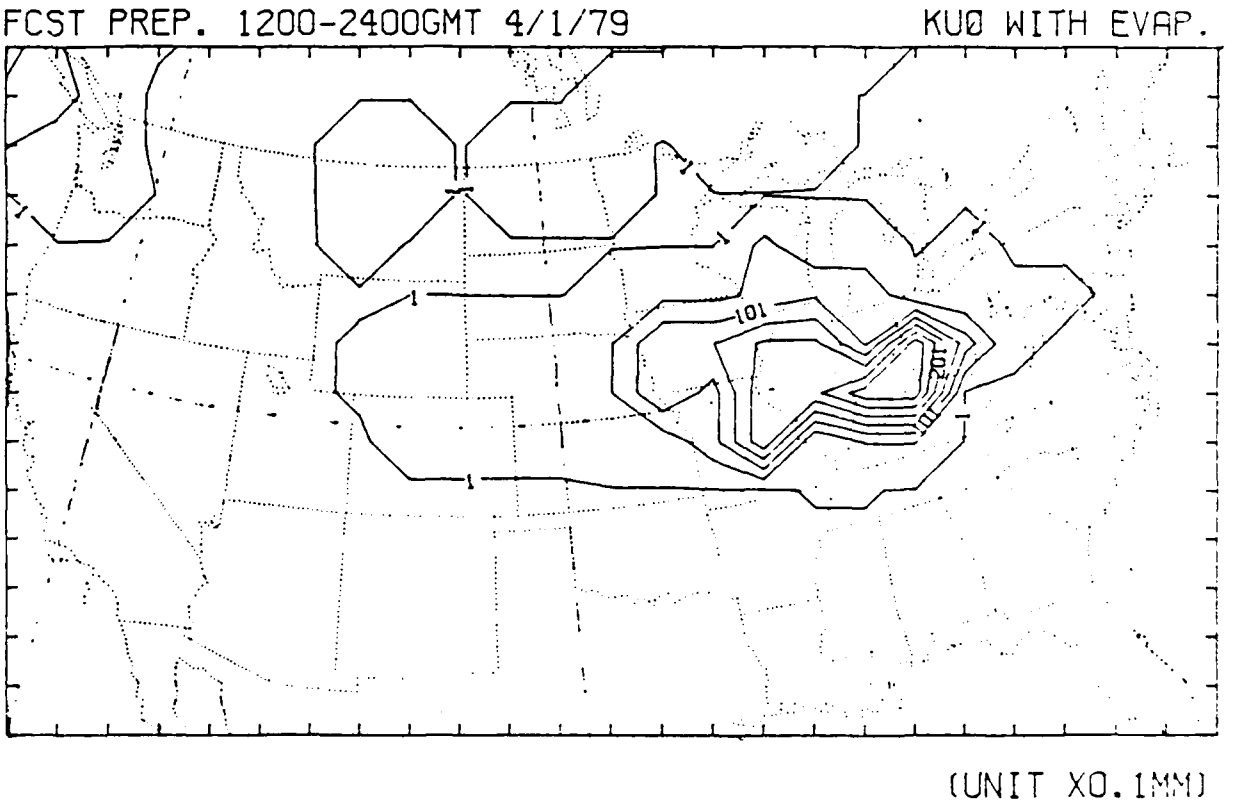

Fig. 33. Model-predicted 12-hr rainfall ending at 2400 GMT 1 April 1979 interpolated over the U.S. from Integration 1 with a contour interval of 5 mm.

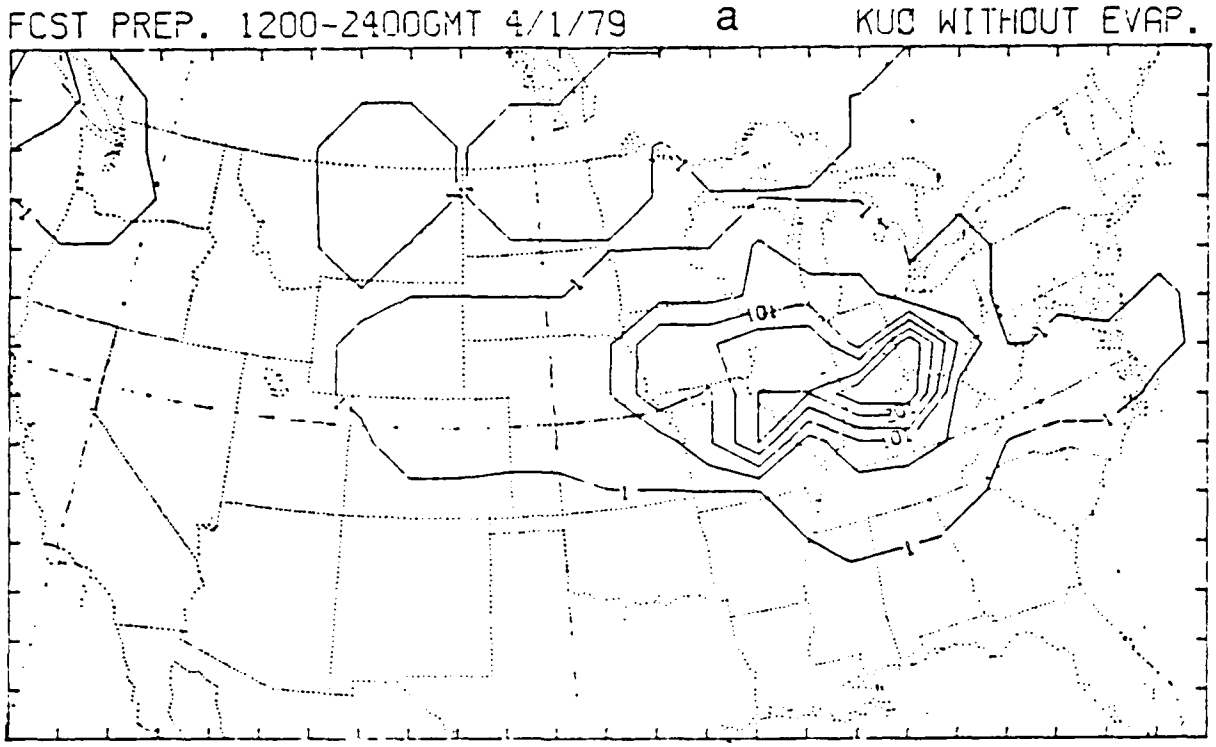

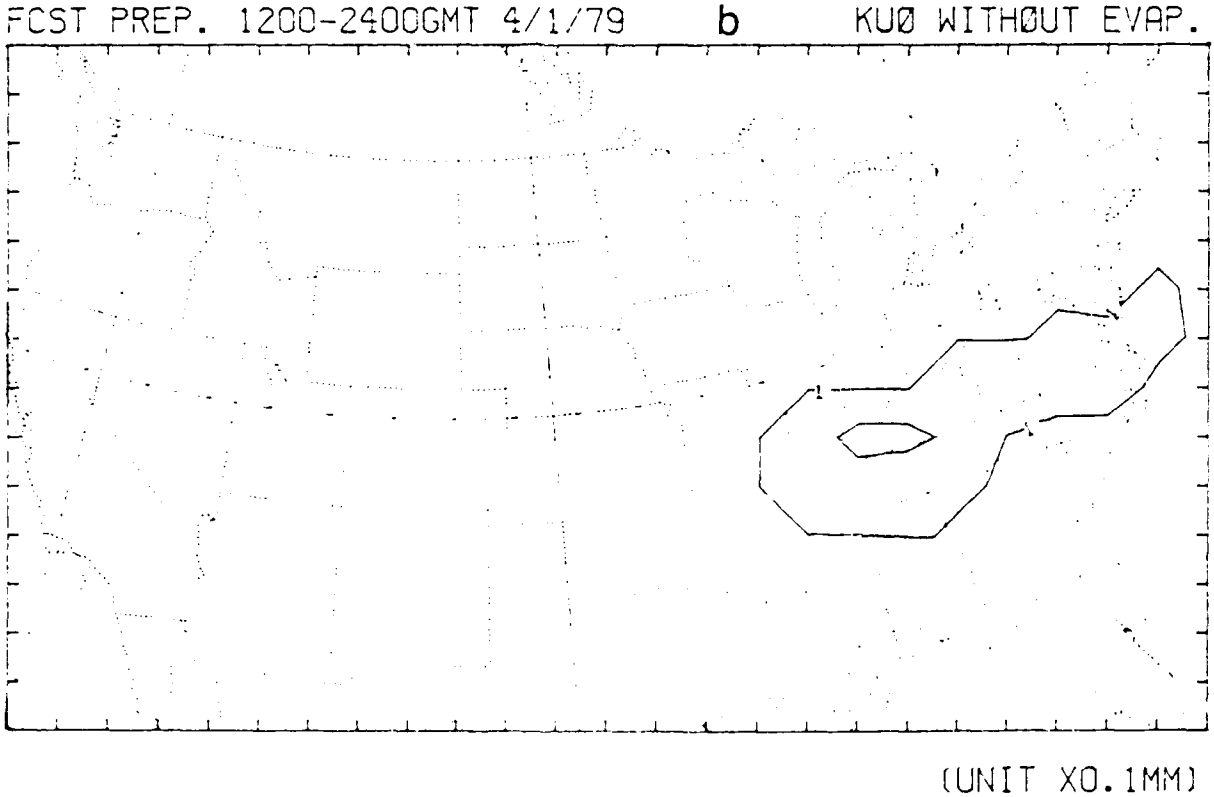

Fig. 34. Model-predicted 12-hr rainfall ending at 2400 GMT 1 April 1979 interpolated over the U.S. from Integration 2 with a contour interval of 5 mm: (a) total precipitation, (b) convective rainfall.

AD-A170 137 A STUDY OF CUMULUS PARAMETERIZATION IN A GLOBAL CIRCULATION MODEL(U) ILLINOIS UNIV AT URBANA DEPT OF ATMOSPHERIC SCIENCES S SOONG ET AL. JUN 85 2/2

UNCLASSIFIED AFGL-TR-85-0160 F19628-82-K-0030 F/G 4/2 NL

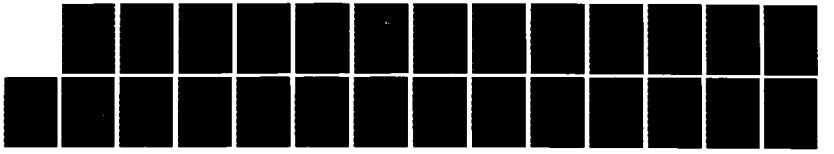

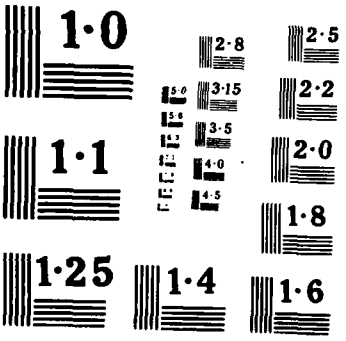
1·0
2·8
2·5
3·15
2·2
3·5
1·1
2·0
4·0
4·5
1·8
1·25
1·4
1·6

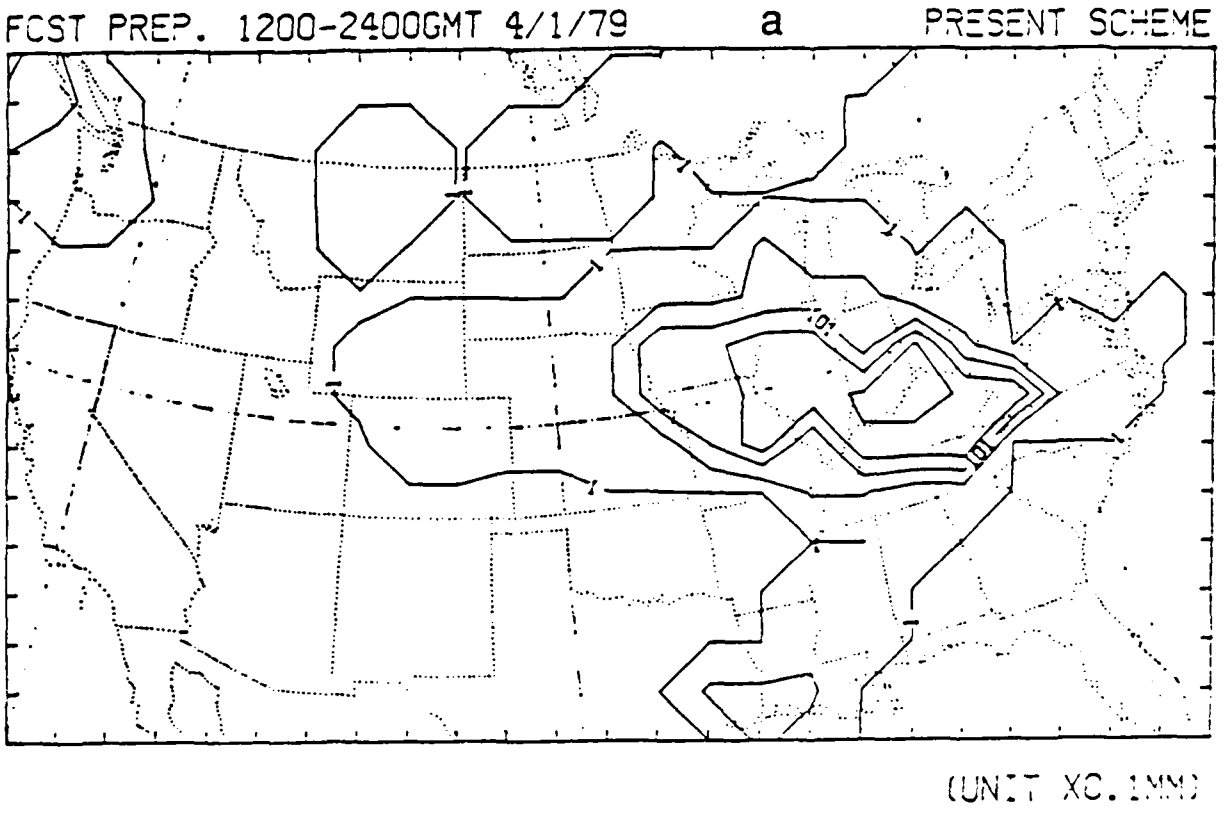

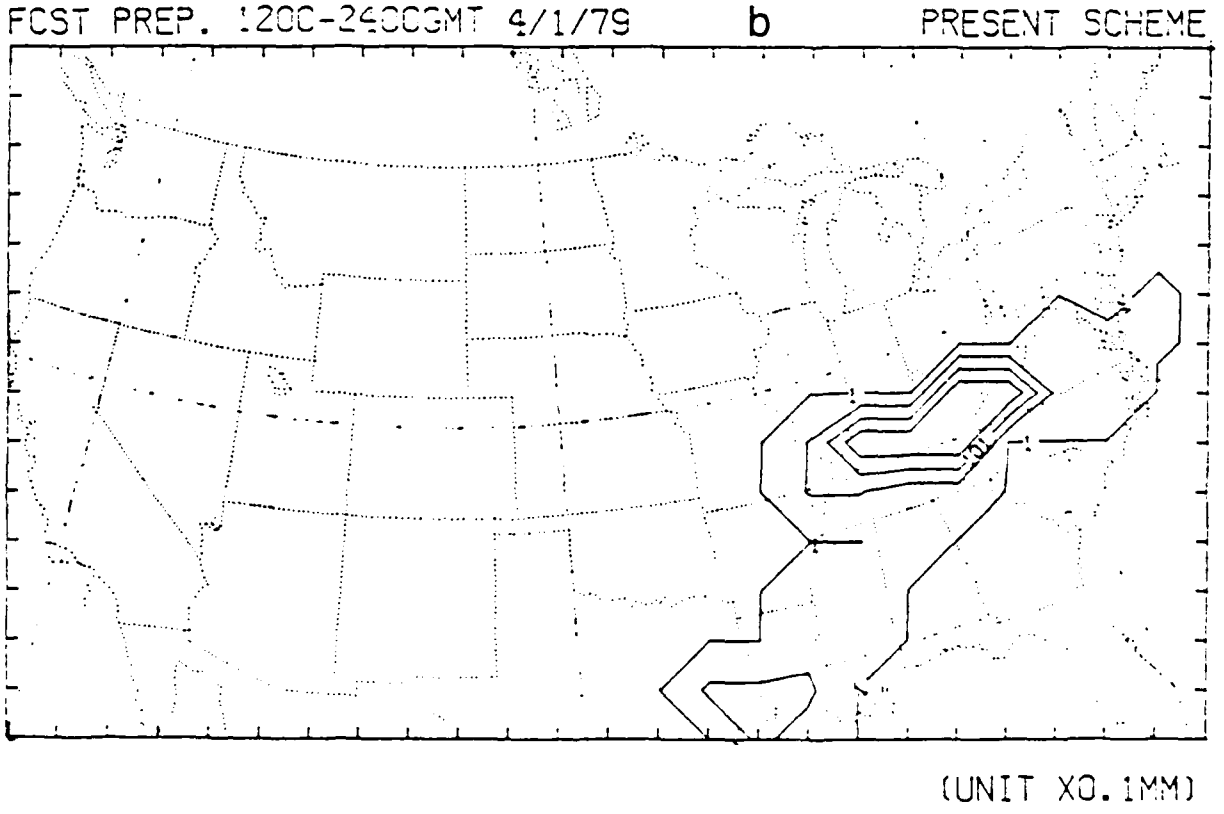

Fig. 35. As in Fig. 34 except for Integration 3.

however, the amount of the predicted rainfall rate is still smaller than the observation and the center of maximum rainfall is too far to the northeast. Fig. 36 shows the results from Integration 4. In Fig. 36a, the predicted total rainfall, the rainfall area covers most of the U.S. except for the West. The maximum rainfall area is over the Minnesota-Iowa border, which is too far northwest compared with the observation. This rainfall is mostly contributed by cumulus clouds, as parameterized by the A-S scheme (Fig. 36b). Another area of convective precipitation is predicted in a band from Tennessee to Louisiana close to the observed rainfall area.

3.2. The April 4, 1979 case

The second 24-hr forecast discussed in this report begins at 00 GMT 4 April 1979. Fig. 37 shows the surface synoptic chart at 1200 GMT 4 April 1979. The main features at this time included a low-pressure system centered over northwest Kentucky, a stationary front over Alabama and a cold front over the North Dakota-Canadian border which extended west and northwestward to North Dakota, Montana, and into Canada. During the next 12 hr, the low-pressure system moved northeastward to the Ohio-Pennsylvania border and produced non-convective rainfall over the East Coast. The stationary front over Alabama also slowly moved northeastward to Georgia with the southern part of this front gradually becoming a cold front during this period. An intensive radar echo associated with this cold front extended the full length of the Atlantic Coastal States (Fig. 38). The cold frontal system over the North Dakota-Canadian border had also moved northeastward into Canada. Several small radar echoes associated with this front were located over North Dakota, South Dakota, Wyoming, and Montana.

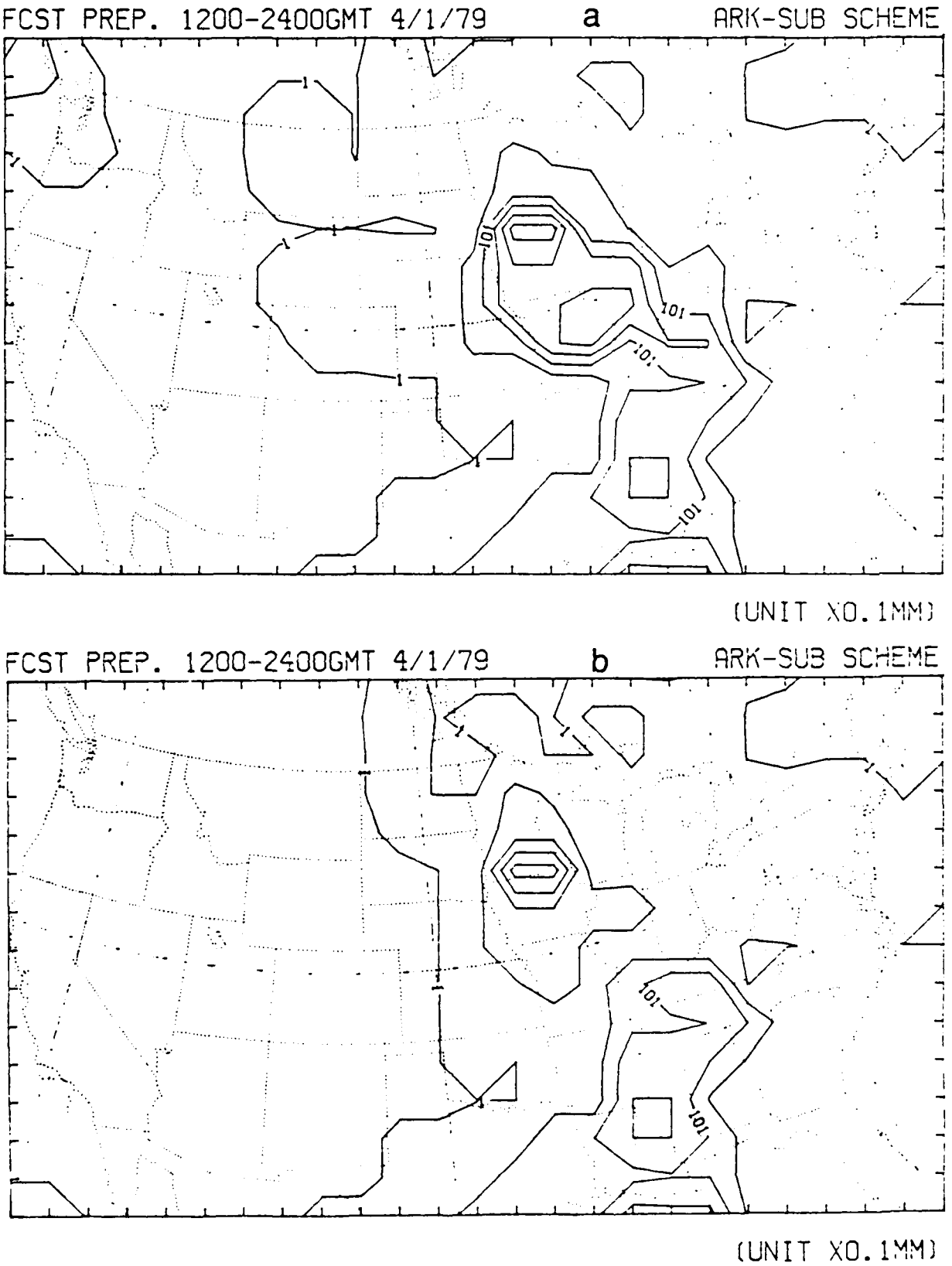

Fig. 36. As in Fig. 34 except for Integration 4.

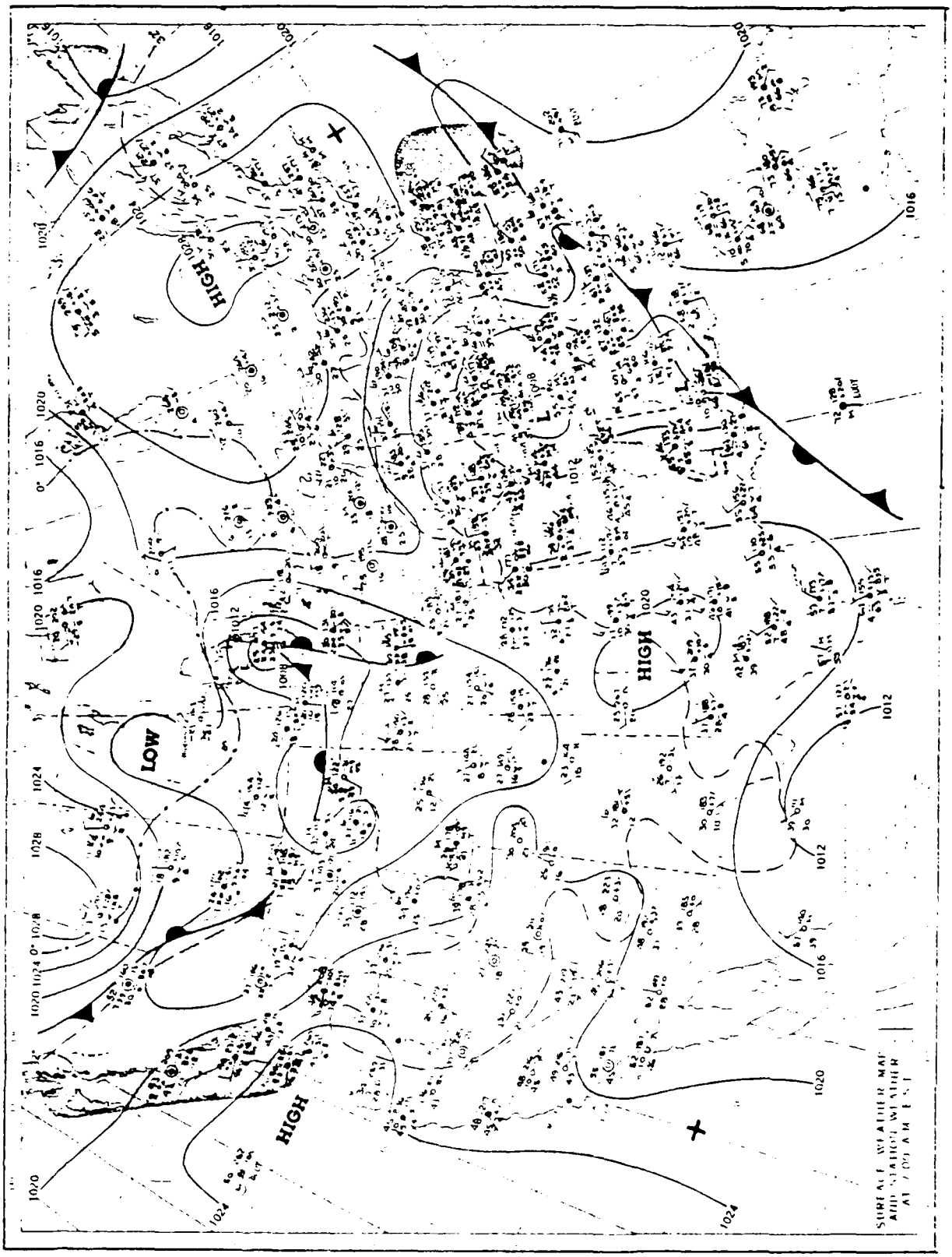

Fig. 37. Surface synoptic chart for 1200 GMT 4 April 1979.

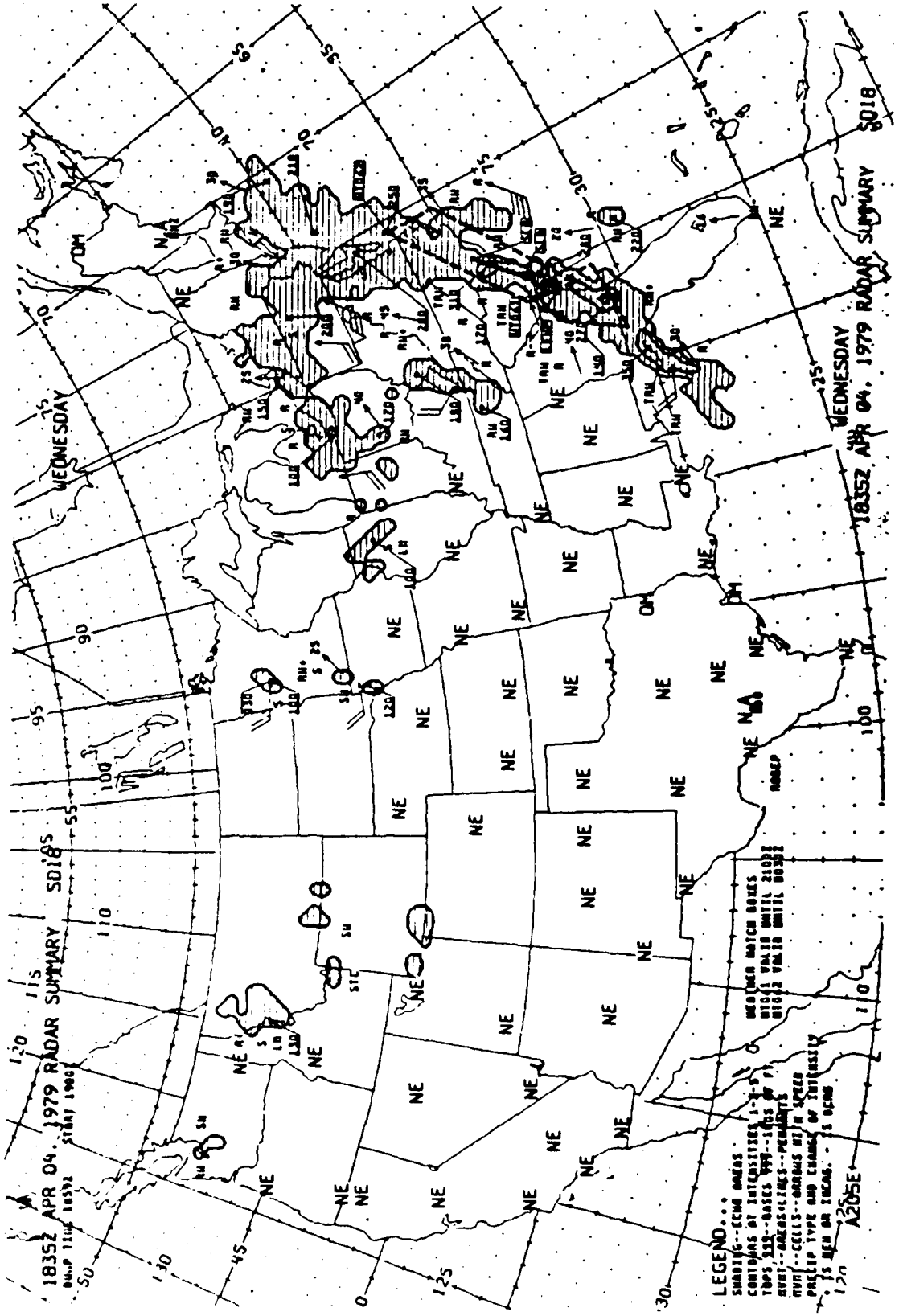

Fig. 38. Radar summary chart at 1835 GMT 4 April 1979.

Fig. 39 shows the observed 12-hr accumulated rainfall ending at 2400 GMT 4 April 1979 over the U.S. Heavy rainfall over the East Coast was again evident with the heaviest area of precipitation over northern Florida. Light rainfall existed from the Iowa-Missouri border northwest to Washington State. Also light rainfall was present over Texas.

Fig. 40 is the predicted 12-hr accumulated total rainfall over the U.S. from Integration 1. The forecast precipitation area is concentrated over the northeast with light rainfall being predicted over the northwestern U.S. The precipitation areas agree somewhat with the observations (Fig. 39), except it totally missed the heavy rainfall over Florida and Texas. The predicted rainfall is mostly due to large-scale condensation and the convective rainfall from this integration is again very small. Fig. 41 is the predicted rainfall from Integration 2 and Fig. 41a is the total rainfall. The predicted rainfall area is essentially the same as that from Integration 1 except it expanded in area from the northeast down to Florida. In Fig. 41b, predicted convective rainfall over Florida is now evident. Also, light convective rainfall is predicted over the borders of Montana, North Dakota, and Canada. However, the amount of convective rainfall is very small compared with that from large-scale condensation. For Integration 3 (Fig. 42), the predicted total rainfall has two centers over the East Coast and is in good agreement with the observation (Fig. 39). Fig. 42b clearly shows that the areas of rainfall over Florida and Texas are the result of convection only. In Fig. 43, from Integration 4, the precipitation area is concentrated over the Northeast Coast and over the ocean off of Florida. Some light rainfall is predicted over Washington State and extending east

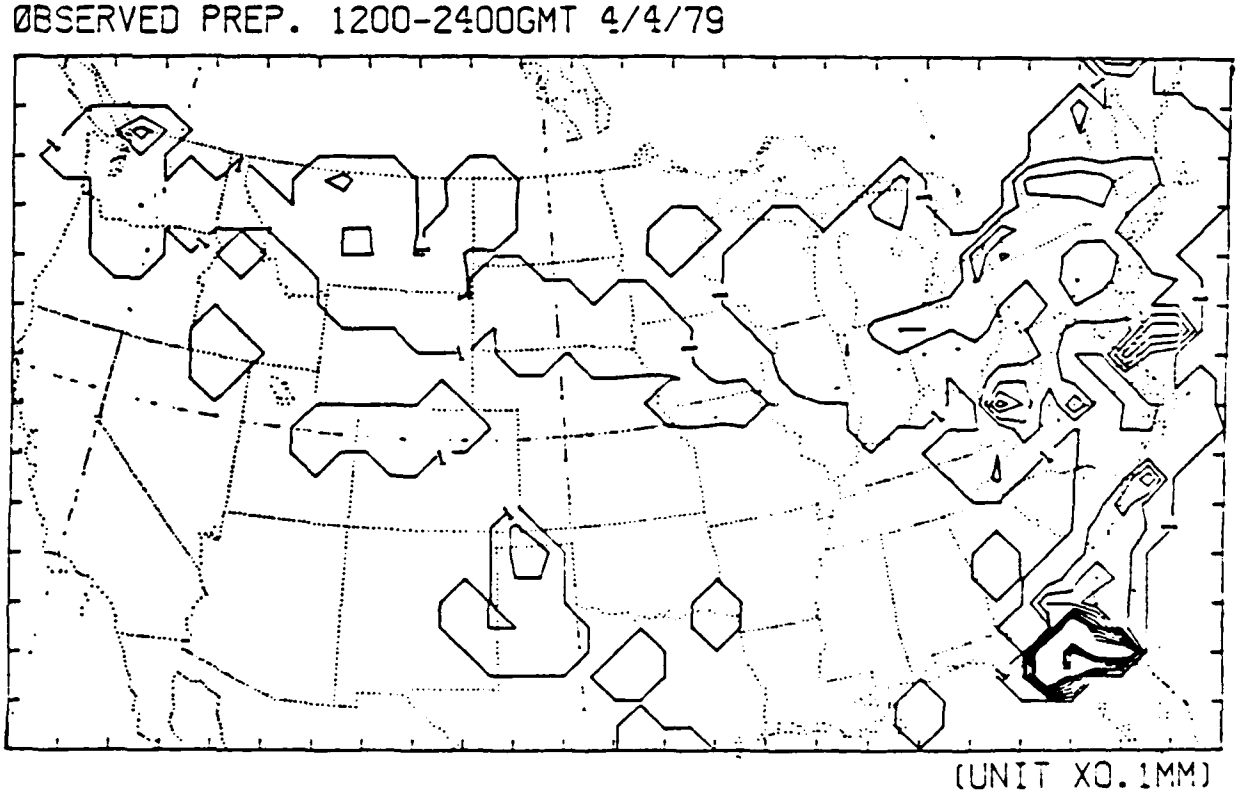

Fig. 39. Observed 12-hr precipitation ending at 2400 GMT 4 April 1979 over the U.S.

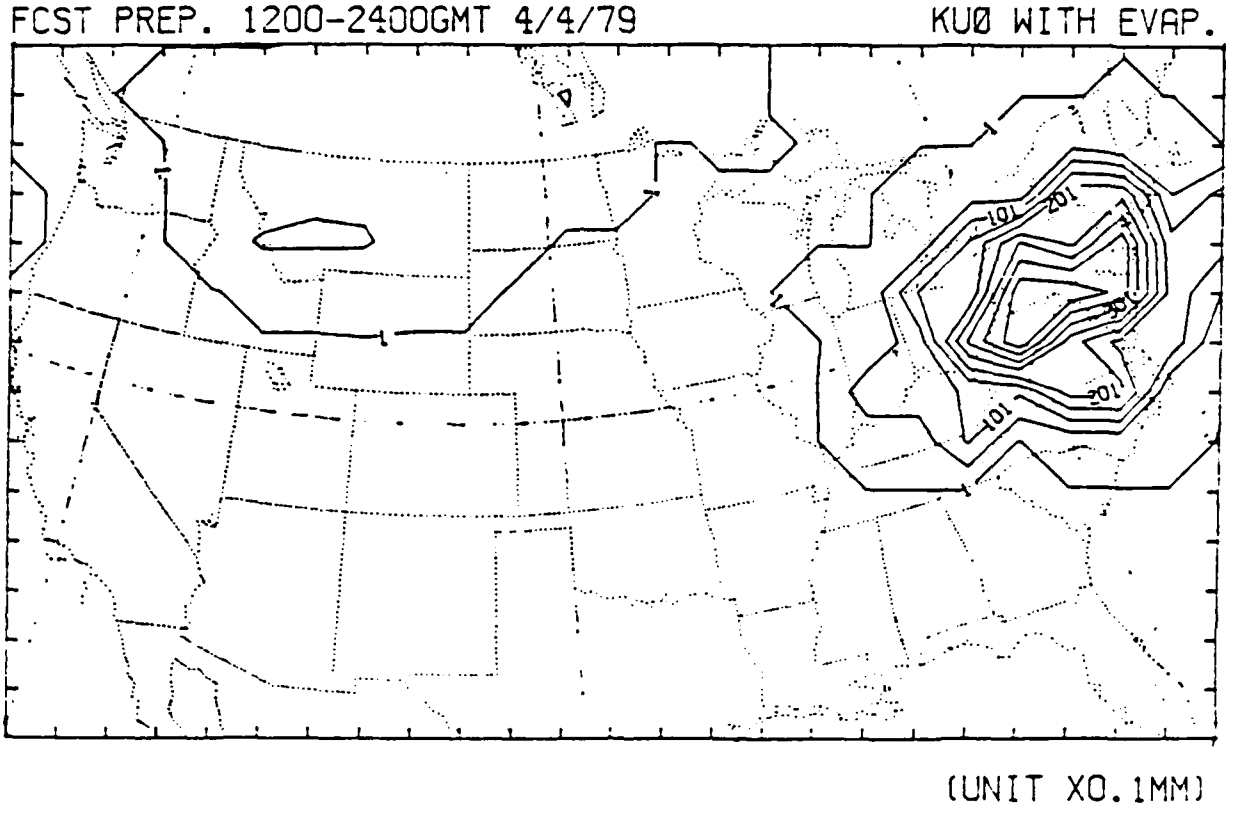

Fig. 40. Model-predicted 12-hr rainfall ending at 2400 GMT 4 April 1979 interpolated over the U.S. from Integration 1 with a contour interval of 5 mm.

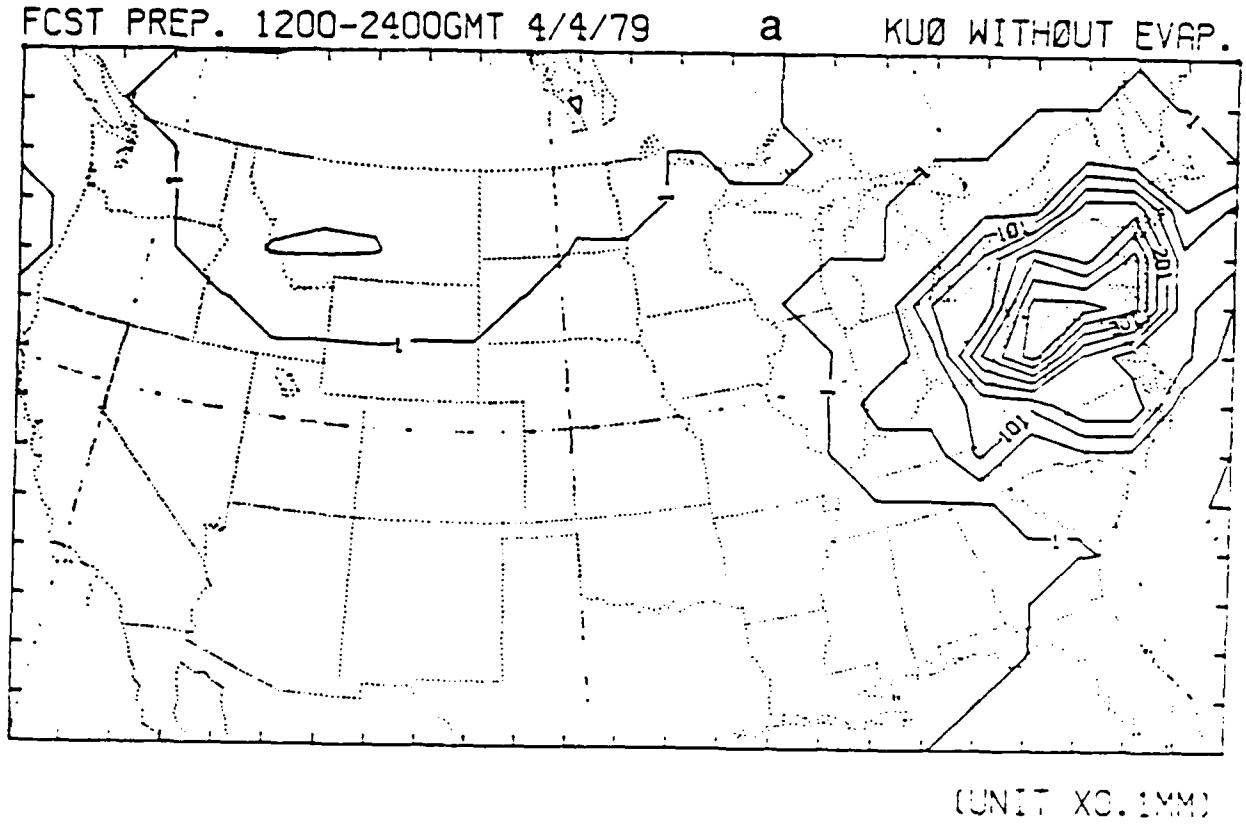

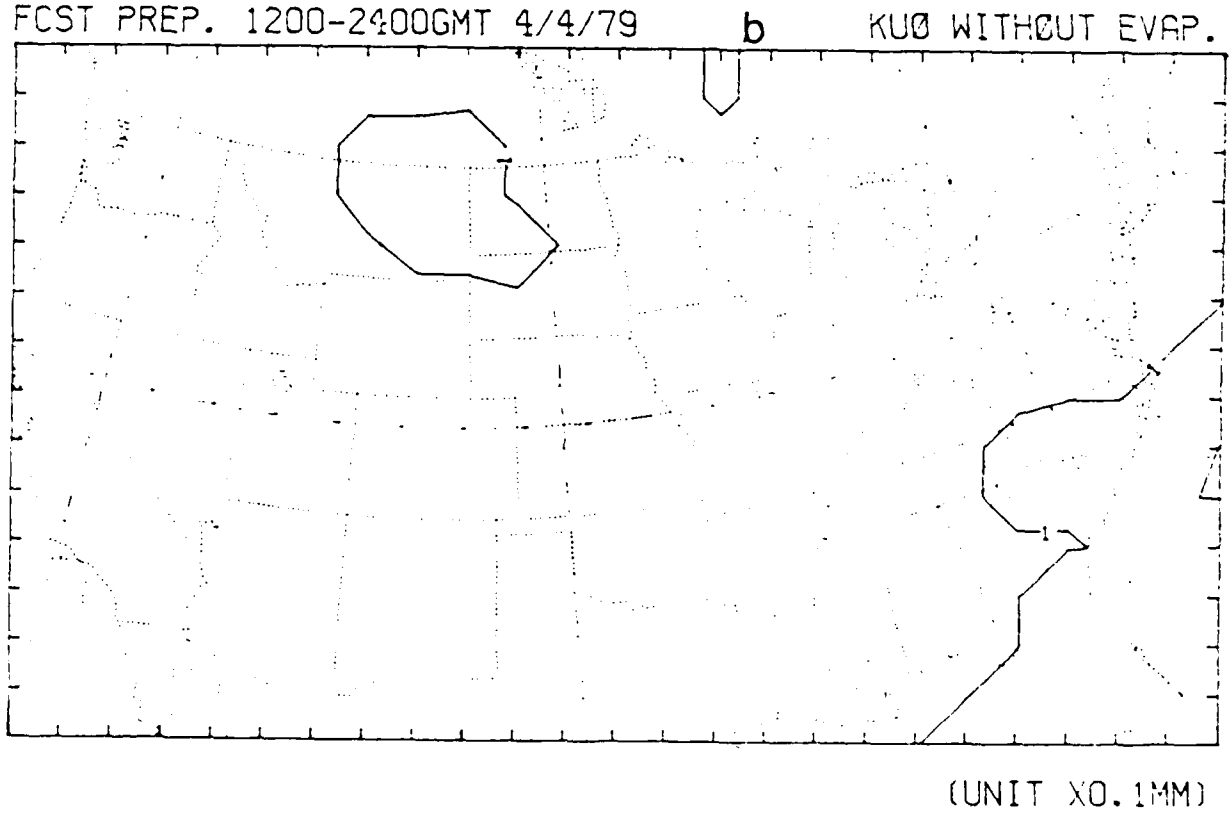

Fig. 41. Model-predicted 12-hr rainfall ending at 2400 GMT 4 April 1979 interpolated over the U.S. from Integration 2 with a contour interval of 5 mm: (a) total rainfall, (b) convective rainfall.

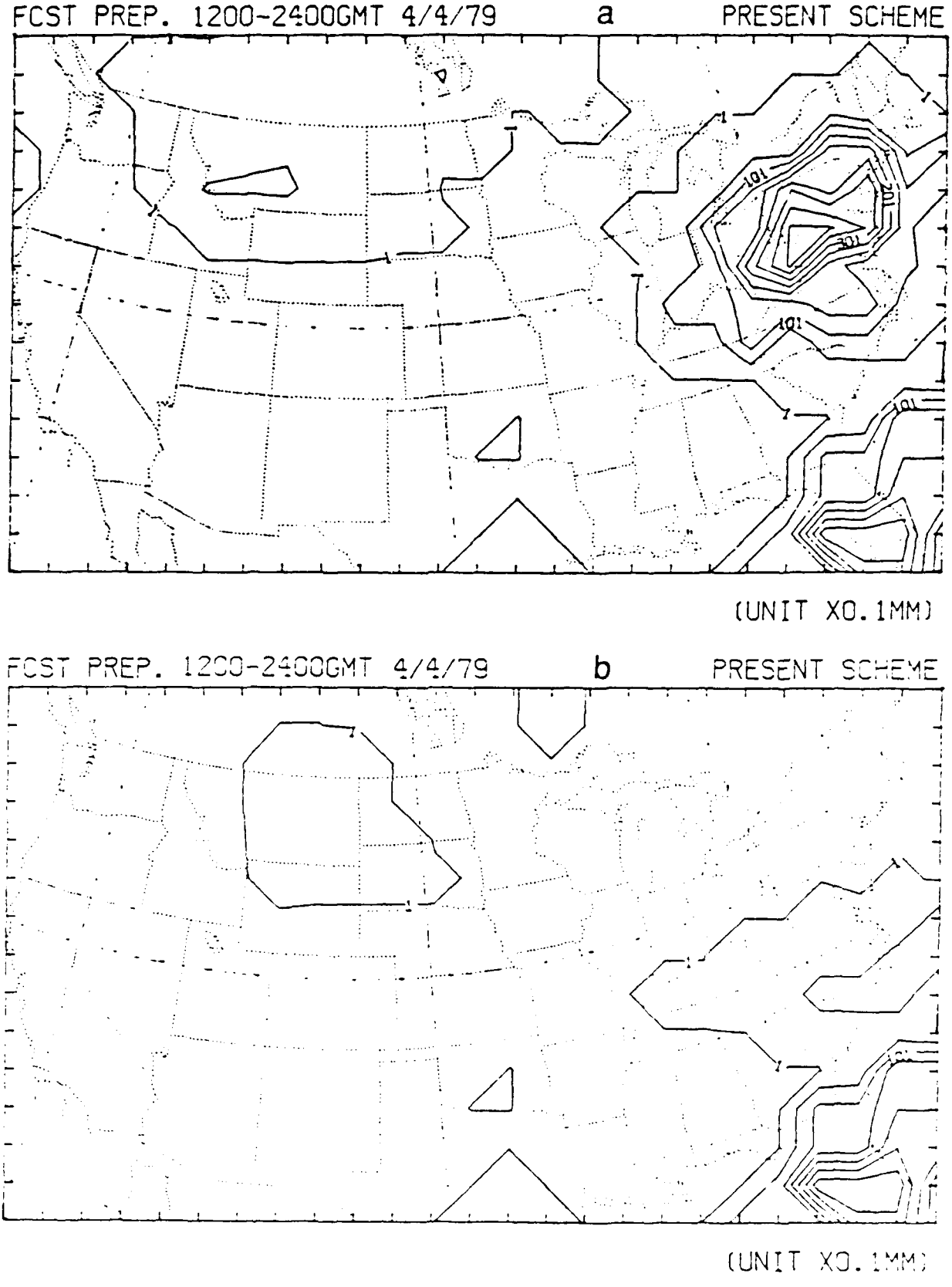

Fig. 42. As in Fig. 41 except for Integration 3.

FCST PREP. 1200-2400GMT 4/4/79 a ARK-SUB SCHEME

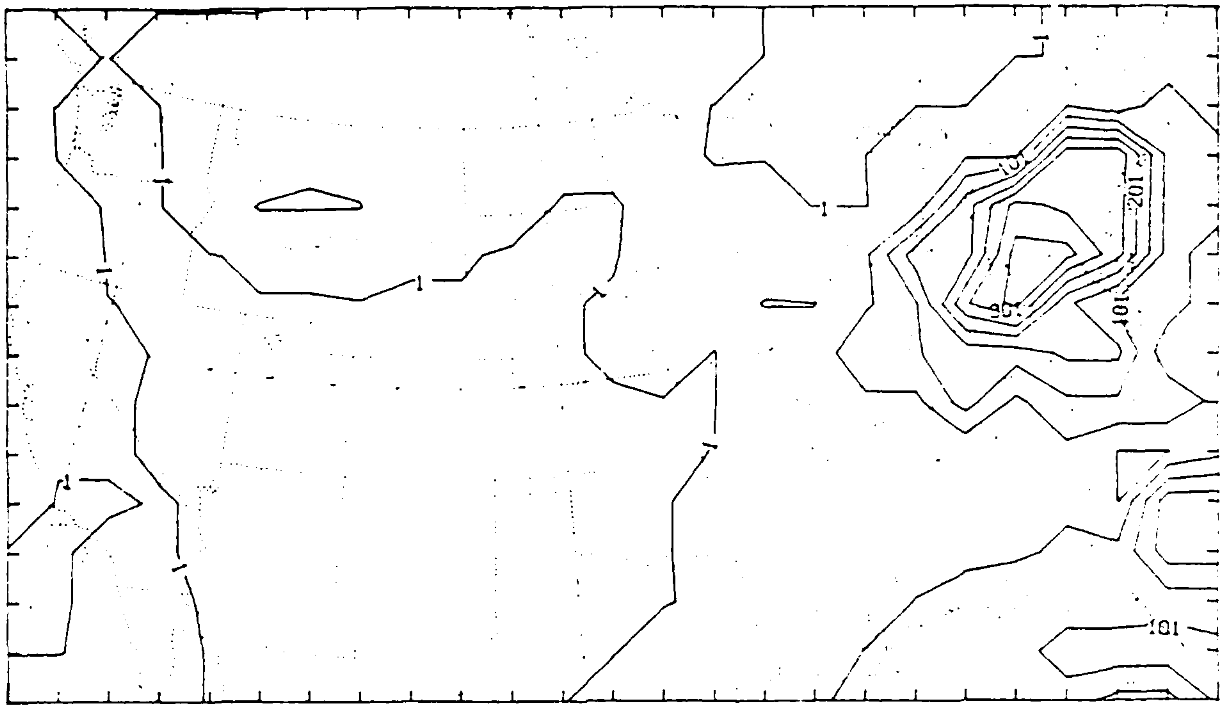

(UNIT X0.1MM)

FCST PREP. 1200-2400GMT 4/4/79 b ARK-SUB SCHEME

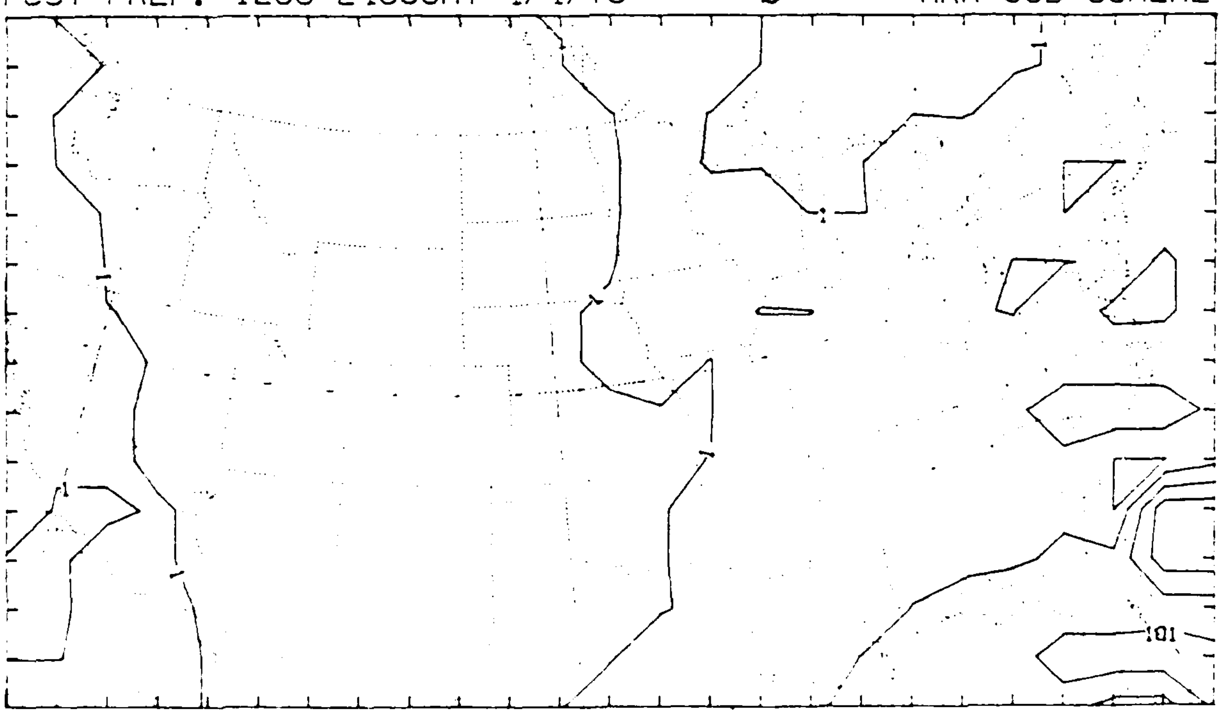

(UNIT X0.1MM)

Fig. 43. As in Fig. 41 except for Integration 4.

and southeast to Texas. It also shows some rainfall over the West Coast. The forecast rainfall area in general agrees with the observations but covers an area much larger than the observation.

3.3. The April 9, 1979 case

The third 24-hr forecast presented in this report starts at 00 GMT 9 April 1979. Fig. 44 shows the surface synoptic conditions at 1200 GMT 9 April 1979. The major features included a low-pressure system centered over West Virginia and a cold front associated with this low located to the south of this low center and extending southward. Another cold front was located over the southwestern part of Canada and extended south and southwestward to California. During the time between 1200 and 2400 GMT, the low-pressure system moved northeastward and the radar echo associated with this system was over the East Coast (Fig. 45). The cold front over Canada moved southward to Montana and southwestward to Wyoming, Utah, Nevada, and California.

Fig. 46 shows the observed 12-hr accumulated rainfall ending at 24 GMT 9 April 1979. Precipitation covers an area from Washington State southeastward down into Texas and Louisiana. Heavy rainfall was produced over the Northeast.

Fig. 47 is the predicted 12-hr accumulated total rainfall from Integration 1. The predicted rainfall areas are mainly over the northeast with patchy areas of light rainfall extending from Washington State southeastward to Texas. As before, the convective rainfall from this integration is very small. Overall, the precipitation pattern matches that in Fig. 46 reasonably well. Fig. 48 shows the forecast rainfall from Integration 2. Due to convection, the predicted rainfall areas over the northeast expanded southward over the Atlantic coastal waters. The rainfall area over the central United States was also mainly due to convection. Fig. 49, from Integration

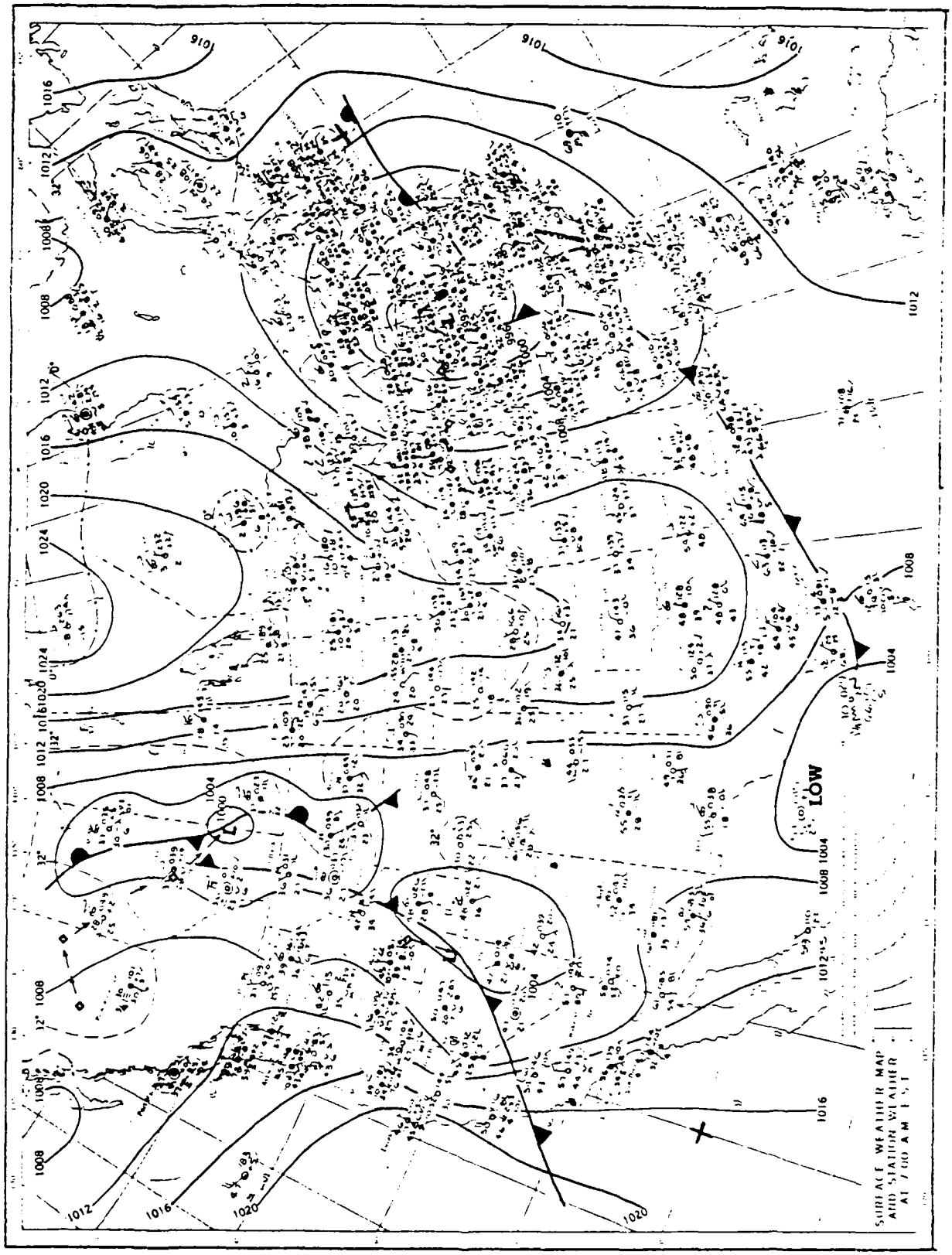

Fig. 44. Surface synoptic chart for 1200 GMT 9 April 1979.

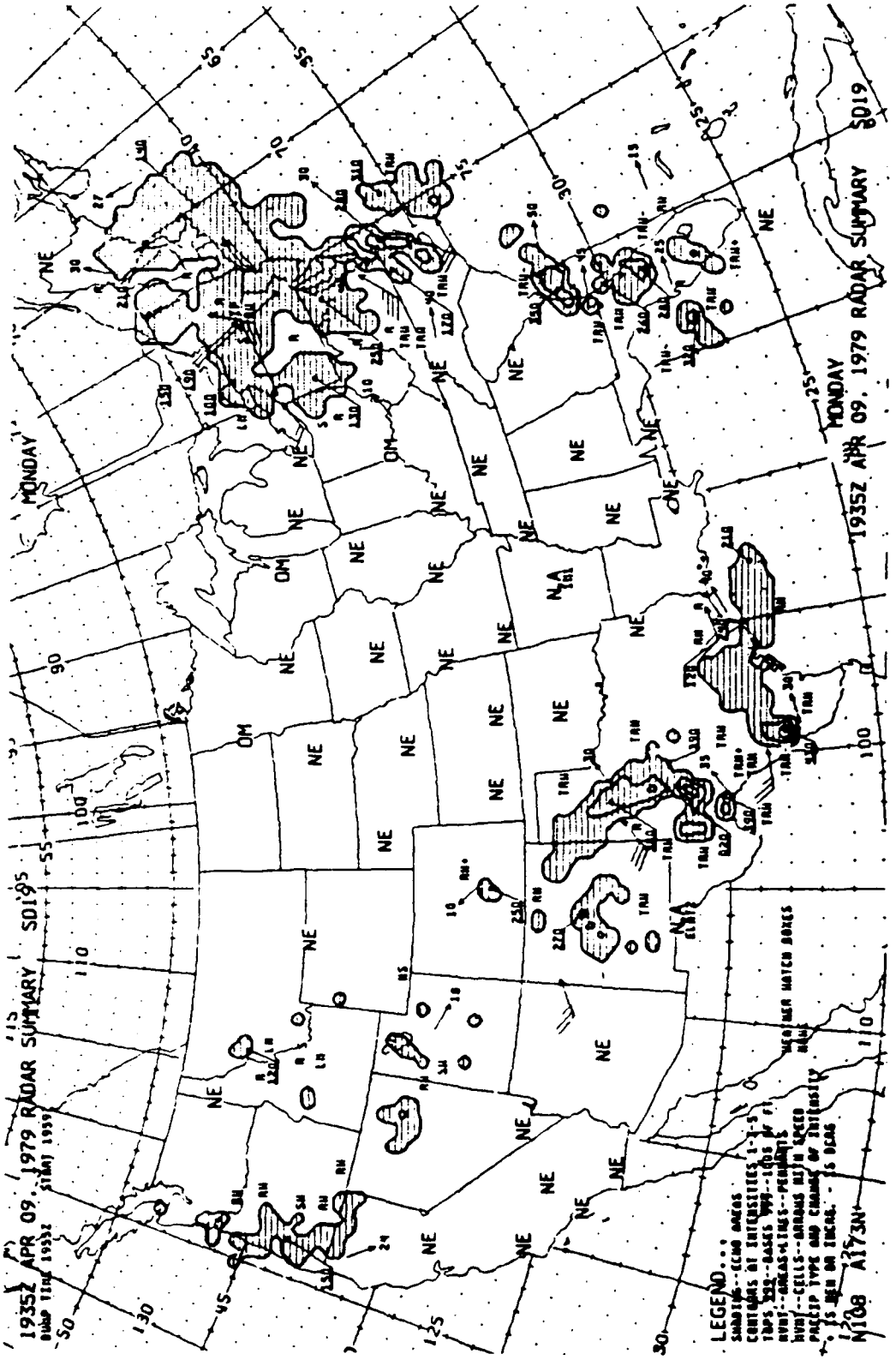

Fig. 45. Radar summary chart at 1935 GMT 9 April 1979.

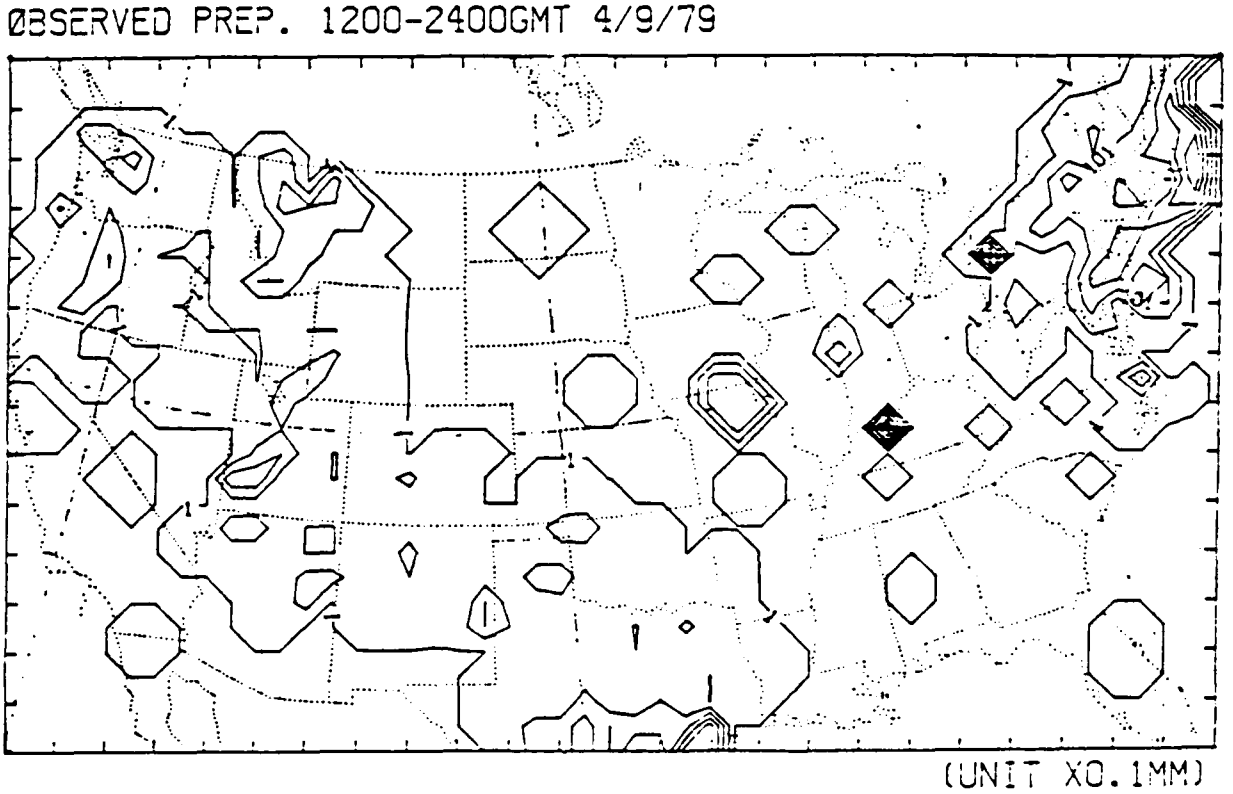

Fig. 46. Observed 12-hr precipitation ending at 2400 GMT 9 April 1979 over the U.S.

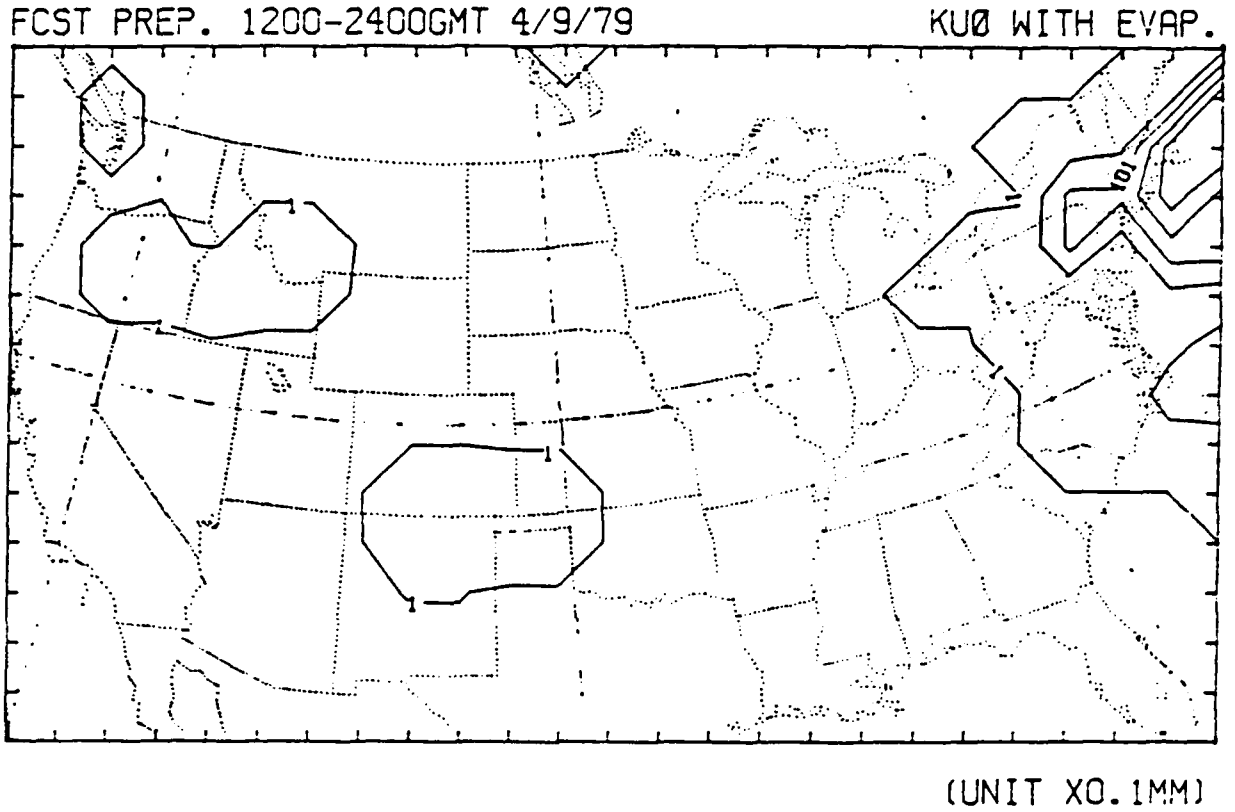

Fig. 47. Model-predicted 12-hr rainfall ending at 2400 GMT 9 April 1979 interpolated over the U.S. from Integration 1 with a contour interval of 5 mm.

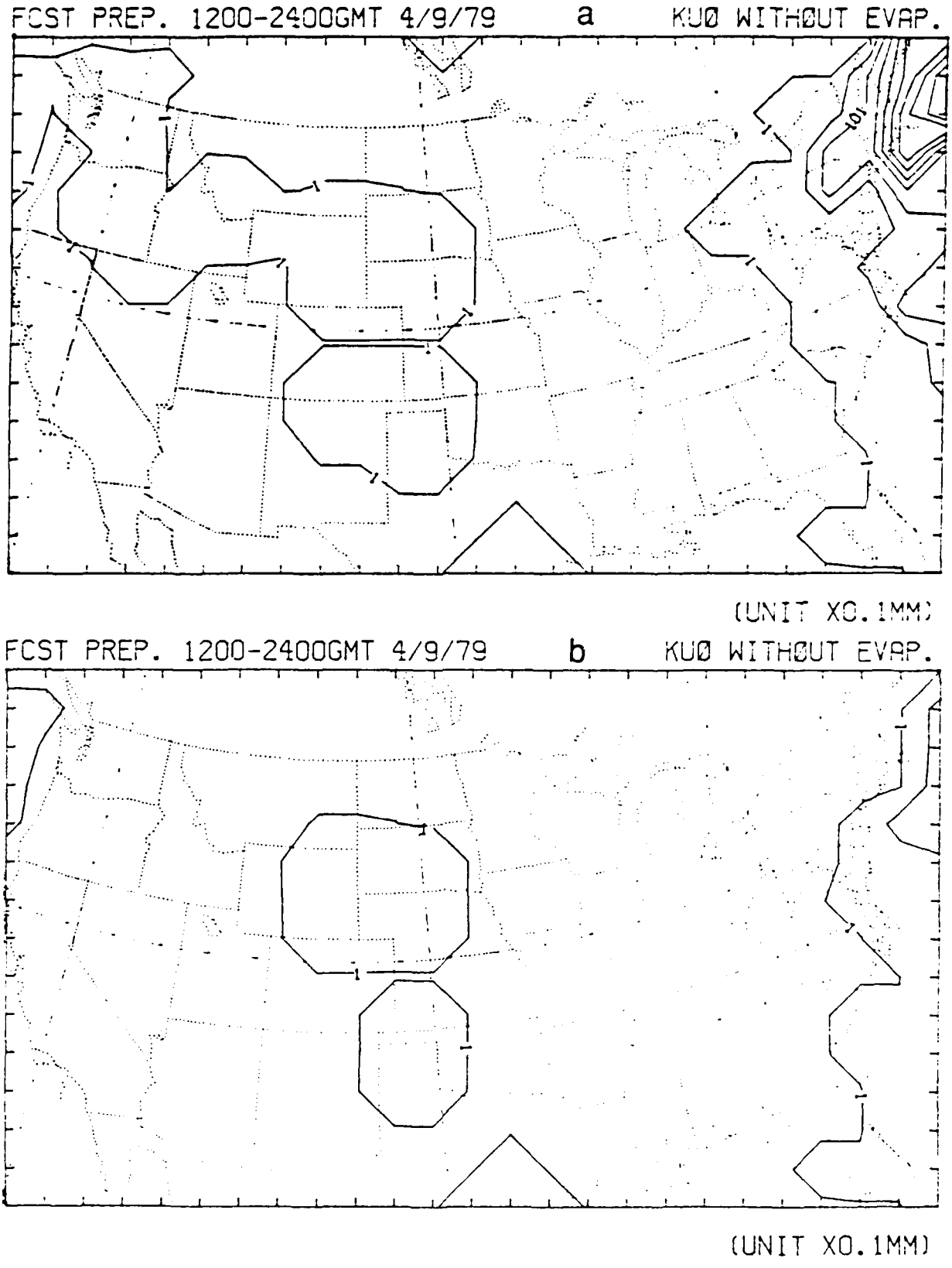

Fig. 48. Model-predicted 12-hr rainfall ending at 2400 GMT 9 April 1979 interpolated over the U.S. from Integration 2 with a contour interval of 5 mm: (a) total rainfall, (b) convective rainfall.

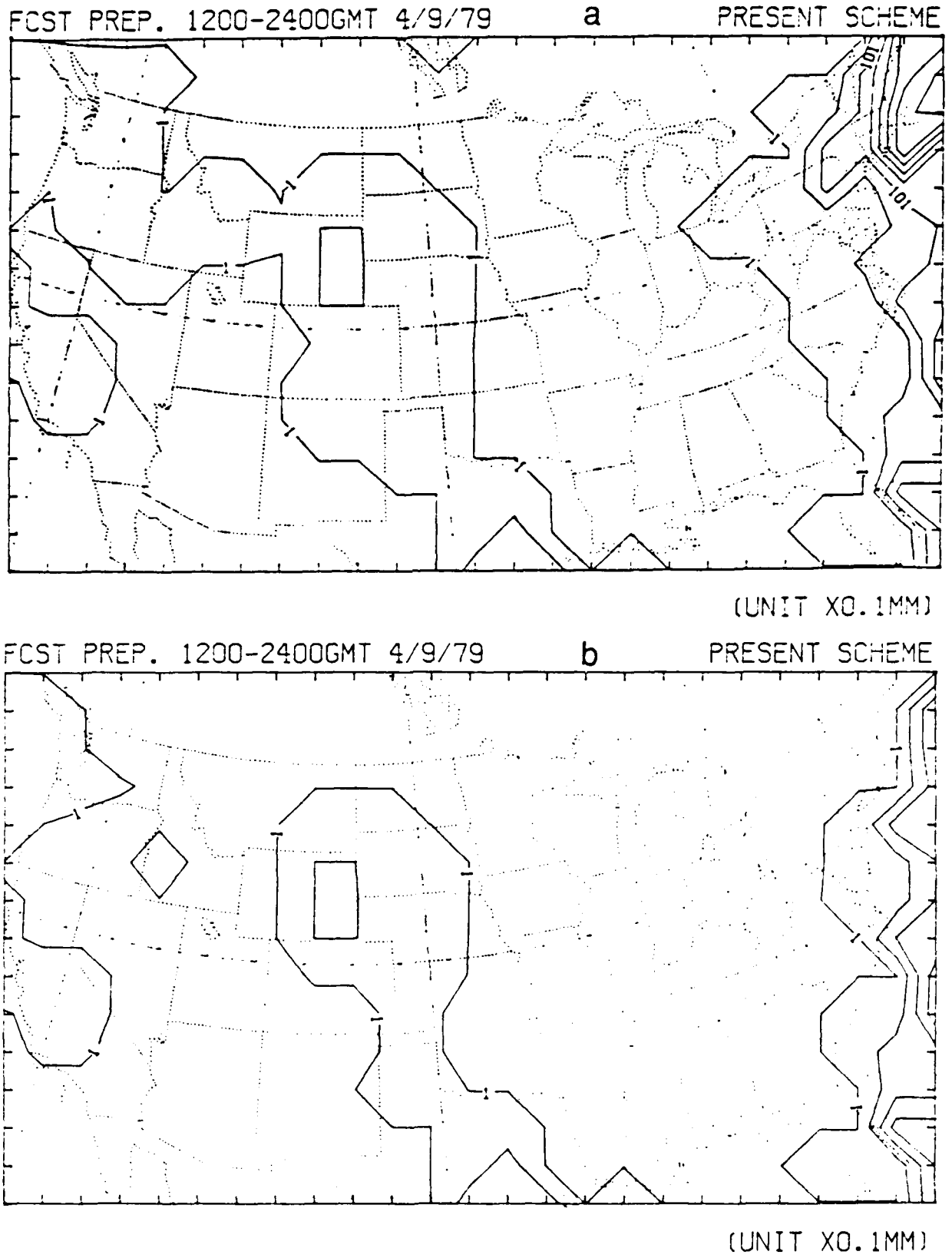

Fig. 49. As in Fig. 48 except for Integration 3.

3, shows that heavy rainfall was produced over the Atlantic coastal area. Any comparison with observations over that area would be misleading because no observations were available. Fig. 50 shows the forecast rainfall from Integration 4. In general, precipitation covers the East Coast and the High Plains area. The area of maximum rainfall, over the Wyoming-Colorado border, has a value above 30 mm, which is much too high compared with the observation. This rainfall is contributed totally by convection due to the A-S scheme.

4. Discussion

The results in the preceding sections have led us to the following conclusions from the four different cumulus parameterization schemes:

(a) In the original AFGL spectral model, Kuo's 1965 scheme was used. In addition, the condensed falling water was allowed to evaporate into the lower layers if they were not saturated. This version of the scheme produced almost no convective rainfall and the total rainfall was mainly contributed by the large-scale condensation. The lack of convective rainfall was caused by the rainfall evaporating before it reached the ground.

(b) Kuo's 1965 scheme without any evaporation of falling rain produced some convective rainfall. However, the amount was still very small compared to that from the large-scale condensation. As discussed in Part One of the report, this version of the scheme used a large portion of the large-scale supply of moisture to moisten the atmosphere, leaving a small portion to precipitation.

(c) The present modified Kuo scheme produced a reasonable amount of convective rainfall because the 'b' parameter in this scheme is always very small. The predicted rainfall area agreed very well with the observations in all three of the test cases.

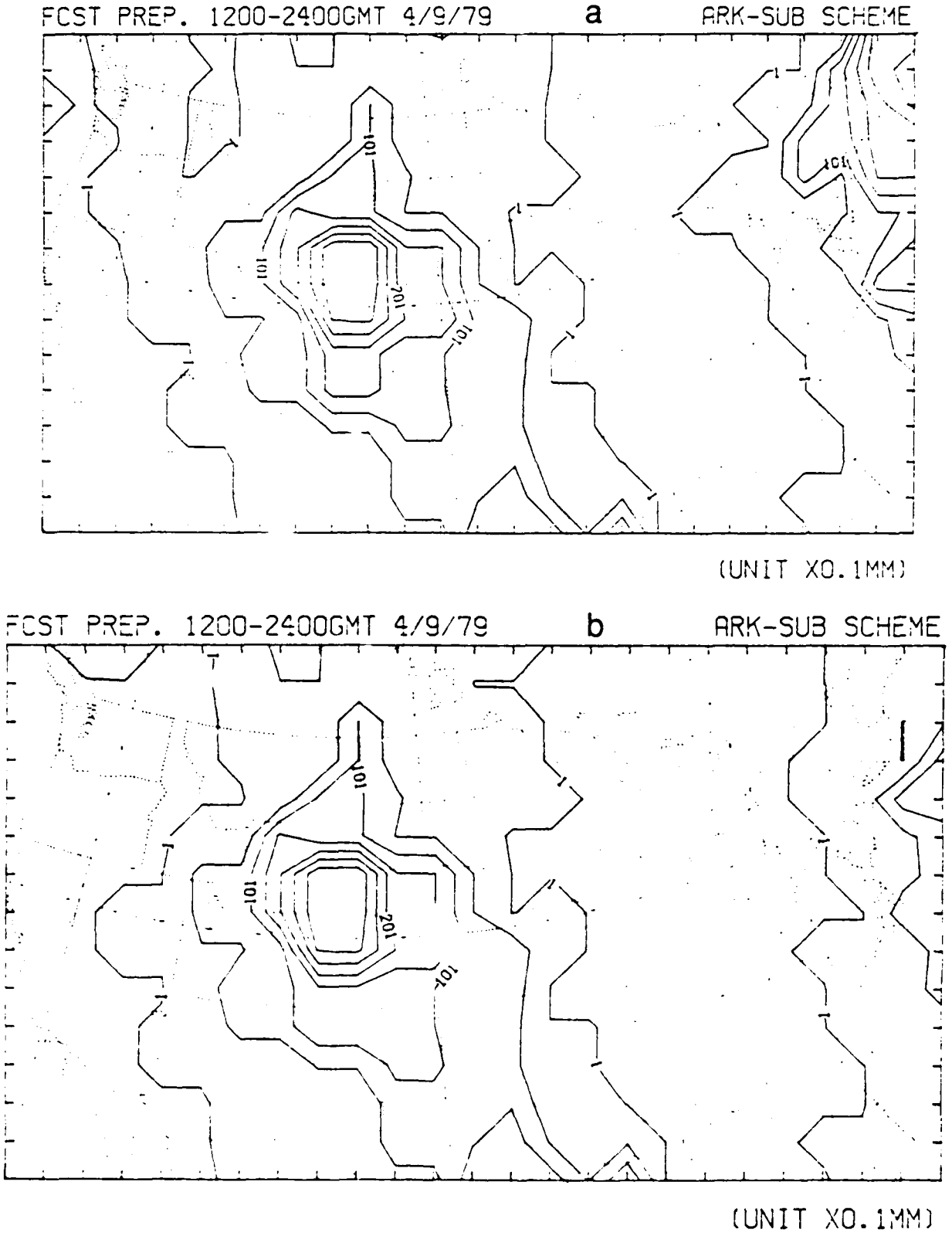

Fig. 50. As in Fig. 48 except for Integration 4.

(d) The A-S scheme tended to produce more convective rainfall than other cumulus parameterization schemes. The predicted rainfall area from this scheme was larger than the observations in the above 3 cases.

This work clearly demonstrated the ability of the AFGL model to predict large-scale stratiform precipitation. With the incorporation of the present modified Kuo scheme, the area of convective precipitation can also be well predicted. However, the predicted convective precipitation area is generally broader and the amount of rainfall smaller than observations. This problem may be attributed to the resolution of the AFGL model in that it cannot resolve the narrow band of the cold front, the major mesoscale rain-producing system. The implementation of the A-S scheme in the AFGL model also produced a reasonable distribution of convective precipitation. The precipitation area is more concentrated and is sometimes produced in an observed clear area. This result may have been caused by the current implementation of the A-S scheme in the AFGL model, in which the cloud base is assumed to be 500 m above the ground surface. This assumption is valid in the tropics, but it may produce unrealistic convective rainfall in dry areas.

Future improvements in precipitation forecasting using the AFGL model include the prediction of mesoscale dynamics related to strong convection and precipitation. A major task in this direction is to incorporate the prediction of the diurnal temperature variation which can significantly affect the structure of mesoscale systems and the time and location of precipitation. The inclusion of boundary layer prediction and radiation, which have already been undertaken by AFGL concurrently with this project, should fulfill this requirement. Once all of these physical processes are integrated to the AFGL model, another task to improve the prediction is to

increase the model resolution. This task can be achieved by either increasing the wave number retained in the AFGL model or using a nested technique for limited area, fine grid prediction. A more comprehensive test of the fine grid model with an extended period of prediction will therefore be needed.

References

Anthes, R. A., 1977: A cumulus parameterization scheme utilizing a one-dimensional cloud model. Mon. Wea. Rev., 105, 270-286.

Arakawa, A., and W. H. Schubert, 1974: Interaction of cumulus cloud ensemble with the large-scale environment, Part I. J. Atmos. Sci., 31, 674-701.

Brenner, S., C.-H. Yang and S. Y. K. Yee, 1982: private communication.

Brown, J. A., 1974: On vertical differencing in the sigma system. NMC Office Note 92, 13 pp.

Chao, H. R., R. M. Bloxam, and L. Cheng, 1979: A GATE A/B scale budget analysis. Atmos. Ocean, 17, 60-76.

Charney, J. G., and A. Eliassen, 1964: On the growth of the hurricane depression. J. Atmos. Sci., 21, 68-75.

Kao, C.-Y. J., and Y. Ogura, 1985: A cumulus parameterization study with special attention to the Arakawa-Schubert scheme. Scientific Report No. 1, AFGL-TR-85-0159, Air Force Geophysics Laboratory, Hanscom Air Force Base, Massachusetts.

Klemp, J. B., and R. B. Wilhelmson, 1978: The simulation of three-dimensional convective storm dynamics. J. Atmos. Sci., 35, 1070-1093.

Kreitzberg, C. W., and D. J. Perkey, 1977: Release of potential instability, Part II: The mechanism of convective/mesoscale interaction. J. Atmos. Sci., 34, 1569-1596.

Krishnamurti, T. N., M. Kanamitsu, R. Godbole, C. B. Chang, F. Carr, and J. H. Chow, 1976: Study of a monsoon depression (II), Dynamical structure. J. Meteor. Soc. Japan, 54, 208-225.

Krishnamurti, T. N., Y. Ramanathan, H.-L. Pan, R. J. Pasch, and J. Molinari, 1980: Cumulus parameterization and rainfall rates I. Mon. Wea. Rev., 108, 465-472.

Krishnamurti, T. N., S.-L. Nam, and R. Pasch, 1983: Cumulus parameterization and rainfall rates II. Mon. Wea. Rev., 111, 815-828.

Kuo, H. L., 1965: On formation and intensification of tropical cyclones through latent release by cumulus convection. J. Atmos. Sci., 22, 40-63.

Kuo, H. L., 1974: Further studies of the parameterization of the influence of cumulus convection on large scale flow. J. Atmos. Sci., 31, 1232-1240.

Molinari, J., 1982: A method of calculating the effects of deep cumulus convection in numerical models. Mon. Wea. Rev., 110, 1527-1534.

Ogura, Y., Y.-L. Chen, J. Russell, and S.-T. Soong, 1979: On the formation of organized convective systems observed over the eastern Atlantic. Mon. Wea. Rev., 107, 426-441.

Phillips, N. A., 1959: Numerical integration of the primitive equation on the hemisphere. Mon. Wea. Rev., 87, 333-345.

Phillips, N. A., 1975: Application of Arakawa's energy conserving layer model to operational numerical weather prediction. NMC Office Note 104, 40 pp.

Phillips, N. A., 1979: The nested grid model. NOAA Tech. Rep. NWS-22, 79 pp.

Robert, A. J., 1966: The integration of a low order spectral form of the primitive meteorological equation. J. Meteor. Soc. Japan, 44, 237-245.

Rosenthal, S. L., 1970: A circularly symmetric primitive equation model of tropical cyclone development containing an explicit water vapor cycle. Mon. Wea. Rev., 98, 643-663.

Song, J. L., and W. M. Frank, 1983: Relationships between deep convection and large-scale processes during GATE. Mon. Wea. Rev., 111, 2145-2160.

Soong, S.-T., and Y. Ogura, 1973: A comparison between axisymmetric and slab-symmetric cumulus cloud models. J. Atmos. Sci., 30, 879-893.

Soong, S.-T., and W.-K. Tao, 1980: Response of deep tropical cumulus clouds to mesoscale processes. J. Atmos. Sci., 37, 2016-2034.

Soong, S.-T., and Y. Ogura, 1982: A numerical study of cloud clusters as a scale interaction problem. WMO Programme on Research in Tropical Meteorology, extended abstracts of papers presented at the MSJ/MJA/WMO/AMS, 115-116.

Sui, C. H., and M. Yarai, 1984: Vorticity budget of the GATE A/B area and its interpretation. 15th Conference on Hurricanes and Tropical Meteorology, AMS, Jan. 9-13, Miami, Florida, 465-472.

Wuchnitz, J., D. Hasselman, and M. Koning, 1977: Wassernahe turbulente vertikal-flusse bei gestorten und ungestorten Bedingungen wahred GATE. Ann. Met. Neue Folge, 12, 23-25.

Yamasaki, M., 1984: Convective clouds in vertical shear flow and CISK applied to easterly waves and squall-line systems, submitted to J. Meteor. Soc. Japan.

END

DTIC

8-86